

The Pennsylvania State University

The Graduate School

The Eberly College of Science

THE EFFECTS OF AEROSOL ACIDITY ON THE MORPHOLOGY AND ICE
NUCLEATION OF AEROSOL PARTICLES

A Dissertation in

Chemistry

by

Delanie J. Losey

© 2017 Delanie J. Losey

Submitted in Partial Fulfillment
of the Requirements
for the Degree of

Doctor of Philosophy

December 2017

The dissertation of Delanie J. Losey was reviewed and approved* by the following

Miriam Arak Freedman
Associate Professor of Chemistry
Dissertation Advisor
Chair of Committee

Paul S. Cremer
Professor of Chemistry
J. Lloyd Huck Chair in Natural Sciences

Christine Keating
Professor of Chemistry

Jose D. Fuentes
Professor of Meteorology

Thomas E. Mallouk
Evan Pugh Professor of Chemistry, Biochemistry and Molecular Biology, and Physics
Head of the Department of Chemistry

*Signatures are on file in the Graduate School

ABSTRACT

Aerosol particle morphology can influence the water uptake, heterogeneous chemistry, and optical properties of the particle. This morphology is known to be dependent on the composition of the particle as well as relative humidity. Recent studies have pointed out the importance of pH in aerosol particles. The pH of systems being investigated during phase transition studies have not investigated the role of pH, which could lead to the deprotonation of the organic component and would affect phase transitions. To investigate the influence of high pH and therefore deprotonation on the phase transitions of 3-methylglutaric acid:ammonium sulfate, sodium hydroxide was used to make solutions with pHs below the pK_{a1} , between the pK_{a1} and pK_{a2} , and above pK_{a2} of 3-methylglutaric acid. Using optical microscopy and an environmental chamber, the separation relative humidity (SRH), mixing relative humidity (MRH), efflorescence relative humidity (ERH) and deliquescence relative humidity (DRH) were recorded for each system. As the pH of the system was increased, the SRH decreased. This was attributed to the increased solubility of the organic component in water when it was deprotonated. The ERH also changed to higher values with added sodium hydroxide. The MRH and DRH values, however, remained constant over all pH. A previously unobserved hysteresis was found between SRH and MRH and the atmospheric implications are discussed. The influence of low pH was also explored in a similar manner, but through addition of concentrated sulfuric acid. Stoichiometric amounts of sulfuric acid was added to six different organic:ammonium sulfate systems to change the salt identity to letovicite, $(NH_4)_3H(SO_4)_2$, and ammonium bisulfate, NH_4HSO_4 . An experiment at low pH was also conducted for each system. In every case, the addition of

sulfuric acid led to an overall decrease in SRH, as expected with changing salt identity. Furthermore, at the lowest pH studied the SRH of four of the six systems were so low that phase separation would not occur in atmospherically relevant conditions. Also, phase separation could occur with no inorganic salt present at all. The ERH and DRH for each system also were affected. These results could affect mass transfer and water uptake for systems at low pH, and can be further explored by investigating the role of pH in particle viscosity and submicron aerosol morphology.

Fly ash can undergo aging in the atmosphere through interactions with sulfuric acid and water. These reactions can lead to physical and chemical changes caused by reaction products or chemical leaching. These changes could influence the amount of soluble material on the particle as well as the ability of the particle to nucleate ice. Both of these affect the fly ash particle's ability to serve as a cloud nucleus. The extent of these changes is expected to be linked to the chemical composition of the fly ash so three fly ash types were investigated. The effect of water- and acid-treatment were assessed using X-ray diffraction, attenuated total reflectance infrared spectroscopy, transmission electron microscopy with selected area electron diffraction and energy dispersive spectroscopy, inductively coupled plasma-atomic emission spectroscopy, Brunauer-Emmett-Teller surface area analysis, and immersion freezing. The results show the presence of soluble material on fly ash and indicate that sulfuric-acid treatment has major physical and chemical effects on fly ash. These effects are dependent on composition of the fly ash. Acid-treatment results in gypsum being created and a variety of metals to be leached, and these changes did affect the immersion ice nucleation activity of the samples. Further studies of these effects on deposition mode freezing are expected for the future.

TABLE OF CONTENTS

List of Figures	vii
List of Tables	x
Acknowledgements	xi
Chapter 1: Introduction	1
1.1 Aerosol Particles	1
1.2 Liquid-Liquid Phase Separation	2
1.3 Ice Nucleation	6
1.4 Liquid-Liquid Phase Separation Experimental	9
1.5 Immersion Freezing Experimental	10
1.6 Scope of Dissertation	13
1.7 References	14
Chapter 2: High pH Dependence of Liquid-Liquid Phase Separation in Organic Aerosol	20
2.1 Abstract	20
2.2 Introduction	21
2.3 Experimental	24
2.4 Results/Discussion	26
2.5 Conclusions/Atmospheric Implications	30
2.6 Supporting Information	32
2.7 References	35
Chapter 3: Low pH Dependence of Morphology in Organic Aerosol	39
3.1 Introduction	39
3.2 Experimental	43
3.3 Results/Discussion	45
3.4 Conclusions/Atmospheric Implications	54

3.5 Supporting Information.....	56
3.6 References.....	57
 Chapter 4: Effect of Acidic Processing on Fly Ash.....	62
4.1 Introduction.....	62
4.2 Experimental.....	68
4.3 Results/Discussion.....	70
4.4 Conclusions/Atmospheric Implications.....	84
4.5 References.....	87
 Chapter 5: Conclusions and Future Directions.....	92
5.1 Conclusions.....	92
5.2 Future Directions.....	94
5.3 Outlook.....	96
5.4 References.....	96

LIST OF FIGURES

Figure 1-1. The growth factor of an aerosol particle vs the relative humidity of the surrounding environment with the efflorescence relative humidity (ERH), deliquescence relative humidity (DRH), and separation relative humidity region (SRH) marked.....	3
Figure 1-2: Side-on view of immersion freezing chamber with an image of particles during a freezing experiment.....	11
Figure 1-3: The fraction frozen at each temperature for different samples with the background freezing due to Millipore water (a) and the n_s plot for each sample with the standard deviation.....	13
Figure 2-1: The three possible phase states observed with optical microscopy: a) a homogeneous particle, b) a phase-separated particle, and c) a crystallized particle and the names of each transition between each phase state (see also Ref. 19). The relative humidity at the time of the picture is recorded for each.....	22
Figure 2-2: The phase transitions for a system of 3-methylglutaric acid/ammonium sulfate with no added NaOH (pH 2.37) compared to a system with a small amount of NaOH (pH 3.65).....	27
Figure 2-3: The efflorescence relative humidity (ERH), separation relative humidity (SRH), deliquescence relative humidity (DRH), and mixing relative humidity (MRH) for the 3-methylglutaric acid/ammonium sulfate/sodium hydroxide system as a function of pH.....	28
Figure 3-1: The separation relative humidity (SRH) for the 3-methylglutaric acid/ammonium sulfate system (pH 2.68) with added sulfuric acid (pH 0.35-1.64) or sodium hydroxide (pHs 3.65-6.45) as a function of pH. The average and standard deviations are found by measuring multiple particles over repeated measurements. Note: The system at pH 0.35 does not phase separate, even when held at 0% relative humidity. *Data from Losey 2016.....	46
Figure 3-2: The separation relative humidity for each organic/ammonium sulfate/sulfuric acid system investigated with organic O:C in parenthesis. Note: 3-methylglutaric acid and 2,2-bis(hydroxymethyl)butyric acid exhibit no phase separation at low pH.....	48

Figure 3-3: The efflorescence relative humidity for each organic/ammonium sulfate/sulfuric acid system investigated with organic O:C in parenthesis. Note: 2-methylglutaric acid and 3-methylglutaric acid do not effloresce at low pH.....53

Figure 3-4: The deliquescence relative humidity for the organic/ammonium sulfate/sulfuric acid systems that effloresced with organic O:C in parenthesis. Note: 3,3-dimethylglutaric acid and diethylmalonic acid did not deliquesce by 95% and are therefore not included.....54

Figure 3-5: The separation relative humidities (a), efflorescence relative humidities (b), and deliquescence relative humidities (c) for each system studied plotted against bulk pH. The regions where the ammonium sulfate (AS), letovicite (L), and ammonium bisulfate (AB) are shown. Note: Ammonium bisulfate is expected to be the identity of the inorganic at low pH as well.....57

Figure 4-1: The XRD data for untreated, acid-treated, and water-treated Class C Joppa and Welsh, Class C/F Clifty, and Class F Miami fly ash. Major components, quartz (Q), gypsum (G), and iron oxide (Fe) are marked on each diffraction pattern.....73

Figure 4-2: The ATR-IR data for untreated, acid-treated, and water-treated Class C Joppa and Welsh, Class C/F Clifty, and Class F Miami fly ash.....74

Figure 4-3: Representative TEM images for Class C and C/F fly ash particles (a and b) and acid-treated Class C and C/F fly ash particles (c and d). Insets in a, b, and c are SAED patterns showing crystallinity.....76

Figure 4-4: EDS spectra of the particles shown in Figure 4-4. The untreated samples are shown in a and b and the acid-treated samples are shown in c and d. The labels from Figure 4-4 correspond to the same letter in this figure. The elements are labeled by symbol in each spectrum. EDS peaks from background signals of C, O, and Cu are denoted by *77

Figure 4-5: Representative TEM images for Class F Miami fly ash particles (a and b) and acid-treated Class F Miami fly ash particles (c and d). Insets in a, b, and c are SAED patterns showing crystallinity.....78

Figure 4-6: EDS spectra of the particles shown in Figure 4-5. The untreated samples are shown in a and b and the acid-treated samples are shown in c and d. The labels from Figure 4-5 correspond to the same letter in this figure. The elements are labeled by symbol in each spectrum. EDS peaks from background signals of C, O, and Cu are denoted by *.....79

Figure 4-7: The ICP-AES results for the supernatant collected from the water-treated and acid-treated Class C Joppa and Welsh, Class C/F Clifty, and Class F Miami fly ash samples.....80

Figure 4-8: The fraction frozen for the water-treated and acid-treated (marked with SA) fly ash samples with the background freezing due to Millipore water (a) and the n_s plot for each sample with the standard deviation.....83

LIST OF TABLES

Table 2-1: Phase transition and ionic strength data for each system as well as control studies with 3-methylglutaric acid (3MGA), ammonium sulfate (AS), and sodium sulfate (SS).....	28
Table 2-2: The calculated average number of water molecules per solute molecule for each system with added sodium hydroxide at approximately 87% RH, immediately after the SRH, and immediately before the ERH.....	35
Table 3-1: The name, structure, molecular weight, and O:C of each organic component as well as pH information for each study.....	45
Table 3-2: Separation relative humidity (SRH), efflorescence relative humidity (ERH) and deliquescence relative humidity (DRH) data for each system. Note: For all systems studied, the mixing relative humidity (MRH) was within error of the SRH and is, therefore, not reported.....	49
Table 3-3: The separation relative humidities (%) for each organic component with ammonium bisulfate and each acid control study.....	51
Table 3-4: The efflorescence relative humidities (%) for the acid control studies. There is no observed deliquescence for any of the systems. The charge state of the sulfuric acid is included based on the pH of the bulk solution.....	53
Table 4-1: The composition of the fly ash samples.....	71
Table 4-2: Crystalline fly ash components identified using XRD.....	73
Table 4-3: The BET and onset, end, and 50% frozen part for each fly ash experiment....	81

ACKNOWLEDGEMENTS

I would like to first start by thanking my advisor, Miriam Freedman. Her constant support, guidance, enthusiasm, and confidence in me has been invaluable during my time at Penn State. She gave me the drive to continue working through the ups and downs of research and life in general. I would also like to acknowledge my committee for their suggestions and guidance as well as Jackie Bortiatynski and Kyle Schmidt for seeing my potential as an educator and allowing me to serve a leadership role in teaching undergraduates organic chemistry.

Second, the people that make up the Freedman Research lab have always been there for me to serve as sounding boards when I needed to discuss data or a building plan, to provide much-needed laughter and encouragement, or to be a coffee break buddy. They were always available to read drafts, provide criticism, and give guidance. The people I'd especially like to acknowledge are Dan Veghte, Sarah Sihvonen, Robbie Parker, Valerie Alstadt, Muhammad Altaf, Joseph Dawson, Esther Chong, and Emily Ott. Other group members that helped to enrich my time here at Penn State include Theresa Kucinski, Alex Ucci, and Josh Haines. I would also like to acknowledge Allison Brooks for her work during her Meteorology REU in Summer 2016.

I would simply not be here today without the friendship of people both at Penn State and from undergrad and high school. These include Anne Sendecki, Kate O'Rourke, Katy Dunlap, and Jill Abrell. They have always reminded me to stay humble, relax when I need to, and not to get overwhelmed.

Finally, my family is the most important part of my life and their unwavering encouragement and support have never failed to remind me why I am here. To my parents, Steve and Tricia, my brothers, Avery and Reilly, my sister-in-law Becca, and my sister-cousin Tori, you are my rocks. I would like to acknowledge as well my grandparents who unfortunately could not see me reach with milestone. I know they are here now and always in spirit. Also, to all of my extended family, grandparents, aunts, uncles, and cousins, thank you for supporting me in my pursuits.

Chapter 1

Introduction

1.1 Aerosol Particles

Aerosol particles are classified as any liquid or solid particle found in the atmosphere.¹ They can be emitted directly as particles called primary aerosol or produced through gas-particle reactions in the air, which are called secondary aerosol. Emission sources can be biogenic or anthropogenic in origin such as dust, sea salt, volcanoes, soot, and ash. Organic aerosol is a major component of fine aerosol in continental aerosol and is especially prevalent over forested areas where it can be directly emitted by vegetation.² Once emitted, the organic aerosol can be quickly oxidized through gas-phase reactions to form secondary organic aerosol which is composed of a variety of functionalities including carboxylic acids, alcohols, aldehydes, and esters.²⁻³ Inorganic components of aerosol are more limited and include salts of NH_4^+ , SO_4^{2-} , NO_3^- , Ca^{2+} , K^+ , Mg^{2+} , Na^+ , and Cl^- .^{1, 4} Due to the widespread emission sources of these aerosol types, organic-inorganic aerosol particles are widespread over the globe.⁵⁻⁶

All aerosol particles can have two effects on the atmosphere. Aerosol particles can directly scatter or absorb light, or they can facilitate cloud formation, which can influence the earth's temperature and energy balance by absorbing or reflecting light. Because of these effects, aerosol particles have been long recognized as having an influence on climate change.⁷ The Intergovernmental Panel on Climate Change has declared that aerosols and their precursors can lead to a cooling or a warming effect. The level of uncertainty for this prediction, however, is still high, especially compared to better understood greenhouse gases like carbon dioxide or methane.

1.2 Liquid-liquid Phase Separation

The phase state of aerosol particles directly influences how the particles interact with their environment. The scattering and absorbing behavior of aerosol particles has been found to directly be affected by the morphology and state of these particles.⁸⁻⁹ The phase state also affects the heterogeneous chemistry and water uptake in which the particles take part.¹⁰⁻¹⁷ Because of this, the morphology and phase state of aerosol particles are of particular interest to atmospheric scientists.

Multiple phase states and morphologies are possible for aerosol particles. When a particle is completely solid, the particle is said to be effloresced. Similarly, a liquid particle is deliquesced. Each of these states are commonly accessed through varying the relative humidity of the environment.⁹ Efflorescence occurs at the efflorescence relative humidity (ERH) which occurs when the relative humidity is lowered so much that the particle becomes saturated and crystallizes out of solution (Figure 1-1). The deliquescence relative humidity (DRH) is considered the point when the particle uptakes

water and becomes liquid. Despite these transitions being inverses of one another, a hysteresis is commonly observed between ERH and DRH. This is common for the phase transitions of aqueous inorganic salt particles as well as mixtures of inorganic and organic compounds.^{9, 18-20} For example, ammonium sulfate has an efflorescence relative humidity (ERH) of 35% RH and a deliquescence relative humidity (DRH) of approximately 79.5% RH due to the activation barrier to forming a nucleus.^{9, 19, 21} These two states are dependent of both the particle composition and the ambient relative humidity (RH).^{9, 18, 22-25}

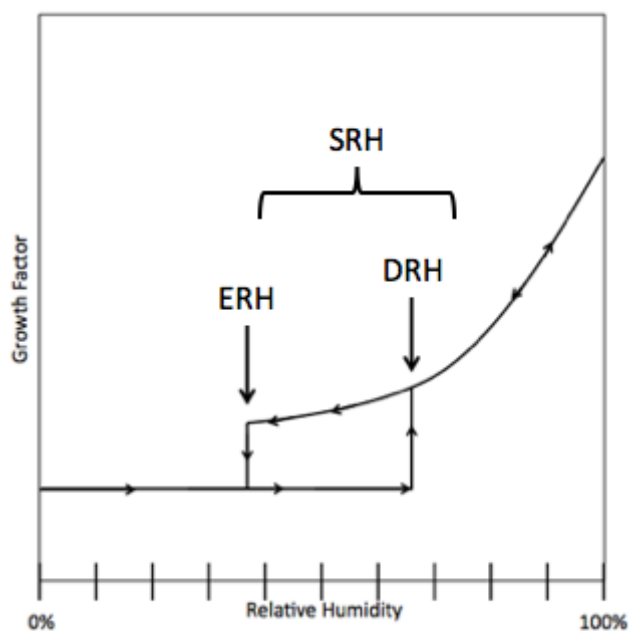


Figure 1-1. The growth factor of an aerosol particle vs the relative humidity of the surrounding environment with the efflorescence relative humidity (ERH), deliquescence relative humidity (DRH), and separation relative humidity region (SRH) marked.

Besides efflorescence and deliquescence, a third possible state is when the particle is separated into two phases. This phase is called liquid-liquid phase separation (LLPS) and is when an organic-inorganic particle separates into an organic-rich and an inorganic rich phase. This transition can occur when the particle is still liquid or upon efflorescence.^{9, 18, 26} As both the organic component and the inorganic salt component become more concentrated at decreasing relative humidity, they are no longer miscible and they form two layers within the particle, an organic-rich and inorganic-rich phase. This point is called the separation relative humidity (SRH) (Figure 1-1). When LLPS occurs, the organic-rich phase is typically on the outside of the particle and the inner phase is an inorganic-rich salt solution.^{20, 25, 27} This is dependent on the surface tensions of the two liquid phases, which lead to the phase with lower surface tension on the outside of the particle.¹⁹ Phase separation has been observed in atmospheric samples and is expected to exist in ambient aerosol.¹⁰

Phase separation not only changes the way that light is scattered or absorbed directly but can influence how the particles interact with gas species and water vapor in the atmosphere.⁸ Phase separation and organic coatings can retard reactive uptake of different gases and water vapor onto aerosol particles.¹⁰⁻¹⁶ In particular, an organic coating in the form of a new phase or surfactants have been shown to decrease the reactive uptake of N_2O_5 which serves as a sink for nitrogen oxides and would lead to increases in NO_x concentrations.^{11-13, 28} When hygroscopic salt particles are coated with secondary organic aerosol formed by the photooxidation of α -pinene, water evaporation rates from these particles is inhibited entirely leading to larger overall particles which in turn affects the optical properties.¹⁴ This can change not only the chemistry that takes

place in the atmosphere, but can dramatically affect how particles can act as cloud condensation nuclei.¹⁷ Phase separation with no salt component is also possible in certain conditions. Studies investigating secondary organic matter resulting from ozonolysis of α -pinene, β -caryophyllene, and limonene and photooxidation of toluene found that at high RH ($> 90\%$) water uptake by water-soluble products results in phase separation.²⁹⁻³⁰ The RH required for this phase transition is much higher than that of most atmospherically relevant cases but is important in cloud condensation nucleus activity.

Predicting if LLPS will occur with certain organic and inorganic systems has been of particular interest for some time.^{20, 26-27, 31-34} Preliminary LLPS studies found that the occurrence of LLPS can be predicted through the use of the O:C ratio within the organic component.^{20, 26} This was determined by combining large arrays of data consisting of one organic compound and one inorganic salt to try to predict the appearance of LLPS. The O:C studies revealed that LLPS was observed for every system with $O:C < 0.5$ and never observed when $O:C > 0.8$.²⁶ For systems with an O:C between 0.5 and 0.8, there was no prevailing reason for their behavior. O:C is particularly useful due to it being a common field measurement for ambient aerosol studies, which have found that in most cases, O:C ranges from 0.2 to 1, making phase separation likely to be present in atmospheric aerosol.^{6, 35-40} The idea behind the O:C ratio is that the ratio can give an idea on how hydrophobic/hydrophilic a compound is. The higher the O:C, the more oxygen there is present in the molecule and the more oxygen present, the more hydrophilic the compound, the harder it is for the compound to salt-out of solution. While O:C is useful for predicting if LLPS may occur, it is not absolute and as atmospheric particles are

complex, many studies have been done to better understand when phase separation occurs and at what SRH can be expected.

Many factors have been shown to affect the presence of phase separation or the location of SRH for different organic-inorganic systems. These include size, the functional groups in the organic component, viscosity, and the identity of the inorganic component.^{27, 32-34} Using cryo-TEM, a size dependence in phase separation has been observed, where particles under a certain threshold diameter are homogeneous unlike their phase-separated, larger counterparts.³³ Song et al. found that in aerosol particles containing mixtures of different organic compounds with different functional groups, such as dicarboxylic acids, aromatic compounds, alcohols, aldehydes, and so on, systems with higher amounts of aromatic compounds, shift the occurrence of phase separation to lower O:C values.²⁷ You et al. explored the effects of viscosity by determining the influence of temperature and organic molecular weight on the SRH.³⁴ They found that only when the viscosity changed drastically at very low temperatures for one of their systems did they see a dependence. The identity of the inorganic component is expected to affect the SRH of different particles based on the Hofmeister Series which organizes ions based on the ability of the ion to salt-out polymers or macromolecules.⁴¹ This has been shown to also affect phase separation in organic-inorganic particles, where salts with high salting-out ability lead to a higher SRH for the system.³²

1.3 Ice Nucleation

The indirect effect of aerosol particles can be observed through the study of cirrus cloud formation. Cirrus clouds are of particular interest due to their ability to impact

climate.^{7, 42-46} Cirrus clouds have the ability to both reflect solar radiation as it enters the atmosphere and absorb the long wave infrared radiation coming from the surface of the earth.⁷ Both of these properties can work against each other to lead to no overall change in global temperature. When cirrus clouds are thin, however, their ability to reflect the light is greatly diminished while their ability to absorb the low energy IR radiation remains present. This in turn leads to a contribution to the global warming rates. They can dehydrate air as it moves through the tropopause into the stratosphere.⁴³⁻⁴⁴ This in turn could affect any water processes such as reactions or cloud formation. They can also serve as sites for heterogeneous reactions that could lead to the destruction of ozone.⁴⁷ As cirrus clouds are made of ice crystals, ice nucleation or the formation of ice crystals in the upper atmosphere is of interest to the scientific community.

Ice can be formed homogeneously or heterogeneously. Homogeneous ice nucleation involves the freezing of pure water droplets at very low temperatures of -40°C.⁴⁸ Heterogeneous ice nucleation, however, is the freezing of water through the use of a foreign substance. Both of these mechanisms are expected to contribute to the formation of cirrus clouds and continue to be heavily studied. While homogeneous ice nucleation has long been thought to be the primary pathway for ice nucleation, recent studies have cast doubt on that mechanism.⁴⁸⁻⁵¹

Heterogeneous nucleation is expected to drastically change the radiative properties of cirrus clouds compared to homogeneous nucleation.⁵² This is due to the sizes of the particles that result from this mechanism.⁵³ Because they can freeze at higher temperatures, they could nucleate before liquid droplets and grow to much larger sizes before homogeneous freezing can initiate.⁵² The surface that enters into the

heterogeneous freezing pathway allows for the water to freeze at higher temperatures closer to 0°C. The ability to nucleate ice at higher temperatures alone, implies that it is more efficient than homogeneous nucleation and can dominate ice nucleation at lower elevations, and in situ studies of cirrus clouds support this. Such studies have found that ice nuclei in certain clouds have a wide range of sizes and low concentrations overall, which is inconsistent with a homogeneous ice nucleation mechanism.^{50, 53}

Heterogeneous ice nucleation can take place through four possible modes.⁵⁴ First, in deposition mode, ice forms directly onto dry, solid particles. In immersion mode, the particle is suspended in a droplet due to previous water uptake and the droplet freezes. Contact freezing is when a particle hits a supercooled droplet initiating freezing, and condensation freezing is when water condenses and then freezes. Each of these freezing modes could occur under different conditions, but immersion freezing will be explored in this dissertation.

DeMott et al. revealed that only a small fraction of the aerosol particles located within a cirrus cloud actually serve as ice nuclei.⁵⁵ This implies that some possible ice nuclei are more efficient at nucleating ice than others. To understand this heterogeneous ice nucleation has been extensively explored to determine what makes a particle a more efficient ice nucleus than another. These studies have investigated, among many other systems, mineral dust, soot, salts, and biological particles as well as the influence of coatings, acidic processing, and viscosity. As a whole, these studies have found many substances that can serve as ice nuclei such as mineral dust, pollen, bacteria, ash, and soot can serve as efficient ice nuclei.⁵⁶ Because these particles are expected to go through aging as they rise to where ice nucleation can occur, the efficiency after acid exposure as

well as after coating with sulfuric acid, ammonium sulfate, and organic compounds is of great interest. Of the studies done thus far on these types of systems, most concluded that the coating or acid exposure led to worse ice nucleation efficiency or no major difference.⁵⁷⁻⁶⁴ Work continues to better understand the surface or chemical properties that make certain ice nuclei better than others.

1.4 Liquid-Liquid Phase Separation Experimental

Aerosol particles are generated in the laboratory from an aqueous solution. A 5 weight percent solution of 1:1 ratio of organic to inorganic in HPLC grade water are first made. Once made, the pH of the solution is recorded. The pH can be changed at this point through addition of acid or base. The solution is then sprayed onto hydrophobically coated slides using a spray bottle and placed inside the environmental chamber located on the microscope stage. To prepare the hydrophobically coated slides, a slide is first cleaned with Alconox solution and then rinsed with ethanol. Once the slides dry, they are cleaned with Rain-X (2 in 1 glass cleaner and repellent). Care is taken to make sure no streaks are on the slide before allowing the slides to dry overnight. Using this method, supermicron particles can be created. Wet and dry nitrogen lines were made by splitting the flow through a dry line and a water bubbler. By adjusting the ratio of nitrogen going through each line, the humidity within the chamber can be controlled precisely. To ensure that the o-rings can keep the chamber sealed and that no pressure buildup occurs in the chamber, a flow of approximately 5 mL/minute is maintained throughout the experiment. The humidity within the chamber is monitored using a Vaisala humidity and temperature probe (HMP 60). The relative humidity (RH) is varied within the chamber from 0 to 95%

in order to observe each phase transition of the particles. The RH is changed with a rate of $\leq 1\%$ /minute. At this rate, the particles are given enough time to equilibrate with the change in RH. ERH, DRH, SRH, and MRH for each system were recorded. Typical experiments start at high relative humidity (90%) until equilibrium is reached, i.e. particle size remains constant, and then decreased to observe the other transitions and subsequently increased to observe DRH. This process can be repeated multiple times with the same slide to ensure reproducibility. Pictures are taken periodically and the RH is recorded for each picture. During a transition period, more pictures are taken to ensure that each event is captured. The pictures are analyzed to determine the RH where each transition occurred for each individual particle so that an average and standard deviation could be determined.

1.5 Immersion Freezing Experimental

To run an immersion freezing experiment, the ideal scenario is to achieve one particle (i.e. nucleus) per droplet. This is attempted by making very low wt% solutions of material in very pure water. Typical wt% values are less than 0.5 wt%, but this can be adjusted depending on how well the material disperses in water. Once the solution is made, it is typically sonicated and then stirred overnight.

Once dispersed and well stirred, 2 μL droplets are added to purchased silanized (hydrophobic) glass slides (Hampton Research, HR3.215). Typical trials contain 30-36 particles. The slide with the particles are then placed inside the chamber on top of the copper block under the camera (Figure 1-2). A low flow line of pre-purified nitrogen is put into the chamber to prevent ice formation on the block and fogging of the glass. The thermocouple is pressed against the copper next to the slide for an accurate reading of

temperature throughout the experiment. The temperature of the copper block is decreased by flowing house nitrogen through a copper coil immersed in liquid nitrogen. To maintain a specific and constant temperature rate, the Styrofoam containing the copper coil and liquid nitrogen is refilled around 7 °C. The flow rate of the nitrogen through the copper coils is determined through cooling trials done previously. As the flow from house may vary or different circumstances change the cooling rate, these cooling trials must be done once a month or whenever the line is moved or changed in any way. The target flow rate is approximately 3 °C/minute.

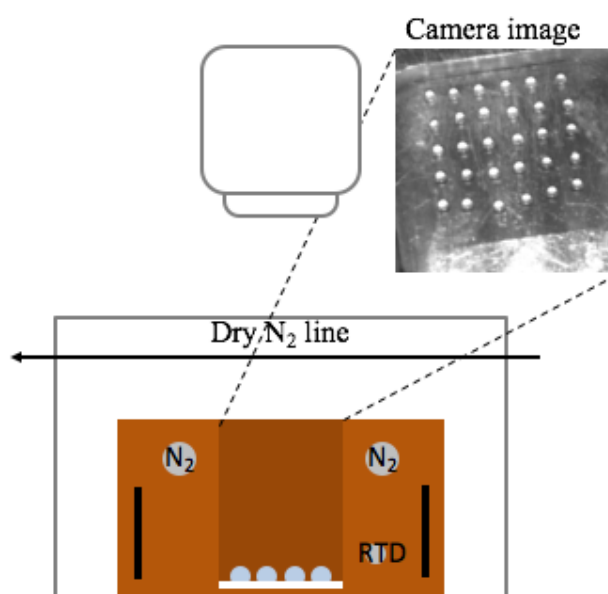


Figure 1-2: Side-on view of immersion freezing chamber with an image of particles during a freezing experiment.

During the course of a typical experiment, a picture of the particles is taken around 2 °C, 0 °C, and then every 0.5 °C until all the particles are frozen. A final picture at -30 °C is taken as well if this value was not reached during the trial. The temperature

rate in °C/minute is recorded. At the end of each trial, the number of particles freezing at each temperature is recorded.

The following calculations are done to analyze the immersion freezing results. The cumulative number of particles frozen at a given temperature ($n(T)$) were recorded to calculate the cumulative fraction of particles frozen (f_{ice}) using the following equation:

$$f_{ice} = \frac{n(T)}{N} \quad (1-1)$$

where N is the total number of particles. In order to rule out background freezing from the Millipore water, freezing experiments were done with pure Millipore water. The combined fraction frozen plots for each sample and the Millipore water are plotted in Figure 1-3a. Using the procedure outlined in O'Sullivan et al., the fraction of particles frozen at a specific temperature, $F(T)$, from each trial was used to calculate $K(T)$, the number of nucleation sites per milliliter water at that temperature for each Millipore and fly ash trial as follows:

$$K(T) = \frac{-\ln(1-F(T))}{V} \times d \quad (1-2)$$

where V is the droplet volume in milliliters and d is the dilution factor.⁶⁵ The average $K(T)$ at each temperature for the Millipore water is then subtracted from the average $K(T)$ calculated for each fly ash experiment. The cumulative number of surface sites per unit area as a function of temperature (n_s) is calculated from the $K(T)$ using the following equation:

$$n_s = K(T) \times C^{-1} \quad (1-3)$$

where C is the total surface area of fly ash in a given volume, which is calculated using the BET surface area and mass percent fly ash in each experiment. The n_s is calculated at each temperature and its standard deviation is calculated using the standard deviation of $K(T)$ over each trial (Figure 1-3b).

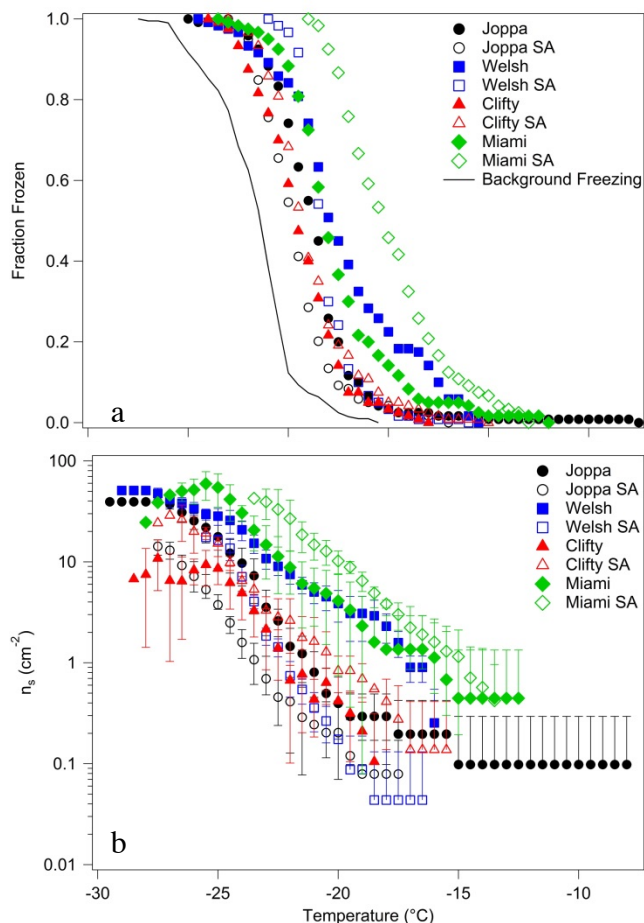


Figure 1-3: The fraction frozen at each temperature for different samples with the background freezing due to Millipore water (a) and the n_s plot for each sample with the standard deviation.

1.6 Scope of Dissertation

This dissertation explores the role of pH in the phase transitions of micron-sized organic-inorganic aerosol particles and the effect of acidic processing on fly ash. Chapter

2 investigates the effect of increased pH on phase transitions of a 3-methylglutaric acid/ammonium sulfate system. Chapter 3 details experiments performed on six different organic compounds at low pH. Chapter 4 shows the effect of sulfuric acid-treatment on different classes of fly ash and explores the change in ice nucleation activity.

1.7 References

1. Seinfeld, J. H.; Pandis, S. N., *Atmospheric Chemistry and Physics: From Air Pollution to Climate Change*. John Wiley & Sons, Inc.: New York, 1998.
2. Kanakidou, M.; Seinfeld, J. H.; Pandis, S. N.; Barnes, I.; Dentener, F. J.; Facchini, M. C.; Van Dingenen, R.; Ervens, B.; Nenes, A.; Nielsen, C. J.; Swietlicki, E.; Putaud, J. P.; Balkanski, Y.; Fuzzi, S.; Horth, J.; Moortgat, G. K.; Winterhalter, R.; Myhre, C. E. L.; Tsigaridis, K.; Vignati, E.; Stephanou, E. G.; Wilson, J. Organic aerosol and global climate modelling: a review. *Atmos. Chem. Phys.* **2005**, 5, 4, 1053-1123.
3. Hallquist, M.; Wenger, J. C.; Baltensperger, U.; Rudich, Y.; Simpson, D.; Claeys, M.; Dommen, J.; Donahue, N. M.; George, C.; Goldstein, A. H.; Hamilton, J. F.; Herrmann, H.; Hoffmann, T.; Iinuma, Y.; Jang, M.; Jenkin, M. E.; Jimenez, J. L.; Kiendler-Scharr, A.; Maenhaut, W.; McFiggans, G.; Mentel, T. F.; Monod, A.; Prévôt, A. S. H.; Seinfeld, J. H.; Surratt, J. D.; Szmigielski, R.; Wildt, J. The formation, properties and impact of secondary organic aerosol: current and emerging issues. *Atmos. Chem. Phys.* **2009**, 9, 14, 5155-5236.
4. Lee, Y. N.; Weber, R.; Ma, Y.; Orsini, D.; Maxwell-Meier, K.; Blake, D.; Meinardi, S.; Sachse, G.; Harward, C.; Chen, T. Y.; Thornton, D.; Tu, F. H.; Bandy, A. Airborne measurement of inorganic ionic components of fine aerosol particles using the particle-into-liquid sampler coupled to ion chromatography technique during ACE-Asia and TRACE-P. *J. Geophys. Res.-Atmos.* **2003**, 108, D23, 1-14.
5. Zhang, Q.; Jimenez, J. L.; Canagaratna, M. R.; Allan, J. D.; Coe, H.; Ulbrich, I.; Alfarra, M. R.; Takami, A.; Middlebrook, A. M.; Sun, Y. L.; Dzepina, K.; Dunlea, E.; Docherty, K.; DeCarlo, P. F.; Salcedo, D.; Onasch, T.; Jayne, J. T.; Miyoshi, T.; Shimojo, A.; Hatakeyama, S.; Takegawa, N.; Kondo, Y.; Schneider, J.; Drewnick, F.; Borrmann, S.; Weimer, S.; Demerjian, K.; Williams, P.; Bower, K.; Bahreini, R.; Cottrell, L.; Griffin, R. J.; Rautiainen, J.; Sun, J. Y.; Zhang, Y. M.; Worsnop, D. R. Ubiquity and dominance of oxygenated species in organic aerosols in anthropogenically-influenced Northern Hemisphere midlatitudes. *Geophys. Res. Lett.* **2007**, 34, 13, 1-6.
6. Chakraborty, A.; Bhattu, D.; Gupta, T.; Tripathi, S. N.; Canagaratna, M. R. Real-time measurements of ambient aerosols in a polluted Indian city: Sources, characteristics, and processing of organic aerosols during foggy and nonfoggy periods. *J. Geophys. Res.-Atmos.* **2015**, 120, 17, 9006-9019.

7. IPCC, 2013: *Summary for Policymakers. In: Climate Change 2013: The Physical Science Basis. Contribution of Working Group I to the Fifth Assessment Report of the Intergovernmental Panel on Climate Change* [Stocker, T.F., D. Qin, G.-K. Plattner, M. Tignor, S.K. Allen, J. Boschung, A. Nauels, Y. Xia, V. Bex and P.M. Midgley (eds.)]. Cambridge University Press, Cambridge, United Kingdom and New York, NY, USA.
8. Freedman, M. A.; Hasenkopf, C. A.; Beaver, M. R.; Tolbert, M. A. Optical Properties of Internally Mixed Aerosol Particles Composed of Dicarboxylic Acids and Ammonium Sulfate. *J. Phys. Chem. A* **2009**, *113*, 48, 13584-13592.
9. Martin, S. T. Phase Transitions of Aqueous Atmospheric Particles. *Chem. Rev.* **2000**, *100*, 9, 3403-3454.
10. You, Y.; Renbaum-Wolff, L.; Carreras-Sospedra, M.; Hanna, S. J.; Hiranuma, N.; Kamal, S.; Smith, M. L.; Zhang, X.; Weber, R. J.; Shilling, J. E.; Dabdub, D.; Martin, S. T.; Bertram, A. K. Images reveal that atmospheric particles can undergo liquid–liquid phase separations. *P. Natl. Acad. Sci. USA*. **2012**, *109*, 33, 13188-13193.
11. Knopf, D. A.; Cosman, L. M.; Mousavi, P.; Mokamati, S.; Bertram, A. K. A Novel Flow Reactor for Studying Reactions on Liquid Surfaces Coated by Organic Monolayers: Methods, Validation, and Initial Results. *J. Phys. Chem. A*. **2007**, *111*, 43, 11021-11032.
12. Cosman, L. M.; Bertram, A. K. Reactive Uptake of N₂O₅ on Aqueous H₂SO₄ Solutions Coated with 1-Component and 2-Component Monolayers. *J. Phys. Chem. A* **2008**, *112*, 20, 4625-4635.
13. Cosman, L. M.; Knopf, D. A.; Bertram, A. K. N₂O₅ Reactive Uptake on Aqueous Sulfuric Acid Solutions Coated with Branched and Straight-Chain Insoluble Organic Surfactants. *J. Phys. Chem. A* **2008**, *112*, 11, 2386-2396.
14. Zelenyuk, A.; Ezell, M. J.; Perraud, V.; Johnson, S. N.; Bruns, E. A.; Yu, Y.; Imre, D.; Alexander, M. L.; Finlayson-Pitts, B. J. Characterization of organic coatings on hygroscopic salt particles and their atmospheric impacts. *Atmos. Environ.* **2010**, *44*, 9, 1209-1218.
15. Davies, J. F.; Miles, R. E. H.; Haddrell, A. E.; Reid, J. P. Influence of organic films on the evaporation and condensation of water in aerosol. *P. Natl. Acad. Sci. USA*. **2013**, *110*, 22, 8807-8812.
16. Hodas, N.; Zuend, A.; Mui, W.; Flagan, R.; Seinfeld, J. Influence of particle-phase state on the hygroscopic behavior of mixed organic–inorganic aerosols. *Atmos. Chem. Phys.* **2015**, *15*, 9, 5027-5045.
17. Petters, M. D.; Kreidenweis, S. M. A single parameter representation of hygroscopic growth and cloud condensation nucleus activity. *Atmos. Chem. Phys.* **2007**, *7*, 8, 1961-1971.
18. Choi, M. Y.; Chan, C. K. The Effects of Organic Species on the Hygroscopic Behaviors of Inorganic Aerosols. *Environ. Sci. Technol.* **2002**, *36*, 11, 2422-2428.
19. Ciobanu, V. G.; Marcolli, C.; Krieger, U. K.; Weers, U.; Peter, T. Liquid–Liquid Phase Separation in Mixed Organic/Inorganic Aerosol Particles. *J. Phys. Chem. A*. **2009**, *113*, 41, 10966-10978.
20. Bertram, A. K.; Martin, S. T.; Hanna, S. J.; Smith, M. L.; Bodsworth, A.; Chen, Q.; Kuwata, M.; Liu, A.; You, Y.; Zorn, S. R. Predicting the relative humidities of

- liquid-liquid phase separation, efflorescence, and deliquescence of mixed particles of ammonium sulfate, organic material, and water using the organic-to-sulfate mass ratio of the particle and the oxygen-to-carbon elemental ratio of the organic component. *Atmos. Chem. Phys.* **2011**, *11*, 21, 10995-11006.
21. Stewart, D. J.; Cai, C.; Naylor, J.; Preston, T. C.; Reid, J. P.; Krieger, U. K.; Marcolli, C.; Zhang, Y. H. Liquid-Liquid Phase Separation in Mixed Organic/Inorganic Single Aqueous Aerosol Droplets. *J. Phys. Chem. A* **2015**, *119*, 18, 4177-4190.
 22. Marcolli, C.; Luo, B.; Peter, T. Mixing of the Organic Aerosol Fractions: Liquids as the Thermodynamically Stable Phases. *J. Phys. Chem. A* **2004**, *108*, 12, 2216-2224.
 23. Parsons, M. T.; Mak, J.; Lipetz, S. R.; Bertram, A. K. Deliquescence of malonic, succinic, glutaric, and adipic acid particles. *J. Geophys. Res.* **2004**, *109*, D6, 1-8.
 24. Parsons, M. T.; Riffell, J. L.; Bertram, A. K. Crystallization of Aqueous Inorganic-Malonic Acid Particles: Nucleation Rates, Dependence on Size, and Dependence on the Ammonium-to-Sulfate Ratio. *J. Phys. Chem. A* **2006**, *110*, 26, 8108-8115.
 25. Song, M.; Marcolli, C.; Krieger, U. K.; Lienhard, D. M.; Peter, T. Morphologies of mixed organic/inorganic/aqueous aerosol droplets. *Faraday Discuss.* **2013**, *165*, 289-316.
 26. You, Y.; Smith, M. L.; Song, M.; Martin, S. T.; Bertram, A. K. Liquid-liquid phase separation in atmospherically relevant particles consisting of organic species and inorganic salts. *Int. Rev. Phys. Chem.* **2014**, *33*, 1, 43-77.
 27. Song, M.; Marcolli, C.; Krieger, U. K.; Zuend, A.; Peter, T. Liquid-liquid phase separation in aerosol particles: Dependence on O:C, organic functionalities, and compositional complexity. *Geophys. Res. Lett.* **2012**, *39*, 19, 1-5.
 28. Dentener, F. J.; Crutzen, P. J. Reaction of N₂O₅ on tropospheric aerosols: Impact on the global distributions of NO_x, O₃, and OH. *J. Geophys. Res. Atmos.* **1993**, *98*, D4, 7149-7163.
 29. Renbaum-Wolff, L.; Song, M.; Marcolli, C.; Zhang, Y.; Liu, P. F.; Grayson, J. W.; Geiger, F. M.; Martin, S. T.; Bertram, A. K. Observations and implications of liquid-liquid phase separation at high relative humidities in secondary organic material produced by α -pinene ozonolysis without inorganic salts. *Atmos. Chem. Phys.* **2016**, *16*, 12, 7969-7979.
 30. Song, M.; Liu, P.; Martin, S. T.; Bertram, A. K. Liquid-liquid phase separation in particles containing secondary organic material free of inorganic salts. *Atmos. Chem. Phys. Discuss.* **2017**, *2017*, 1-29.
 31. Song, M.; Marcolli, C.; Krieger, U. K.; Zuend, A.; Peter, T. Liquid-liquid phase separation and morphology of internally mixed dicarboxylic acids/ammonium sulfate/water particles. *Atmos. Chem. Phys.* **2012**, *12*, 5, 2691-2712.
 32. You, Y.; Renbaum-Wolff, L.; Bertram, A. K. Liquid-liquid phase separation in particles containing organics mixed with ammonium sulfate, ammonium bisulfate, ammonium nitrate or sodium chloride. *Atmos. Chem. Phys.* **2013**, *13*, 23, 11723-11734.
 33. Veghte, D. P.; Altaf, M. B.; Freedman, M. A. Size Dependence of the Structure of Organic Aerosol. *J. Am. Chem. Soc.* **2013**, *135*, 43, 16046-16049.

34. You, Y.; Bertram, A. K. Effects of molecular weight and temperature on liquid–liquid phase separation in particles containing organic species and inorganic salts. *Atmos. Chem. Phys.* **2015**, *15*, 3, 1351–1365.
35. Aiken, A. C.; DeCarlo, P. F.; Kroll, J. H.; Worsnop, D. R.; Huffman, J. A.; Docherty, K. S.; Ulbrich, I. M.; Mohr, C.; Kimmel, J. R.; Sueper, D.; Sun, Y.; Zhang, Q.; Trimborn, A.; Northway, M.; Ziemann, P. J.; Canagaratna, M. R.; Onasch, T. B.; Alfarra, M. R.; Prevot, A. S. H.; Dommen, J.; Duplissy, J.; Metzger, A.; Baltensperger, U.; Jimenez, J. L. O/C and OM/OC Ratios of Primary, Secondary, and Ambient Organic Aerosols with High-Resolution Time-of-Flight Aerosol Mass Spectrometry. *Environ. Sci. Technol.* **2008**, *42*, 12, 4478–4485.
36. Jimenez, J. L.; Canagaratna, M. R.; Donahue, N. M.; Prevot, A. S. H.; Zhang, Q.; Kroll, J. H.; DeCarlo, P. F.; Allan, J. D.; Coe, H.; Ng, N. L.; Aiken, A. C.; Docherty, K. S.; Ulbrich, I. M.; Grieshop, A. P.; Robinson, A. L.; Duplissy, J.; Smith, J. D.; Wilson, K. R.; Lanz, V. A.; Hueglin, C.; Sun, Y. L.; Tian, J.; Laaksonen, A.; Raatikainen, T.; Rautiainen, J.; Vaattovaara, P.; Ehn, M.; Kulmala, M.; Tomlinson, J. M.; Collins, D. R.; Cubison, M. J.; Dunlea, J.; Huffman, J. A.; Onasch, T. B.; Alfarra, M. R.; Williams, P. I.; Bower, K.; Kondo, Y.; Schneider, J.; Drewnick, F.; Borrmann, S.; Weimer, S.; Demerjian, K.; Salcedo, D.; Cottrell, L.; Griffin, R.; Takami, A.; Miyoshi, T.; Hatakeyama, S.; Shimono, A.; Sun, J. Y.; Zhang, Y. M.; Dzepina, K.; Kimmel, J. R.; Sueper, D.; Jayne, J. T.; Herndon, S. C.; Trimborn, A. M.; Williams, L. R.; Wood, E. C.; Middlebrook, A. M.; Kolb, C. E.; Baltensperger, U.; Worsnop, D. R. Evolution of Organic Aerosols in the Atmosphere. *Science* **2009**, *326*, 5959, 1525–1529.
37. Ng, N. L.; Canagaratna, M. R.; Zhang, Q.; Jimenez, J. L.; Tian, J.; Ulbrich, I. M.; Kroll, J. H.; Docherty, K. S.; Chhabra, P. S.; Bahreini, R.; Murphy, S. M.; Seinfeld, J. H.; Hildebrandt, L.; Donahue, N. M.; DeCarlo, P. F.; Lanz, V. A.; Prévôt, A. S. H.; Dinar, E.; Rudich, Y.; Worsnop, D. R. Organic aerosol components observed in Northern Hemispheric datasets from Aerosol Mass Spectrometry. *Atmos. Chem. Phys.* **2010**, *10*, 10, 4625–4641.
38. Canagaratna, M. R.; Jimenez, J. L.; Kroll, J. H.; Chen, Q.; Kessler, S. H.; Massoli, P.; Hildebrandt Ruiz, L.; Fortner, E.; Williams, L. R.; Wilson, K. R.; Surratt, J. D.; Donahue, N. M.; Jayne, J. T.; Worsnop, D. R. Elemental ratio measurements of organic compounds using aerosol mass spectrometry: characterization, improved calibration, and implications. *Atmos. Chem. Phys.* **2015**, *15*, 1, 253–272.
39. Choi, J. H.; Ryu, J.; Jeon, S.; Seo, J.; Yang, Y.-H.; Pack, S. P.; Choung, S.; Jang, K.-S. In-depth compositional analysis of water-soluble and -insoluble organic substances in fine (PM_{2.5}) airborne particles using ultra-high-resolution 15T FT-ICR MS and GC×GC-TOFMS. *Environ. Pollut.* **2017**, *225*, Supplement C, 329–337.
40. Xue, J.; Li, Y.; Xie, X.; Xiong, C.; Liu, H.; Chen, S.; Nie, Z.; Chen, C.; Zhao, J. Characterization of organic aerosol in Beijing by laser desorption ionization coupled with Fourier Transform Ion Cyclotron Resonance Mass spectrometry. *Atmos. Environ.* **2017**, *159*, Supplement C, 55–65.
41. Zhang, Y.; Cremer, P. S. Interactions between macromolecules and ions: the Hofmeister series. *Curr. Opin. Chem. Biol.* **2006**, *10*, 6, 658–663.

42. Chen, T.; Rossow, W. B.; Zhang, Y. Radiative Effects of Cloud-Type Variations. *J. Climate*. **2000**, *13*, 1, 264-286.
43. Luo, B. P.; Peter, T.; Fueglistaler, S.; Wernli, H.; Wirth, M.; Kiemle, C.; Flentje, H.; Yushkov, V. A.; Khattatov, V.; Rudakov, V.; Thomas, A.; Borrmann, S.; Toci, G.; Mazzinghi, P.; Beuermann, J.; Schiller, C.; Cairo, F.; Di Donfrancesco, G.; Adriani, A.; Volk, C. M.; Strom, J.; Noone, K.; Mitev, V.; MacKenzie, R. A.; Carslaw, K. S.; Trautmann, T.; Santacesaria, V.; Stefanutti, L. Dehydration potential of ultrathin clouds at the tropical tropopause. *Geophys. Res. Lett.* **2003**, *30*, 11, 1-4.
44. Jensen, E.; Pfister, L. Transport and freeze-drying in the tropical tropopause layer. *J. Geophys. Res.-Atmos.* **2004**, *109*, D2, 1-16.
45. Mitchell, D. L.; Rasch, P.; Ivanova, D.; McFarquhar, G.; Nousiainen, T. Impact of small ice crystal assumptions on ice sedimentation rates in cirrus clouds and GCM simulations. *Geophys. Res. Lett.* **2008**, *35*, 9, 1-5.
46. Fueglistaler, S.; Dessler, A. E.; Dunkerton, T. J.; Folkins, I.; Fu, Q.; Mote, P. W. Tropical tropopause layer. *Rev. Geophys.* **2009**, *47*, 1, 1-31.
47. Borrmann, S.; Solomon, S.; Dye, J. E.; Luo, B. The potential of cirrus clouds for heterogeneous chlorine activation. *Geophys. Res. Lett.* **1996**, *23*, 16, 2133-2136.
48. Vali, G. Ice nucleation—A review. *Nucleation and atmospheric aerosols* **1996**, 271-279.
49. Haag, W.; Kärcher, B. The impact of aerosols and gravity waves on cirrus clouds at midlatitudes. *J. Geophys. Res.-Atmos.* **2004**, *109*, D12, 1-18.
50. Froyd, K. D.; Murphy, D. M.; Lawson, P.; Baumgardner, D.; Herman, R. L. Aerosols that form subvisible cirrus at the tropical tropopause. *Atmos. Chem. Phys.* **2010**, *10*, 1, 209-218.
51. Cziczo, D. J.; Froyd, K. D.; Hoose, C.; Jensen, E. J.; Diao, M.; Zondlo, M. A.; Smith, J. B.; Twohy, C. H.; Murphy, D. M. Clarifying the Dominant Sources and Mechanisms of Cirrus Cloud Formation. *Science* **2013**, *340*, 6138, 1320-1324.
52. Cantrell, W.; Heymsfield, A. Production of Ice in Tropospheric Clouds: A Review. *Bull. Amer. Meteor. Soc.* **2005**, *86*, 6, 795-807.
53. DeMott, P. J.; Rogers, D. C.; Kreidenweis, S. M.; Chen, Y.; Twohy, C. H.; Baumgardner, D.; Heymsfield, A. J.; Chan, K. R. The role of heterogeneous freezing nucleation in upper tropospheric clouds: Inferences from SUCCESS. *Geophys. Res. Lett.* **1998**, *25*, 9, 1387-1390.
54. Murray, B.; O'Sullivan, D.; Atkinson, J.; Webb, M. Ice nucleation by particles immersed in supercooled cloud droplets. *Chem. Soc. Rev.* **2012**, *41*, 19, 6519-6554.
55. DeMott, P. J.; Prenni, A. J.; Liu, X.; Kreidenweis, S. M.; Petters, M. D.; Twohy, C. H.; Richardson, M. S.; Eidhammer, T.; Rogers, D. C. Predicting global atmospheric ice nuclei distributions and their impacts on climate. *Proc. Natl. Acad. Sci. U.S.A.* **2010**, *107*, 25, 11217-11222.
56. Murray, B.; O'Sullivan, D.; Atkinson, J.; Webb, M. Ice nucleation by particles immersed in supercooled cloud droplets. *Chem. Soc. Rev.* **2012**, *41*, 19, 6519-6554.

57. Eastwood, M. L.; Cremel, S.; Wheeler, M.; Murray, B. J.; Girard, E.; Bertram, A. K. Effects of sulfuric acid and ammonium sulfate coatings on the ice nucleation properties of kaolinite particles. *Geophys. Res. Lett.* **2009**, *36*, 2, 1-5.
58. Cziczo, D. J.; Froyd, K. D.; Gallavardin, S. J.; Moehler, O.; Benz, S.; Saathoff, H.; Murphy, D. M. Deactivation of ice nuclei due to atmospherically relevant surface coatings. *Environ. Res. Lett.* **2009**, *4*, 4, 044013.
59. Sullivan, R.; Petters, M.; DeMott, P.; Kreidenweis, S.; Wex, H.; Niedermeier, D.; Hartmann, S.; Clauss, T.; Stratmann, F.; Reitz, P. Irreversible loss of ice nucleation active sites in mineral dust particles caused by sulphuric acid condensation. *Atmos. Chem. Phys.* **2010**, *10*, 23, 11471-11487.
60. Chernoff, D. I.; Bertram, A. K. Effects of sulfate coatings on the ice nucleation properties of a biological ice nucleus and several types of minerals. *J. Geophys. Res.-Atmos.* **2010**, *115*, D20, 1-12.
61. Niedermeier, D.; Hartmann, S.; Shaw, R.; Covert, D.; Mentel, T.; Schneider, J.; Poulain, L.; Reitz, P.; Spindler, C.; Clauss, T. Heterogeneous freezing of droplets with immersed mineral dust particles—measurements and parameterization. *Atmos. Chem. Phys.* **2010**, *10*, 8, 3601-3614.
62. Yang, Z.; Bertram, A. K.; Chou, K. C. Why Do Sulfuric Acid Coatings Influence the Ice Nucleation Properties of Mineral Dust Particles in the Atmosphere? *J. Phys. Chem. Lett.* **2011**, *2*, 11, 1232-1236.
63. Tobo, Y.; DeMott, P. J.; Raddatz, M.; Niedermeier, D.; Hartmann, S.; Kreidenweis, S. M.; Stratmann, F.; Wex, H. Impacts of chemical reactivity on ice nucleation of kaolinite particles: A case study of levoglucosan and sulfuric acid. *Geophys. Res. Lett.* **2012**, *39*, 19, 1-5.
64. Sihvonon, S. K.; Schill, G. P.; Lykтей, N. A.; Veghte, D. P.; Tolbert, M. A.; Freedman, M. A. Chemical and Physical Transformations of Aluminosilicate Clay Minerals Due to Acid Treatment and Consequences for Heterogeneous Ice Nucleation. *J. Phys. Chem. A* **2014**, *118*, 38, 8787-8796.
65. O'Sullivan, D.; Murray, B. J.; Ross, J. F.; Whale, T. F.; Price, H. C.; Atkinson, J. D.; Umo, N. S.; Webb, M. E. The relevance of nanoscale biological fragments for ice nucleation in clouds. *Sci. Rep.-UK* **2015**, *5*, 8082.

Chapter 2

High pH Dependence of Liquid-Liquid Phase Separation in Organic Aerosol

Reprinted with permission from: Losey, D. J.; Parker, R. G.; Freedman, M. A., pH Dependence of Liquid–Liquid Phase Separation in Organic Aerosol. *J. Phys. Chem. Lett.* **2016**, 7, 19, 3861-3865. Copyright 2017 American Chemical Society

Author Contributions: Losey collected and analyzed all data and is primary author. Parker served in discussions and editing.

2.1 Abstract

Atmospheric aerosol particles influence climate through their direct and indirect effects. These impacts depend in part on the morphology of the particles, which is determined by their composition. The effect of pH on morphology was investigated using particles composed of 3-methylglutaric acid and ammonium sulfate by manipulating the starting pH of the bulk solution through the addition of aqueous sodium hydroxide. Efflorescence, deliquescence, phase separation, and mixing transitions were observed with optical microscopy. Due to changes in its protonation states, the solubility of the

organic component increases with increasing pH, which shifts the location of the separation relative humidity (SRH) from 78.7% for the fully protonated acid to 63.9% for the fully deprotonated acid. Surprisingly, this shift in the SRH leads to a hysteresis between the SRH and the mixing relative humidity (MRH). Particle pH has the greatest effect on phase transitions that require nucleus formation, i.e. efflorescence and SRH.

2.2 Introduction

Aerosol particles can directly influence climate through the scattering and absorption of light or indirectly as cloud condensation nuclei, ice nuclei, and participants in heterogeneous chemistry. The chemical and physical properties of aerosol particles that control their effects on climate stem in part from the particle phase state, which depends on the relative humidity and composition (Figure 2-1).¹⁻⁴ In the aqueous state, particularly, high concentrations of salt can result in reduced organic solubility, leading to liquid-liquid phase separation (LLPS).^{1, 5} LLPS is of particular interest to the atmospheric community because organic coatings can affect heterogeneous chemistry and therefore atmospheric composition,⁶⁻¹¹ as well as altering water evaporation and condensation rates of aerosol particles.¹²⁻¹⁴ One phenomenon that governs the phase state of aerosol particles is the presence or absence of a hysteresis between inverse transitions. Hysteresis is commonly observed for the phase transitions of aqueous inorganic salt particles as well as mixtures of inorganic and organic compounds.^{1, 15-17} For example, ammonium sulfate has an efflorescence relative humidity (ERH) of 35% RH and a deliquescence relative humidity (DRH) of approximately 79.5% RH due to the activation barrier to forming a nucleus.^{1, 15, 18} This activation barrier is also theorized to be present in phase separation processes that occur through a nucleation and growth mechanism,^{1, 19} but a hysteresis has

not been previously observed between the separation relative humidity (SRH) and the mixing relative humidity (MRH), where the two liquid phases mix into one phase.^{1-2, 18}

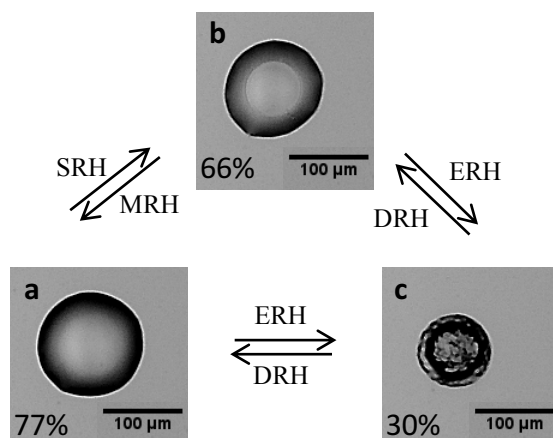


Figure 2-1: The three possible phase states observed with optical microscopy: a) a homogeneous particle, b) a phase-separated particle, and c) a crystallized particle and the names of each transition between each phase state (see also Ref. 5). The relative humidity at the time of the picture is recorded for each.

The pH of aerosol particles varies depending on the composition, location, season, and size of the particles studied.²⁰⁻²⁴ Aerosol particle pH has been estimated to be as high as 7-9 for coarse-mode freshly emitted sea spray aerosol, but most studies find a much lower pH.²⁰ Studies of fine aerosol during the Southern Oxidant and Aerosol Study (SOAS), Southeastern Center for Air Pollution and Epidemiology (SCAPE), and the Wintertime Investigation of Transport, Emissions, and Reactivity (WINTER) campaigns have identified pH values as low as -0.51 and up to 3.1 depending on the season and location.^{22, 24} Attempts to track pH directly in particles have only been performed twice before. Raman spectroscopy was used to probe the sulfate and bisulfate stretches in inorganic particles composed of sulfuric acid and magnesium sulfate over the course of a humidity cycle, and a fluorescent pH dye was used to probe the organic phase of an organic-inorganic particle.²⁵⁻²⁶ These showed that the pH of the particle varied by less

than one pH unit over the course of an experiment. This low variability of pH over the course of an RH cycling experiment would not generally affect the protonation state of the organic compound. Because the protonation state of the organic acid could only vary under atmospherically relevant conditions, however, we have altered the pH of the bulk solution from which the aerosol particles are generated in order to investigate the effect of the protonation state of the organic acid on aerosol phase transitions.

The acidity of particles has been shown to influence the reactive uptake of certain gases in the atmosphere, the solar absorption of bound nitrophenols on aerosol surfaces, and the heterogeneous reactions of gaseous isoprene, α -pinene, and primary organic aerosol.^{21, 27-32} While the effects of particle acidity on these processes have been documented,^{28, 33-34} the effect of pH on phase transitions of the particle itself have yet to be explored. Carboxylic acids, which can be directly emitted from combustion sources or more commonly produced by oxidation of olefins in the atmosphere, make up about 25% of nonmethane hydrocarbons.³⁵⁻³⁶ The protonation state, and consequently solubility, of these organic acids varies as a function of pH, where dicarboxylic acids are more soluble at higher pH, when they are more deprotonated.³⁷ The solubility of the organic component of a system directly impacts the propensity for salting out (i.e. the solubility of the organic compound impacts the salt concentration at which the organic component becomes insoluble in aqueous solution). The solubility of the organic component can be quantified using the Setchenov equation as follows:

$$\log(s_0/s) = kc_s \quad (2-1)$$

where s_0 and s are the solubilities of the organic component in water and in the ionic solution, c_s is the concentration of salt in the ionic solution, and k is the Setchenov

constant.³⁸⁻³⁹ This phenomenon has been explored in polymer systems that contain carboxylic acids by probing the lower critical solution temperature (LCST), the temperature above which the system is phase separated. At values of pH above the pK_a of the carboxylic acid groups, the LCST occurs at higher temperatures due to the increase in solubility attributed to the deprotonation of the acidic groups.⁴⁰⁻⁴¹ These differences in solubility could potentially change the position of phase transitions for systems relevant to organic aerosol.

In this paper, the effect of pH is examined using particles composed of 3-methylglutaric acid ($pK_{a1} = 4.24$, $pK_{a2} = 5.41$) and ammonium sulfate. The starting pH of the solution is manipulated through dropwise addition of aqueous sodium hydroxide. To probe the effect of the solubility of the organic compound at each protonation state of 3-methylglutaric acid, the target pH values are located below pK_{a1} , above pK_{a2} , and between both pK_a s of 3-methylglutaric acid. The relative humidities at which the phase transitions, ERH, DRH, SRH, and MRH, occur are observed with optical microscopy. To study the effect of each protonation state of 3-methylglutaric acid on the phase transitions, the pH values used are higher than may commonly be present in atmospheric aerosol particles. The effects on the phase transitions, however, may be relevant for other atmospherically relevant organic acids with lower pK_a s.

2.3 Experimental Methods

Aerosol particles containing 3-methylglutaric acid (Alfa Aesar, 95% purity) and ammonium sulfate (EMD, GR ACS) were generated in the laboratory from an aqueous solution. A 5.0 wt.% solution of 3-methylglutaric acid and ammonium sulfate in a 1:1 ratio by mass was made in ultrapure water (HPLC grade, Fisher). The pH of the solution

was adjusted using aqueous NaOH (5.29 M) until the desired pH was achieved (3.65, 5.17, and 6.45). Control studies were performed with aqueous solutions of 5.0 wt.% 3-methylglutaric acid/ammonium sulfate in a 1:1 ratio by mass without NaOH, 2.5 wt.% ammonium sulfate or 3-methylglutaric acid with NaOH added (pH 7.27 and 6.11, respectively), and 5 wt.% 3-methylglutaric acid. Sodium hydroxide, a strong base, is used to modify the pH of the bulk solution in order to use a minimum amount of base to change the pH. In contrast, use of a weak base would have a more significant impact on the composition of the solution. High ionic strength solutions were made using the 1:1 by mass 3-methylglutaric acid:ammonium sulfate solution and then adding additional sodium sulfate or ammonium sulfate to achieve high ionic strength. Each solution was then sprayed onto slides coated with a commercial silanizing agent, which results in a hydrophobic surface, to produce supermicron particles. This method results in a distribution of particle sizes with minimal variation in pH (< 0.5 units). These small changes in pH are not sufficient to change the protonation state of the organic acid as long as the solution is not near the pK_a . The RH in the laboratory is not controlled, but the particles remain aqueous during the transfer to the environmental chamber. The particles are placed inside an environmental chamber on a microscope stage. Precisely adjusting the ratio of wet and dry nitrogen that flows through the chamber controls the relative humidity within, which was measured using a Vaisala humidity and temperature probe (HMP 60). The probe is calibrated using saturated salt solutions of known equilibrium relative humidity: potassium hydroxide (9%), sodium chloride (75%), and ammonium sulfate (81%); and further checked for accuracy by verifying that the ERH and DRH of ammonium sulfate particles are located at 35% and 79.5%, respectively.^{15, 42}

The relative humidity (RH) was varied within the chamber from 0 to 95% in order to observe each phase transition of the particles. The RH was changed at a rate of $\leq 1\%/min$, which allows the particles enough time to equilibrate with the change in RH. ERH, DRH, SRH, and MRH for each system were recorded by cycling the RH from high to low values and then back up to high values.

2.4 Results and Discussion

The effect of sodium hydroxide on the phase transitions of 3-methylglutaric acid and ammonium sulfate was first quantified (Figure 2-2). The efflorescence relative humidity (ERH) is unchanged with the addition of base, but each of the other phase transitions are affected. Even with a small change in pH, 2.37 to 3.65, the SRH changes to a higher value, 72.9% to 78.7% (Figure 2-2, Table 2-1). The MRH for each system matches the SRH for the same system resulting in no hysteresis between the transitions. The deliquescence relative humidity (DRH) decreases with the addition of sodium hydroxide from 81.0% to 74.3%. We would expect that the systems with and without sodium hydroxide would have different positions of at least some of their phase transitions due to the difference in composition. Below, we only consider the system with the added base in order to compare the behavior of particles with the same constituents and different values of the bulk pH.

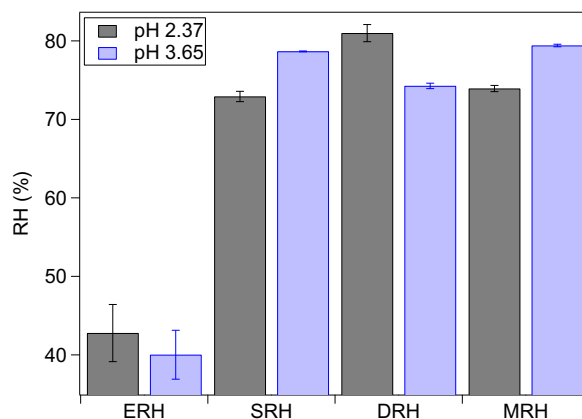


Figure 2-2: The phase transitions for a system of 3-methylglutaric acid/ammonium sulfate with no added NaOH (pH 2.37) compared to a system with a small amount of NaOH (pH 3.65).

As demonstrated in Figure 2-3 and Table 2-1, SRH has a strong dependence on the pH, decreasing 14.8% over the different pH values studied. With the addition of sodium hydroxide, the pH of the system rises and 3-methylglutaric acid becomes more deprotonated. Once deprotonated, the organic component becomes charged and can interact with the salt (i.e. ammonium sulfate) and water through ion-ion and ion-dipole interactions, respectively, leading to an increase in solubility. These interactions prevent the salting-out of the organic component at high relative humidity. These ion-ion and ion-dipole interactions can persist until efflorescence due to the high ratio of water molecules to solute molecules that remains in the particle bulk even immediately prior to ERH, where the number of water molecules to solute molecules is approximately 50:1 at the two higher pH values (Table 2-2). This high ratio implies that the deprotonated state of the organic component continues through phase separation to immediately before efflorescence. This change in SRH is independent of ionic strength and the addition of sodium into the system. When excess ammonium sulfate or sodium sulfate is added to the system to achieve high ionic strength, the SRH rises rather than decreases (Table 2-1). Note that the ionic strength of ambient particles may be greater than in this study.

Bertram et al. have shown that SRH is not influenced by the organic:sulfate ratio and ERH and DRH have only minimal dependence on this ratio.¹⁷

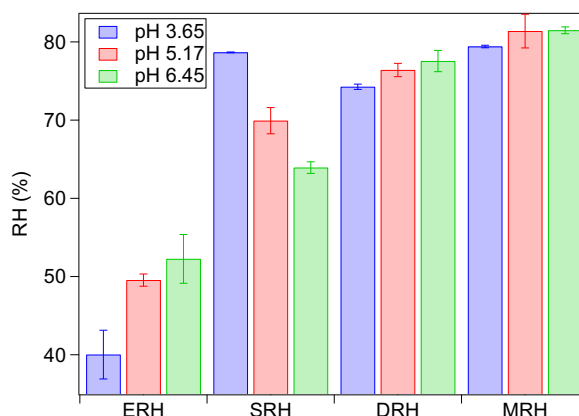


Figure 2-3: The efflorescence relative humidity (ERH), separation relative humidity (SRH), deliquescence relative humidity (DRH), and mixing relative humidity (MRH) for the 3-methylglutaric acid/ammonium sulfate/sodium hydroxide system as a function of pH.

Table 2-1: Phase transition and ionic strength data for each system as well as control studies with 3-methylglutaric acid (3MGA), ammonium sulfate (AS), and sodium sulfate (SS).

System	pH	Ionic Strength (M)	ERH (%)	SRH (%)	DRH (%)	MRH (%)
3MGA/AS/NaOH	3.65	0.60	40.0 ± 3.1	78.7 ± 0.1	74.3 ± 0.3	79.4 ± 0.2
3MGA/AS/NaOH	5.17	1.02	49.6 ± 0.8	69.9 ± 1.7	76.4 ± 0.9	81.4 ± 2.2
3MGA/AS/NaOH	6.45	1.05	52.3 ± 3.1	63.9 ± 0.7	77.6 ± 1.4	81.5 ± 0.4
Control Studies						
3MGA/AS	2.37	0.50	42.8 ± 3.6	72.9 ± 0.7	81.0 ± 1.1	73.9 ± 0.4
AS/NaOH	7.27	2.27	38.1 ± 1.6	---	79.6 ± 2.6	---
3MGA/NaOH	6.11	0.34	53.3 ± 3.0	---	71.1 ± 1.4	---
3MGA	2.15	0.00	---	---	---	---
3MGA/AS/SS	2.69	1.09	49.8 ± 1.2	82.1 ± 3.0	74.1 ± 0.2	85.7 ± 0.9
3MGA/AS	2.89	1.09	40.0 ± 3.5	76.6 ± 0.8	79.5 ± 0.4	77.6 ± 0.4

The ERH increases at higher pH (Figure 2-3, Table 2-1). At pH 3.65, the ERH is the same as that of ammonium sulfate within experimental error,¹⁵ but at pH 5.17, it rises to 49.6% and subsequently to 52.3% at pH 6.45. This change is most likely due to the change in protonation state of the 3-methylglutaric acid because the system without added NaOH matches the pH 3.65 results (Figure 2-2, Table 2-1). To confirm this, control studies of each component and sodium hydroxide were performed. According to Table 1, at high pH, ammonium sulfate/NaOH and 3-methylglutaric acid/NaOH have ERH values of 38.1% and 53.3%, respectively. As a result, we hypothesize that the ERH at the higher pH values is controlled by the crystallization of the organic component, perhaps in the form of a carboxylate salt. Choi and Chan have previously hypothesized that the organic component crystallizes first at an RH of 48.3% for succinic acid/ammonium sulfate, with the ammonium sulfate then crystallizing heterogeneously on the succinic acid seed crystal at this higher RH.¹⁶

The pH of the system as well as ionic strength was found to have little effect on the locations of the deliquescence and mixing transitions (Figure 2-3, Table 2-1). The DRH values for each system are all fairly consistent between 74.3% and 77.6%. These values are between those found for ammonium sulfate/NaOH and 3-methylglutaric acid/NaOH. Water uptake is largely independent of ion concentration as seen in the parameterizations developed by Bertram and co-workers.¹⁷ This idea is supported by experiments performed with 3-methylglutaric acid/ammonium sulfate at different ionic strengths (Table 2-1). Because each solution has similar composition and the DRH only weakly depends on the inorganic concentration, this transition is expected to be constant across the systems containing NaOH. Similarly, the MRH location, which is also

controlled by water uptake, is consistently around 80% for each of the systems containing sodium hydroxide.

Surprisingly, a hysteresis between SRH and MRH is observed at pH values of 5.17 and 6.45 (Figure 2-3, Table 2-1). At low pH, both with and without NaOH, this hysteresis is not present (Figures 2-2 and 2-3, Table 2-1). While the MRH phase transition was observed at approximately the same RH for all of the solutions containing NaOH, the SRH drops with increasing pH due to the increasing solubility of the organic component. This hysteresis is independent of ionic strength and the presence of sodium in the system, as seen in Table 2-1. Both of the high ionic strength studies with excess ammonium sulfate and the ammonium sulfate/sodium sulfate mixture show no hysteresis between the SRH and MRH phase transitions. Instead, the hysteresis appears to be dependent on the protonation state of 3-methylglutaric acid. It may therefore be present for systems containing organic acids with low pK_{as} at atmospherically relevant pH values. This hysteresis will affect the overall expected phase state of these particles in the atmosphere.

2.5 Conclusions and Atmospheric Implications

The presence of a hysteresis between two states, such as ERH and DRH, underlines the importance of the RH history of the particle needed to predict its phase state. For example, at 70% RH, an ammonium sulfate particle could be either solid or liquid depending on what the RH was previously. The same principle can be applied to the hysteresis between SRH and MRH, leading to phase separated particles being more likely phase separated for a greater amount of time. The presence of this hysteresis makes

factoring in aerosol pH essential to understanding the phase state of particles in the atmosphere.

The results seen in this study are expected to shift when investigating smaller particles. The particles (20 – 200 μm in diameter) investigated in this study demonstrate a slight size dependence that is accounted for in the standard deviation for each phase transition. A stronger size dependence in both ERH and DRH has been identified between 100 nm and 3-10 μm sized particles of mixtures of ammonium sulfate with succinic or adipic acid, where smaller particles exhibited a lower DRH and ERH compared to larger particles.⁴³ In contrast, when investigating sizes <100 nm, the Kelvin effect will increase DRH and ERH.⁴⁴⁻⁴⁵ Similarly, the Kelvin effect should increase the SRH making it easier to phase separate these particles due to the higher salt concentrations at small diameters if the particles undergo phase separation. We have previously, however, observed systems where large particles phase separate while small particles remain homogeneous, and as a result, SRH may not occur for sufficiently small particles.⁴⁶⁻⁴⁸

In summary, the pH of aerosol particles greatly affects the phase state of particles composed of ammonium sulfate, 3-methylglutaric acid, and sodium hydroxide. Due to changes in protonation states, the solubility of the organic component increases with increasing pH, which significantly shifts the location of SRH from 78.7% at low pH to 63.9% at high pH. At the same time, the MRH of the system remains consistent around 80%, resulting in a hysteresis between these phase transitions at the higher values of pH. The depression in SRH with rising pH is expected to be present in any dicarboxylic acid aerosol system and should be a consideration when mimicking atmospheric particles.

Furthermore, the presence of the hysteresis between MRH and SRH in this system suggests an overall underestimation of the role that liquid-liquid phase separated particles play in the atmospheric environment and should be explored further for more complex aerosol compositions.

2.6 Supporting Information

Summary

This supporting information contains details of the calculation of ionic strength and the number of water molecules per solute molecule for the systems detailed in the manuscript.

Ionic strength calculation

The ionic strength, μ , of a solution is given by the equation

$$\mu = \frac{1}{2} \sum_i c_i z_i^2 \quad (2.2)$$

where c_i is the concentration of the ion and z_i is the charge of the ion.⁴⁹ Our solution is made using ammonium sulfate, 3-methylglutaric acid (3MGA), sodium hydroxide, and water. Ammonium sulfate forms its component ions, NH_4^+ and SO_4^{2-} upon dissolution. Some of the SO_4^{2-} can form HSO_4^- , but we assume that H_2SO_4 is not formed because it is a strong acid. 3MGA can be doubly protonated, singly protonated (3MGA^-), and doubly deprotonated (3MGA^{2-}). Sodium hydroxide will form its component ions, Na^+ and OH^- , in solution. Because NaOH completely dissociates in aqueous solution, the Na^+ concentration is calculated based on the volume of NaOH solution added. Water can dissociate to form H_3O^+ and OH^- . The concentrations of NH_4^+ , SO_4^{2-} , HSO_4^- , OH^- , H_3O^+ ,

3MGA^- , and 3MGA^{2-} were calculated using the equations below and inputted into equation 2.2:

For NH_4^+ :

$$[\text{NH}_4^+] = 2[(\text{NH}_4)_2\text{SO}_4]_0 \quad (2.3)$$

where $[(\text{NH}_4)_2\text{SO}_4]_0$ is the initial concentration of ammonium sulfate.

For SO_4^{2-} :

$$[\text{SO}_4^{2-}] = [(\text{NH}_4)_2\text{SO}_4]_0 - [\text{HSO}_4^-] \quad (2.4)$$

For HSO_4^- :

$$\text{pH} = \text{pK}_a + \log \left(\frac{[(\text{NH}_4)_2\text{SO}_4]_0 - [\text{HSO}_4^-]}{[\text{HSO}_4^-]} \right) \quad (2.5)$$

For OH^- :

$$10^{-(14-\text{pH})} = [\text{OH}^-] \quad (2.6)$$

For H_3O^+ :

$$10^{-\text{pH}} = [\text{H}_3\text{O}^+] \quad (2.7)$$

For 3MGA^- and 3MGA^{2-} :

$$\text{pH} = \text{pK}_{a1} + \log \left(\frac{[3\text{MGA}^-]}{[3\text{MGA}]} \right) \quad (2.8)$$

$$\text{pH} = \text{pK}_{a2} + \log \left(\frac{[3\text{MGA}^{2-}]}{[3\text{MGA}^-]} \right) \quad (2.9)$$

$$[3\text{MGA}] + [3\text{MGA}^-] + [3\text{MGA}^{2-}] = [3\text{MGA}]_0 \quad (2.10)$$

where $[3\text{MGA}]_0$ is the initial concentration of 3-methylglutaric acid.⁴⁹

The results for ionic strength are given in Table 2-1 in the manuscript.

The Number of Water Molecules per Solute Molecule

When particles were first introduced into the chamber, they were held at high RH (80-90%) for 15 minutes to equilibrate. After 15 minutes, the particle concentration is

assumed to be approximately 5.0 wt.%, the same as the initially made solution. To calculate the number of water molecules per solute molecule, we consider the solutes as 3-methylglutaric acid (3MGA) in its protonated and deprotonated forms, ammonium, and sulfate; sodium is not included. We use the initial concentration of 3MGA and ammonium sulfate (AS) in the calculations. Taking 3MGA and AS to have equal weight fractions in the solution, we calculate that 1 g of solute contains 8.897×10^{21} molecules of solute using the molecular weights of the two components. Using this number and the weight percent of the solution, we calculate that there are approximately 75.1 water molecules to solute molecules. At the separation relative humidity and immediately prior to the efflorescence relative humidity, the ratio of the area equivalent diameters of a given particle at the final and initial RH was determined. The area of each particle was found using ImageJ software. These ratios were used to determine the number of water molecules per solute molecule at these RH values. Calculations from 10-19 particles were averaged together over multiple runs. The results are shown in Table 2-2. This calculation is an upper estimate due to the assumption that the concentration of the particles at high relative humidity was the same as the starting bulk solution. It is known that aerosol particles lose water in order to achieve equilibrium saturation.²⁶ This assumption was made so that a starting concentration could be determined. The effects of phase separation are also not considered.

Table 2-2: The calculated average number of water molecules per solute molecule for each system with added sodium hydroxide at approximately 87% RH, immediately after the SRH, and immediately before the ERH.

pH	Phase State	RH	Average # H ₂ O molecules/solute molecule
3.66	High RH	87.3%	75.1
	After SRH	78.6%	67.9
	Before ERH	42%	57.1
5.17	High RH	87%	75.1
	After SRH	69.1%	54.1
	Before ERH	52%	47.7
6.74	High RH	87%	75.1
	After SRH	62.8%	53.3
	Before ERH	61.5%	53.0

2.7 References

1. Ciobanu, V. G.; Marcolli, C.; Krieger, U. K.; Weers, U.; Peter, T. Liquid–Liquid Phase Separation in Mixed Organic/Inorganic Aerosol Particles. *J. Phys. Chem. A*. **2009**, *113*, 41, 10966-10978.
2. Song, M.; Marcolli, C.; Krieger, U. K.; Zuend, A.; Peter, T. Liquid-liquid phase separation and morphology of internally mixed dicarboxylic acids/ammonium sulfate/water particles. *Atmos. Chem. Phys.* **2012**, *12*, 5, 2691-2712.
3. Song, M.; Marcolli, C.; Krieger, U. K.; Zuend, A.; Peter, T. Liquid-liquid phase separation in aerosol particles: Dependence on O:C, organic functionalities, and compositional complexity. *Geophys. Res. Lett.* **2012**, *39*, 19, 1-5.
4. Parsons, M. T.; Mak, J.; Lipetz, S. R.; Bertram, A. K. Deliquescence of malonic, succinic, glutaric, and adipic acid particles. *J. Geophys. Res.* **2004**, *109*, D6, 1-8.
5. You, Y.; Renbaum-Wolff, L.; Carreras-Sospedra, M.; Hanna, S. J.; Hiranuma, N.; Kamal, S.; Smith, M. L.; Zhang, X.; Weber, R. J.; Shilling, J. E.; Dabdub, D.; Martin, S. T.; Bertram, A. K. Images reveal that atmospheric particles can undergo liquid–liquid phase separations. *P. Natl. Acad. Sci. USA*. **2012**, *109*, 33, 13188-13193.
6. Thornton, J. A.; Abbatt, J. P. D. N₂O₅ Reaction on Submicron Sea Salt Aerosol: Kinetics, Products, and the Effect of Surface Active Organics. *J. Phys. Chem. A*. **2005**, *109*, 44, 10004-10012.

7. McNeill, V. F.; Patterson, J.; Wolfe, G. M.; Thornton, J. A. The effect of varying levels of surfactant on the reactive uptake of N_2O_5 to aqueous aerosol. *Atmos. Chem. Phys.* **2006**, *6*, 6, 1635-1644.
8. Knopf, D. A.; Cosman, L. M.; Mousavi, P.; Mokamati, S.; Bertram, A. K. A Novel Flow Reactor for Studying Reactions on Liquid Surfaces Coated by Organic Monolayers: Methods, Validation, and Initial Results. *J. Phys. Chem. A* **2007**, *111*, 43, 11021-11032.
9. Park, S.-C.; Burden, D. K.; Nathanson, G. M. The Inhibition of N_2O_5 Hydrolysis in Sulfuric Acid by 1-Butanol and 1-Hexanol Surfactant Coatings. *J. Phys. Chem. A* **2007**, *111*, 15, 2921-2929.
10. Cosman, L. M.; Bertram, A. K. Reactive Uptake of N_2O_5 on Aqueous H_2SO_4 Solutions Coated with 1-Component and 2-Component Monolayers. *J. Phys. Chem. A* **2008**, *112*, 20, 4625-4635.
11. Cosman, L. M.; Knopf, D. A.; Bertram, A. K. N_2O_5 Reactive Uptake on Aqueous Sulfuric Acid Solutions Coated with Branched and Straight-Chain Insoluble Organic Surfactants. *J. Phys. Chem. A* **2008**, *112*, 11, 2386-2396.
12. Petters, M. D.; Kreidenweis, S. M. A single parameter representation of hygroscopic growth and cloud condensation nucleus activity. *Atmos. Chem. Phys.* **2007**, *7*, 8, 1961-1971.
13. Zelenyuk, A.; Ezell, M. J.; Perraud, V.; Johnson, S. N.; Bruns, E. A.; Yu, Y.; Imre, D.; Alexander, M. L.; Finlayson-Pitts, B. J. Characterization of organic coatings on hygroscopic salt particles and their atmospheric impacts. *Atmos. Environ.* **2010**, *44*, 9, 1209-1218.
14. Davies, J. F.; Miles, R. E. H.; Haddrell, A. E.; Reid, J. P. Influence of organic films on the evaporation and condensation of water in aerosol. *P. Natl. Acad. Sci. USA* **2013**, *110*, 22, 8807-8812.
15. Martin, S. T. Phase Transitions of Aqueous Atmospheric Particles. *Chem. Rev.* **2000**, *100*, 9, 3403-3454.
16. Choi, M. Y.; Chan, C. K. The Effects of Organic Species on the Hygroscopic Behaviors of Inorganic Aerosols. *Environ. Sci. Technol.* **2002**, *36*, 11, 2422-2428.
17. Bertram, A. K.; Martin, S. T.; Hanna, S. J.; Smith, M. L.; Bodsworth, A.; Chen, Q.; Kuwata, M.; Liu, A.; You, Y.; Zorn, S. R. Predicting the relative humidities of liquid-liquid phase separation, efflorescence, and deliquescence of mixed particles of ammonium sulfate, organic material, and water using the organic-to-sulfate mass ratio of the particle and the oxygen-to-carbon elemental ratio of the organic component. *Atmos. Chem. Phys.* **2011**, *11*, 21, 10995-11006.
18. Stewart, D. J.; Cai, C.; Naylor, J.; Preston, T. C.; Reid, J. P.; Krieger, U. K.; Marcolli, C.; Zhang, Y. H. Liquid-Liquid Phase Separation in Mixed Organic/Inorganic Single Aqueous Aerosol Droplets. *J. Phys. Chem. A* **2015**, *119*, 18, 4177-4190.
19. Papon, P.; Leblond, J.; Meijer, P. H. E., *The Physics of Phase Transitions: Concepts and Applications*. Springer: 1999.
20. Fridlind, A. M.; Jacobson, M. Z. A study of gas-aerosol equilibrium and aerosol pH in the remote marine boundary layer during the First Aerosol Characterization Experiment (ACE 1). *J. Geophys. Res-Atmos.* **2000**, *105*, D13, 17325-17340.

21. Yao, X.; Ling, T. Y.; Fang, M.; Chan, C. K. Size dependence of in situ pH in submicron atmospheric particles in Hong Kong. *Atmos. Environ.* **2007**, *41*, 2, 382-393.
22. Guo, H.; Xu, L.; Bougiatioti, A.; Cerully, K. M.; Capps, S. L.; Hite Jr, J. R.; Carlton, A. G.; Lee, S. H.; Bergin, M. H.; Ng, N. L.; Nenes, A.; Weber, R. J. Fine-particle water and pH in the southeastern United States. *Atmos. Chem. Phys.* **2015**, *15*, 9, 5211-5228.
23. Bougiatioti, A.; Nikolaou, P.; Stavroulas, I.; Kouvarakis, G.; Weber, R.; Nenes, A.; Kanakidou, M.; Mihalopoulos, N. Particle water and pH in the eastern Mediterranean: source variability and implications for nutrient availability. *Atmos. Chem. Phys.* **2016**, *16*, 7, 4579-4591.
24. Guo, H.; Sullivan, A. P.; Campuzano-Jost, P.; Schroder, J. C.; Lopez-Hilfiker, F. D.; Dibb, J. E.; Jimenez, J. L.; Thornton, J. A.; Brown, S. S.; Nenes, A.; Weber, R. J. Fine particle pH and the partitioning of nitric acid during winter in the northeastern United States. *J. Geophys. Res.-Atmos.* **2016**, *121*, 17, 1-22.
25. Rindelaub, J. D.; Craig, R. L.; Nandy, L.; Bondy, A. L.; Dutcher, C. S.; Shepson, P. B.; Ault, A. P. Direct Measurement of pH in Individual Particles via Raman Microspectroscopy and Variation in Acidity with Relative Humidity. *J. Phys. Chem. A* **2016**, *120*, 6, 911-917.
26. Dallemagne, M. A.; Huang, X. Y.; Eddingsaas, N. C. Variation in pH of Model Secondary Organic Aerosol during Liquid-Liquid Phase Separation. *J. Phys. Chem. A* **2016**, *120*, 18, 2868-2876.
27. Jang, M.; Czoschke, N. M.; Lee, S.; Kamens, R. M. Heterogeneous Atmospheric Aerosol Production by Acid-Catalyzed Particle-Phase Reactions. *Science* **2002**, *298*, 5594, 814-817.
28. Limbeck, A.; Kulmala, M.; Puxbaum, H. Secondary organic aerosol formation in the atmosphere via heterogeneous reaction of gaseous isoprene on acidic particles. *Geophys. Res. Lett.* **2003**, *30*, 19, 1-4.
29. Iinuma, Y.; Böge, O.; Gnauk, T.; Herrmann, H. Aerosol-chamber study of the α -pinene/O₃ reaction: influence of particle acidity on aerosol yields and products. *Atmos. Environ.* **2004**, *38*, 5, 761-773.
30. Surratt, J. D.; Lewandowski, M.; Offenberg, J. H.; Jaoui, M.; Kleindienst, T. E.; Edney, E. O.; Seinfeld, J. H. Effect of Acidity on Secondary Organic Aerosol Formation from Isoprene. *Environ. Sci. Technol.* **2007**, *41*, 15, 5363-5369.
31. Zhou, S.; Wang, Z.; Gao, R.; Xue, L.; Yuan, C.; Wang, T.; Gao, X.; Wang, X.; Nie, W.; Xu, Z.; Zhang, Q.; Wang, W. Formation of secondary organic carbon and long-range transport of carbonaceous aerosols at Mount Heng in South China. *Atmos. Environ.* **2012**, *63*, 203-212.
32. Hinrichs, R. Z.; Buczek, P.; Trivedi, J. J. Solar Absorption by Aerosol-Bound Nitrophenols Compared to Aqueous and Gaseous Nitrophenols. *Environ. Sci. Technol.* **2016**, *50*, 11, 5661-5667.
33. Gao, S.; Ng, N. L.; Keywood, M.; Varutbangkul, V.; Bahreini, R.; Nenes, A.; He, J.; Yoo, K. Y.; Beauchamp, J. L.; Hodyss, R. P.; Flagan, R. C.; Seinfeld, J. H. Particle Phase Acidity and Oligomer Formation in Secondary Organic Aerosol. *Environ. Sci. Technol.* **2004**, *38*, 24, 6582-6589.

34. Zhang, Q.; Jimenez, J. L.; Worsnop, D. R.; Canagaratna, M. A Case Study of Urban Particle Acidity and Its Influence on Secondary Organic Aerosol. *Environ. Sci. Technol.* **2007**, *41*, 9, 3213-3219.
35. Chebbi, A.; Carlier, P. Carboxylic acids in the troposphere, occurrence, sources, and sinks: A review. *Atmos. Environ.* **1996**, *30*, 24, 4233-4249.
36. Khare, P.; Kumar, N.; Kumari, K. M.; Srivastava, S. S. Atmospheric formic and acetic acids: An overview. *Rev. Geophys.* **1999**, *37*, 2, 227-248.
37. Chowhan, Z. T. pH-solubility profiles of organic carboxylic acids and their salts. *J. Pharm. Sci.-US* **1978**, *67*, 9, 1257-1260.
38. Grover, P. K.; Ryall, R. L. Critical Appraisal of Salting-Out and Its Implications for Chemical and Biological Sciences. *Chem. Rev.* **2005**, *105*, 1, 1-10.
39. You, Y.; Smith, M. L.; Song, M.; Martin, S. T.; Bertram, A. K. Liquid-liquid phase separation in atmospherically relevant particles consisting of organic species and inorganic salts. *Int. Rev. Phys. Chem.* **2014**, *33*, 1, 43-77.
40. Liu, X.-M.; Wang, L.-S. A one-pot synthesis of oleic acid end-capped temperature- and pH-sensitive amphiphilic polymers. *Biomaterials* **2004**, *25*, 10, 1929-1936.
41. Pineda-Contreras, B. A.; Schmalz, H.; Agarwal, S. pH dependent thermoresponsive behavior of acrylamide-acrylonitrile UCST-type copolymers in aqueous media. *Polym. Chem.* **2016**, *7*, 10, 1979-1986.
42. Greenspan, L. Humidity fixed points of binary saturated aqueous solutions. *J. Res. NBS A Phys. Ch.* **1977**, *81*, 1, 89-96.
43. Laskina, O.; Morris, H. S.; Grandquist, J. R.; Qin, Z.; Stone, E. A.; Tivanski, A. V.; Grassian, V. H. Size Matters in the Water Uptake and Hygroscopic Growth of Atmospherically Relevant Multicomponent Aerosol Particles. *J. Phys. Chem. A* **2015**, *119*, 19, 4489-4497.
44. Biskos, G.; Malinowski, A.; Russell, L. M.; Buseck, P. R.; Martin, S. T. Nanosize Effect on the Deliquescence and the Efflorescence of Sodium Chloride Particles. *Aerosol Sci. Tech.* **2006**, *40*, 2, 97-106.
45. Biskos, G.; Russell, L. M.; Buseck, P. R.; Martin, S. T. Nanosize effect on the hygroscopic growth factor of aerosol particles. *Geophys. Res. Lett.* **2006**, *33*, 7, 1-4.
46. Veghte, D. P.; Altaf, M. B.; Freedman, M. A. Size Dependence of the Structure of Organic Aerosol. *J. Am. Chem. Soc.* **2013**, *135*, 43, 16046-16049.
47. Veghte, D. P.; Bittner, D. R.; Freedman, M. A. Cryo-Transmission Electron Microscopy Imaging of the Morphology of Submicrometer Aerosol Containing Organic Acids and Ammonium Sulfate. *Anal. Chem.* **2014**, *86*, 5, 2436-2442.
48. Altaf, M. B.; Zuend, A.; Freedman, M. A. Role of nucleation mechanism on the size dependent morphology of organic aerosol. *Chem. Commun.* **2016**, *52*, 59, 9220-9223.
49. Harris, D. C., *Quantitative Chemical Analysis*. Seventh ed.; W. H. Freeman and Company: New York, 2007.

Chapter 3

Low pH Dependence of Morphology in Organic Aerosol

Author Contributions: Losey is responsible for most data collection and experimental design and is the primary author. Emily-Jean E. Bankes served in the rest of the data collection, numerous discussions, and editing.

3.1 Introduction

Aerosol particles can affect the environment directly by scattering or absorbing light in the atmosphere and indirectly by serving as cloud condensation nuclei. Because the scattering, absorbing, and cloud condensation properties of aerosol particles are greatly affected by the physical state of the particle, it is important to know in which phase the particles are present in the atmosphere.¹ Aerosol particles can undergo deliquescence (DRH), efflorescence (ERH), phase separation (SRH), and mixing (MRH) at different relative humidities, which are affected by relative humidity and the composition of the particle. Phase separation can influence the optical properties of the

aerosol particle, the heterogeneous chemistry in which the particle participates in the atmosphere, and evaporation and condensation rates.

The pH of aerosol particles is an ongoing discussion within the atmospheric community. It has been shown that pH is influenced by particle composition, size, and location. Fine particle aerosol studies have determined pH ranges from as low as -0.51 and up to 3.1 depending on the season or location.²⁻⁴ Some events such as haze or biomass burning can cause aerosol pH to be as high as 3.0-4.9 for haze events. These pH measurements have been shown to be very sensitive to size as well, where PM₁ and PM_{2.5} have an average measured pH of 1.9 and 2.7.⁵ The influence of this low pH on phase transitions, especially phase separation, has not yet been explored.

Phase separation has been well studied with most studies concluding that its occurrence is mostly dependent on the O:C ratio of the organic component, but more recent studies have identified that the inorganic salt identity and the pH of the solution can affect the SRH as well.⁶⁻⁷ The salting-out ability, as predicted by the Hofmeister Series, of different inorganic salts has been shown to directly correlate to the SRH in aerosol particles by You et al.⁷ In this paper, the SRH trend was as follows: $(\text{NH}_4)_2\text{SO}_4 \geq \text{NH}_4\text{HSO}_4 \geq \text{NaCl} \geq \text{NH}_4\text{NO}_3$, which is consistent with the Hofmeister series where the salt with the highest salting-out ability has the highest SRH.⁸ A previous study from our group has explored the effect of a high pH on SRH.⁶ This study found that when the organic component is deprotonated at high pH, the SRH decreases. The influence of low pH and changing the inorganic salt are explored in this paper.

Ammonium sulfate aerosol is ubiquitous in the continental atmosphere due to its emission sources from industry and agriculture.⁹ Thermodynamic principles have long

dictated that the sulfate should be completely neutralized due to the ammonium:sulfate ratio being above 2 in most cases, but this is not always the case.¹⁰⁻¹¹ Letovicite, $(\text{NH}_4)_3\text{H}(\text{HSO}_4)_2$, and ammonium bisulfate, NH_4HSO_4 , have also been shown to be present in high amounts.¹²⁻¹⁶ Letovicite is an intermediate form between ammonium sulfate and ammonium bisulfate due to its intermediate ammonium:sulfate ratio of 1.5, verses 2.0 and 1.0 for the other compounds. Letovicite is commonly studied along with ammonium sulfate and ammonium bisulfate as its efflorescence and deliquescence behavior can influence the behavior of ammonium sulfate and ammonium bisulfate if they are found in the same environment.¹⁷⁻²⁵ It has been well studied as an ice nucleus for heterogeneous ice nucleation and as a component for homogeneous ice nucleation of cirrus clouds.²⁶⁻³² The pKa of bisulfate is 2.00,³³ so the low pH of atmospheric aerosol indicates that bisulfate should be the primary identity present. Also, it has been predicted that the volatilization of ammonia and/or organic coatings on inorganic particles prevent full neutralization.¹⁰⁻¹¹ Weber et al. suggested that aerosol pH is insensitive to decreases in sulfate emissions due to the partitioning of ammonia between the gas and particle phase which effectively buffers the pH between 0 and 2.¹⁰ Likewise, Silvern et al. investigated what prevents the uptake of ammonia onto aerosol particles.¹¹ By implementing a kinetic mass transfer limitation, the discrepancy between the particle-phase ammonium:sulfate ratio and observed gaseous ammonia concentrations could be mitigated. The kinetic mass transfer limitation was assumed to be due to an organic coating present on the particles, a consequence of liquid-liquid phase separation. While letovicite and its occurrence in atmospheric aerosol particles has been extensively studied, its role in phase separation of aerosol particles has not yet been investigated.

Several studies have used Raman spectroscopy and fluorescent dyes to determine the pH of individual particles.³⁴⁻³⁶ Raman spectroscopy has been used to track sulfate and bisulfate stretches to determine pH during a humidity cycle.³⁴ This research has expanded to determine pH using multiple acid-base equilibria and Debye-Hückel activity calculations,³⁶ but these tools are still being developed and are still only accurate for well-controlled systems. A fluorescent pH dye has also been employed to track pH of the organic phase during a humidity cycle in an organic/inorganic system that undergoes phase separation.³⁵ The experiments that have tracked pH during humidity cycles have not observed a more than a one pH unit difference during the cycle, so pH of the bulk system is most important when determining the effects of pH on phase separation.

Sulfuric acid is known to be an important contributor to new particle formation and many studies have explored its role in heterogeneous chemistry and phase state of aerosol particles. Particle acidity in general has been well documented and is known to affect heterogeneous chemistry of atmospheric species, reactive uptake of gas species on particles, and solar absorption of aerosol particle-bound nitrophenols.³⁷⁻⁴⁴ Sulfuric acid-containing aerosol have been studied to understand their effects on viscosity of the particles. These studies have found that sulfuric acid-containing aerosol particles become more viscous with decreasing temperatures and/or increased weight percent.⁴⁵⁻⁴⁶ This increase in viscosity with added sulfuric acid could inhibit crystallization, water uptake, or crystal growth of these particles.⁴⁷⁻⁴⁹ The effect of viscosity on phase separation has been previously investigated by You et al. by viewing phase separation of high molecular weight organic components at low temperatures.⁵⁰ This study found that viscosity played some role in lowering the SRH of the studied systems, but there was no strong

dependence. Most of the organic compounds investigated in this study are carboxylic acids. Carboxylic acids are estimated to make up about 25% non-methane hydrocarbons in the atmosphere and are common products of olefin oxidation or can be emitted directly during combustion.⁵¹⁻⁵² Alcohols can be directly released from biogenic sources and have been identified as products of certain combustion processes.⁵³⁻⁵⁵

In this study, the effect of the addition of sulfuric acid to particles containing an organic compound and ammonium sulfate is investigated. Through the addition of sulfuric acid, the stoichiometric ratio between ammonium and sulfate can be manipulated to achieve letovicite and ammonium bisulfate. The effect of having excess sulfate is also investigated for systems with an atmospherically relevant low pH at 0.35. The organic compounds investigated were chosen to achieve a wide range of O:C ratios and a range of SRHs. They are 2-methylglutaric acid, 3-methylglutaric acid, 2,2-Bis(hydroxymethyl)butyric acid, 3,3-dimethylglutaric acid, diethylmalonic acid, and 1,2,6-hexanetriol. The relative humidities at which the phase transitions, ERH, DRH, SRH, and MRH, occur were observed with optical microscopy.

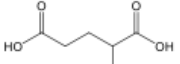
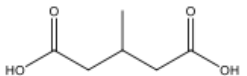
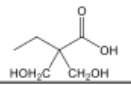

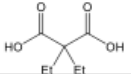
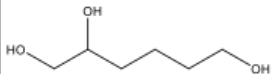
3.2 Experimental Methods

Aerosol particles containing a variety of organic components and ammonium sulfate (EMD, GR ACS) were generated in the laboratory from an aqueous solution. The organic components investigated were 2-methylglutaric acid, 3-methylglutaric acid, 2,2-bis(hydroxymethyl)butyric acid, 3,3-dimethylglutaric acid, diethylmalonic acid, and 1,2,6-hexanetriol (Table 3-1). A 5.0 wt.% solution of an organic component and ammonium sulfate in a 1:1 ratio by mass was made in ultrapure water (HPLC grade, Fisher), except for 2,2-bis(hydroxymethyl)butyric acid which was in a 0.6:0.4 ratio of

inorganic:organic to guarantee phase separation. This ratio was chosen because Bertram and coworkers found that an organic:sulfate mass ratio of less than 1 was required for phase separation on some compounds with O:C near 0.7.⁵⁶ The identity of the inorganic component was changed to ammonium bisulfate or letovicite through addition of concentrated sulfuric acid to achieve an ammonium:sulfate stoichiometric ratio of 1:1 and 2:3, respectively. To mimic the low pH in aerosol particles that is expected from recent studies,^{3-4, 10} additional concentrated sulfuric acid was added to reach a pH of approximately 0.35. The pH of each system was recorded. It is expected that this bulk pH should remain mostly constant even after the particles are aerosolized. Previous work by Dallemagne et al. saw little change in the pH in aerosol particles when decreasing the relative humidity (RH) from 80 to 65%.³⁵ Even though a small change in pH after aerosolizing may occur, the ammonium:sulfate ratio will not change. Furthermore, the protonation state of the organic component and the salt identity are not expected to change in the low pH case. In every case, the pH of the solutions varied with added sulfuric acid, even with small addition of sulfuric acid (i.e. between letovicite and ammonium bisulfate) (Figure 3-1). Each solution was tested using the setup described previously, in an environmental chamber where RH can be changed by varying the ratio between wet and dry nitrogen lines.⁶ The RH was increased or decreased within the chamber anywhere from 0 to 95% to observe each phase transition of the particles. The RH was changed at a rate of $\leq 1\%/min$, which allows the particles enough time to equilibrate with the change in RH. ERH, DRH, SRH, and MRH for each system were recorded by starting at high RH, decreasing the RH to observe SRH and ERH, and then increasing the RH to observe MRH and DRH. Control studies of 2.5 wt.% ammonium

sulfate with concentrated sulfuric acid added to achieve ammonium bisulfate and letovicite were performed as well as 2.5 wt.% of each organic component with only sulfuric acid. To further explore systems made out of just an organic component and acid in water, 2.5 wt.% of select organic compound solutions with the same molar equivalent of phosphoric acid, hydrochloric acid, and/or glacial acetic acid as the sulfuric acid control studies were made.

Table 3-1: The name, structure, molecular weight, and O:C of each organic component as well as pH information for each study.

Name	Structure	MW (g/mol)	O:C	pH of solution of:			
				Ammonium sulfate	Letovicite	Ammonium bisulfate	Low pH
2-methylglutaric acid		146.14	0.67	2.78 ± 0.01	1.48 ± 0.04	0.94 ± 0.01	0.34 ± 0.01
3-methylglutaric acid		146.14	0.67	2.68 ± 0.07	1.64 ± 0.01	1.16 ± 0.01	0.35 ± 0.00
2,2-Bis(hydroxymethyl) butyric acid		148.16	0.67	2.96 ± 0.02	1.33 ± 0.01	0.75 ± 0.02	0.34 ± 0.01
3,3-dimethylglutaric acid		160.17	0.57	2.54 ± 0.01	1.44 ± 0.02	0.94 ± 0.01	0.34 ± 0.04
Diethylmalonic acid		160.17	0.57	1.87 ± 0.09	1.53 ± 0.07	1.15 ± 0.12	0.34 ± 0.03
1,2,6-Hexanetriol		134.17	0.50	5.16 ± 0.08	1.69 ± 0.03	1.20 ± 0.00	0.34 ± 0.01

3.3 Results and Discussion

Our previous work explored the effect of adding sodium hydroxide to aqueous 3-methylglutaric acid/ammonium sulfate.⁶ This study found that with addition of sodium hydroxide, the organic component became deprotonated, and as its solubility changed, the SRH decreased. A similar trend is evident when sulfuric acid is added to the 3-methylglutaric acid/ammonium sulfate system (Figure 3-1). As more sulfuric acid is added and the pH decreases, the SRH decreases from 72.9% at pH 2.68, where no sulfuric acid is added, to no observable SRH at pH 0.35. This trend at low pH follows the

expected trend from the Hofmeister Series, where when ammonium sulfate, letovicite, and ammonium bisulfate make up the inorganic component of the system at pH 2.68, 1.64, and 1.16, respectively, the SRH decreases to reflect the decreased salting-out ability of the salt. This trend continues at pH 0.35 although ammonium bisulfate is expected to be the primary inorganic salt identity. This implies that there are increased interactions between the organic component and the sulfuric acid which is preventing the phase separation. Unlike the studies done previously on 3-methylglutaric acid/ammonium sulfate at high pH, sulfuric acid system showed no hysteresis between the SRH and MRH.

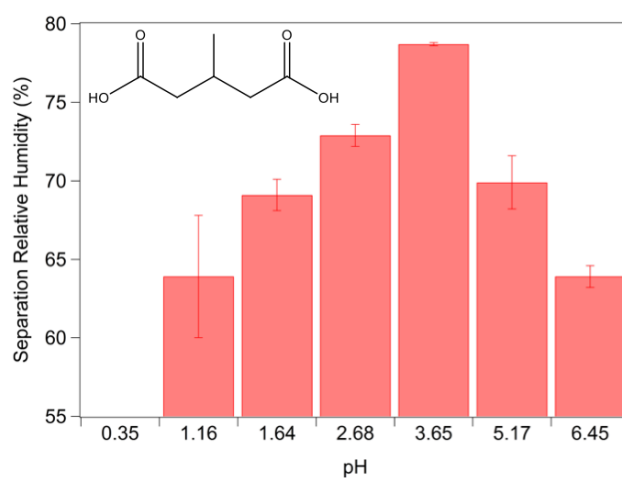


Figure 3-1: The separation relative humidity (SRH) for the 3-methylglutaric acid/ammonium sulfate system (pH 2.68) with added sulfuric acid (pH 0.35-1.64) or sodium hydroxide (pHs 3.65-6.45) as a function of pH. The average and standard deviations are found by measuring multiple particles over repeated measurements. Note: The system at pH 0.35 does not phase separate, even when held at 0% relative humidity. *Data from Losey 2016

Five organic systems were studied in addition to 3-methylglutaric acid to explore how the SRH is influenced based on salt identity/acidity (Figure 3-2 and Table 3-2). In every case, the SRH decreased with addition of sulfuric acid from ammonium sulfate to low pH. The amount of sulfuric acid added was the same for each of the letovicite studies and the ammonium bisulfate studies, but the amount added to achieve low pH varied based on the system. The overall identity of the salt in each system is expected to be the same not only due to the same stoichiometric ratio between the ammonium and sulfate ions but also because of pH measurements of each system. In every case, the pH of the ammonium sulfate, letovicite, and ammonium bisulfate solutions were in a range that did not overlap (Table 3-1, Figure 3-5 in Supporting Information). The degree of change with additional sulfuric acid varied based on the organic studied. The greatest change in SRH with additional sulfuric acid is evident for 2-methylglutaric acid, 3-methylglutaric acid, 2,2-bis(hydroxymethyl)butyric acid, and 1,2,6-hexanetriol. Each of these systems see a change of at least 45% in their SRH from ammonium sulfate to low pH. Two of these systems, 3-methylglutaric acid and 2,2-bis(hydroxymethyl)butyric acid, do not phase separate at low pH. This high dependence on sulfuric acid addition is independent on the O:C, but instead seems to be loosely dependent on the starting SRH of the organic/ammonium sulfate system. This large change with sulfuric acid is not as pronounced with two of the systems. For 3,3-dimethylglutaric acid and diethylmalonic acid, the SRH with ammonium sulfate as the inorganic component was 90.3% and 93.9%, respectively. With addition of sulfuric acid, the SRH for these systems stayed consistent or decreased slightly until low pH where a statistically significant drop in SRH is seen. The SRH dropped from 87.2% to 73.9% for 3,3-dimethylglutaric acid and 91.8%

to 84.8% for diethylmalonic acid when going from ammonium bisulfate to low pH. The overall trend of the SRH decreasing as the inorganic salt identity changes agrees with You et al. which found that the SRH decreases as the salting-out ability of the inorganic component decreases, according to the Hofmeister series.⁷ These results are consistent across each organic component studied no matter which functional groups were present.

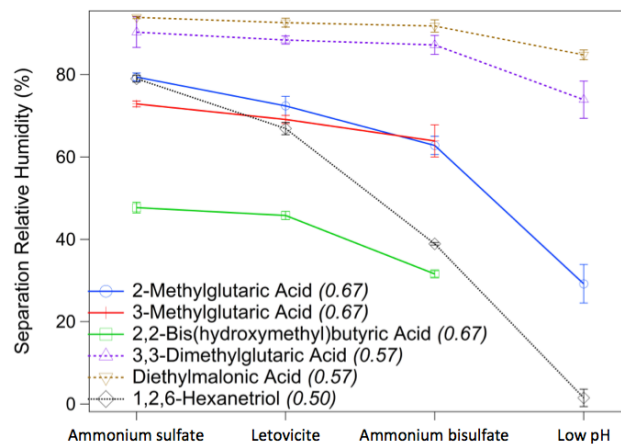


Figure 3-2. The separation relative humidity for each organic/ammonium sulfate/sulfuric acid system investigated with organic O:C in parenthesis. Note: 3-methylglutaric acid and 2,2-bis(hydroxymethyl)butyric acid exhibit no phase separation at low pH.

Table 3-2: Separation relative humidity (SRH), efflorescence relative humidity (ERH) and deliquescence relative humidity (DRH) data for each system. Note: For all systems studied, the mixing relative humidity (MRH) was within error of the SRH and is, therefore, not reported.

	2-Methylglutaric Acid	3-Methylglutaric Acid	2,2-Bis(hydroxymethyl)butyric Acid	3,3-Dimethylglutaric Acid	Diethylmalonic Acid	1,2,6-Hexanetriol
SRH	79.4 ± 1.0	72.9 ± 0.7	47.7 ± 1.3	90.3 ± 3.7	93.9 ± 0.3	79.0 ± 0.8
ERH	40.6 ± 3.9	42.8 ± 3.6	38.2 ± 2.0	40.9 ± 4.7	42.8 ± 7.1	37.6 ± 2.0
DRH	81.2 ± 1.1	81.0 ± 1.1	81.3 ± 2.5	---	---	81.4 ± 1.7
SRH	72.4 ± 2.3	69.1 ± 1.0	45.8 ± 1.0	88.4 ± 1.0	92.6 ± 1.1	66.9 ± 1.5
ERH	33.0 ± 6.6	35.4 ± 6.4	25.6 ± 3.4	47.0 ± 12.9	41.0 ± 9.0	31.9 ± 4.8
DRH	76.2 ± 3.8	93.5 ± 3.0	74.0 ± 4.9	---	---	77.4 ± 1.3
SRH	62.8 ± 2.2	63.9 ± 3.9	31.6 ± 0.8	87.2 ± 2.3	91.8 ± 1.5	38.9 ± 0.3
ERH	6.1 ± 2.1	17.4 ± 3.1	6.2 ± 5.8	49.7 ± 7.5	61.1 ± 8.9	23.7 ± 1.6
DRH	51.9 ± 3.1	65.2 ± 0.3	51.9 ± 0.5	---	---	67.2 ± 1.2
SRH	29.2 ± 4.7	---	2.6 ± 1.9	73.9 ± 4.5	84.8 ± 1.2	1.5 ± 2.1
ERH	---	---	0.4 ± 1.1	46.8 ± 11.3	65.9 ± 9.0	1.5 ± 2.1
DRH	---	---	31.8 ± 0.6	---	---	30.2 ± 0.6

To better understand what is controlling the phase separation behavior of the organic/inorganic/sulfuric acid systems, solutions containing only an organic component and sulfuric acid were investigated. When sulfuric acid alone is added, 2-methylglutaric acid, 3,3-dimethylglutaric acid, and diethylmalonic acid all phase separate (Table 3). Phase separation with no salt component has been demonstrated before in previous studies investigating secondary organic matter resulting from ozonolysis of α -pinene, β -caryophyllene, and limonene and photooxidation of toluene.⁵⁷⁻⁵⁸ This phase separation occurs upon water uptake and requires relative humidities greater than 90%. Because this happens at such high relative humidity, it is unlikely to occur in most atmospherically relevant cases but is important in cloud condensation nucleus activity. The SRH values recorded with sulfuric acid show that this phase separation can occur and persist at atmospherically relevant relative humidity, for the 3,3-dimethylglutaric acid and

diethylmalonic acid systems. The low SRH, 34.1%, for 2-methylglutaric acid implies that this would be less prevalent in atmospherically relevant conditions. The other systems do not phase separate at any relative humidity. These systems all have a lower SRH when compared to ammonium bisulfate, except 3-methylglutaric acid which has the same SRH within experimental error as 2-methylglutaric acid, and therefore are less likely to salt out already. The removal of the inorganic salt from the mixture makes them even less likely to phase separate.

The behavior of the organic/sulfuric acid systems can help understand the organic/ammonium sulfate/sulfuric acid experiments. The 3,3-dimethylglutaric acid and diethylmalonic acid systems have very high SRH with or without the presence of ammonium sulfate. This suggests that the phase separation for these two systems is dependent on the excess sulfate in solution and not the inorganic salt. This is not the case for 2-methylglutaric acid. The phase separation of the 2-methylglutaric acid/sulfuric acid system is much lower than that of the 2-methylglutaric acid/ammonium sulfate/sulfuric acid system implying that the interaction between the inorganic salt and the organic component is what drives the separation.

The presence of phase separation without the presence of an inorganic salt was further investigated using different acids. These results showed the following trend in salting out abilities: $\text{HSO}_4^- > \text{H}_3\text{PO}_4 > \text{Cl}^- \approx \text{CH}_3\text{COOH}$. Sulfuric acid, as bisulfate, is the most salting out due to its ability to cause phase separation at relative humidities above 95% for 3,3-dimethylglutaric acid and diethylmalonic acid and phase separate 2-methylglutaric acid at 34.1% (Table 4-3). Phosphoric acid, on the other hand, only leads to phase separation for the 3,3-dimethylglutaric acid and diethylmalonic acid systems.

Both of which phase separate at >95%. The addition of hydrochloric acid or acetic acid lead to no phase separation regardless of the organic component present. This trend in salting-out ability follows with current knowledge of the Hofmeister series. To the authors' knowledge, phosphoric acid and acetic acid in their completely protonated state have not been explicitly studied and added to the series; however, their positions can be inferred from the location of their deprotonated states.

Table 3-3: The separation relative humidities (%) for each organic component with ammonium bisulfate and each acid control study.*

	NH ₄ HSO ₄	HSO ₄ ⁻	H ₃ PO ₄	Cl ⁻	CH ₃ COOH
2-Methylglutaric acid	62.8 ± 2.2	34.1 ± 4.1	---	---	---
3-Methylglutaric acid	73.9 ± 3.9	---	---	---	
2,2-Bis(hydroxymethyl)butyric acid	31.6 ± 0.8	---	---		
3,3-Dimethylglutaric acid	87.2 ± 2.3	>95	>95	---	---
Diethylmalonic acid	91.8 ± 1.5	>95	>95	---	---
1,2,6-Hexanetriol	38.9 ± 0.3	---	---		

* The charge state of each acid is included based on the pH of the bulk solution. Systems that did not phase separate are dashed and systems not studied are shaded in gray.

The ERH of each system changed drastically with subsequent additions of sulfuric acid (Table 3-2, Figure 3-3). For 2-methylglutaric acid, 3-methylglutaric acid, 2,2-bis(hydroxymethyl)butyric acid, and 1,2,6-hexanetriol, the ERH decreased with addition of sulfuric acid and both methylglutaric acids have no ERH at low pH. Control studies reveal that ammonium sulfate, letovicite, and ammonium bisulfate have ERH values of 35%, 27.3% ± 4.3 and 7.1% ± 3.7, respectively.¹⁸ A solution containing ammonium sulfate at pH 0.35 has no ERH. The ammonium sulfate systems all are within experimental error of the ammonium sulfate ERH and are therefore expected to be

controlled by the crystallization of the inorganic component. Likewise, the ERH for 2-methylglutaric acid/letovicite, 3-methylglutaric acid/letovicite, 2,2-bis(hydroxymethyl)butyric acid/letovicite, 1,2,6-hexanetriol/letovicite, 2-methylglutaric acid/ammonium bisulfate, and 2,2-bis(hydroxymethyl)butyric acid/ammonium bisulfate are all controlled by the crystallization of the inorganic component, based on the value for ERH for these systems. The ERH for the 3,3-dimethylglutaric acid/letovicite and 3,3-dimethylglutaric acid/ammonium bisulfate systems overlap with the 3,3-dimethylglutaric acid/sulfuric acid results and thus indicates that the efflorescence is controlled by the crystallization of the organic component (Table 3-4). This organic-controlled efflorescence has been seen previously.^{6, 59} For diethylmalonic acid/letovicite system as well as the ammonium bisulfate systems containing 3-methylglutaric acid, diethylmalonic acid, and 1,2,6-hexanetriol, it is not clear what leads to crystallization as these values do not support a crystallization mechanism led by the inorganic or organic component. The salt-containing systems at low pH, however, must be controlled by the crystallization of the organic component since no ERH for the control study of ammonium sulfate at pH 0.35 was found. This resulted in very low or unmeasured ERH values for all the organic systems except for 3,3-dimethylglutaric acid and diethylmalonic acid which maintained a high ERH that overlapped with the results from ammonium bisulfate, supporting a similar mechanism of crystallization. For the systems that do not effloresce, 2-methylglutaric acid and 3-methylglutaric acid, or have very low efflorescence, 2,2-bis(hydroxymethyl)butyric acid and 1,2,6-hexanetriol, the efflorescence could be inhibited by the viscosity of the particles. Viscosity-inhibited efflorescence has been previously reported where the viscosity of different solutions increases with higher mass

fractions of sulfuric acid.⁴⁵ The increased viscosity can inhibit the nucleation of the new phase even when it is thermodynamically favored.³⁰

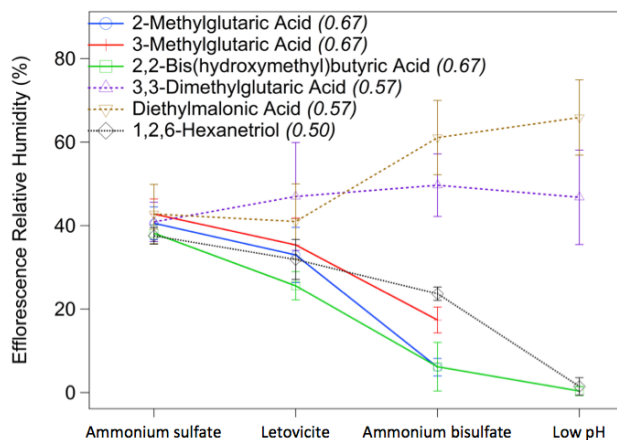


Figure 3-3: The efflorescence relative humidity for each organic/ammonium sulfate/sulfuric acid system investigated with organic O:C in parenthesis. Note: 2-methylglutaric acid and 3-methylglutaric acid do not effloresce at low pH.

Table 3-4: The efflorescence relative humidities (%) for the acid control studies. There is no complete deliquescence for any of the systems. The charge state of the sulfuric acid is included based on the pH of the bulk solution.*

	Low pH	HSO_4^- (AB)	HSO_4^- (L)	No Acid
3-Methylglutaric acid		---	$35.8 \pm 12.1^\dagger$	---
3,3-dimethylglutaric acid	57.2 ± 7.2	48.6 ± 14.8	44.6 ± 13.4	42.3 ± 14.2
Diethylmalonic acid	66.4 ± 3.7	73.4 ± 6.3	72.7 ± 5.8	64.7 ± 7.8

* The charge state of each acid is included based on the pH of the bulk solution. Systems that did not effloresce are dashed and systems not studied are shaded in gray.

† Not all of the particles effloresce for this 3-methylglutaric acid system.

With one exception, the DRH for every system studied decreases with addition of sulfuric acid (Figure 3-4). This result is unsurprising as the DRH of letovicite and ammonium bisulfate show a similar trend and DRH is expected to be dictated by the DRH of the inorganic component according to the parameterizations by Bertram and

coworkers.⁵⁶ The DRH of ammonium sulfate, letovicite, and ammonium bisulfate are 80%, 73.5% \pm 0.9, and 34.6% \pm 3.4, respectively.¹⁸ As with the ERH results, the results for the systems containing ammonium sulfate overlap with the pure inorganic salt. This is true also for every system with letovicite, except 3-methylglutaric acid. While the ammonium bisulfate DRH is lower than that of letovicite, it is much lower (15-35%) than the measured DRH of all the systems. Because none of these organic compounds effloresce when sulfuric acid is added, it is unknown what is causing this large difference in DRH. Likewise, because the ammonium sulfate/sulfuric acid system at low pH does not effloresce, it cannot, therefore, be determined what is driving this process.

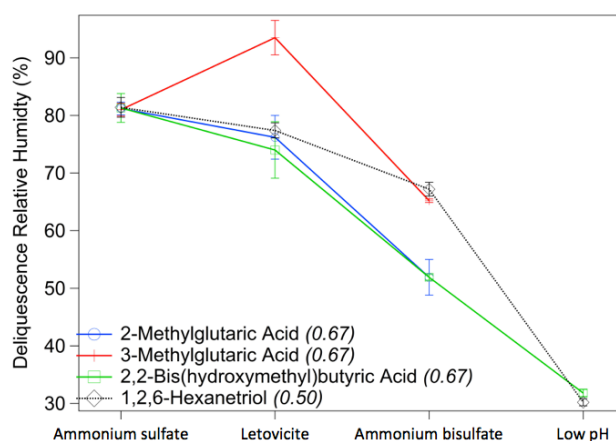


Figure 3-4: The deliquescence relative humidity for the organic/ammonium sulfate/sulfuric acid systems that effloresced with organic O:C in parenthesis. Note: 3,3-dimethylglutaric acid and diethylmalonic acid did not deliquesce by 95% and are therefore not included.

3.4 Conclusions and Atmospheric Implications

The addition of sulfuric acid to both decrease the pH of the system and change the inorganic salt identity has major effects on the phase transitions of the organic/inorganic

systems investigated in this study. As more sulfuric acid is added and the ammonium to sulfate ratio is changed from 2:1, to 3:2 and 1:1 and so on, the SRH decreases, making phase separation less favored. This effect is more pronounced with systems that have a SRH less than 80%. As shown by the organic/sulfuric acid phase separation studies, it is possible for a system with no salt to phase separate, although this only is true for certain systems. Further studies with different acids revealed that the SRH for different acids follow the trend: $\text{HSO}_4^- > \text{H}_3\text{PO}_4 > \text{HCl} \approx \text{CH}_3\text{COOH}$, which mirrors what is expected based on the Hofmeister series. The ERH of each system varies greatly with pH and is usually controlled by the crystallization of the organic or inorganic component. Several systems do not effloresce with high sulfuric acid content. This is likely due to the high viscosity expected of these particles which can prevent crystallization. The DRH of each of the systems tend to decrease with increasing sulfuric acid, except for 3,3-dimethylglutaric acid and diethylmalonic acid which never exhibit a deliquescence.

Combined with the results from the high pH studies done previously, these results underline the importance of pH in phase transition studies. The pH and inorganic salt identities investigated here imply that phase separation may not occur for certain systems, especially at low pH. At the lowest pH values studied, four of the six systems would likely not phase separate under atmospherically relevant conditions. The inorganic salt identity also has a major impact on the phase separation of particles. When the inorganic salt is letovicite or ammonium bisulfate, the SRH decreases, making phase separation less likely. All of these results indicate that the prevalence of phase separation may be overestimated in regions of low pH.

3.5 Supporting Information

Figure 3-5 shows the SRH, ERH, and DRH results from Figures 3-2, 3-3, and 3-4 plotted against the bulk pH of each system investigated. From this figure, it is clear that none of the pHs investigated for the ammonium sulfate, letovicite, and ammonium bisulfate systems overlap. This is true even when the starting pH of the ammonium sulfate/organic system varies over four pH units, depending on the organic component studied. These pH values also overlap with the pH values recorded for the ammonium sulfate, letovicite, and ammonium bisulfate control studies done with no organic component present.

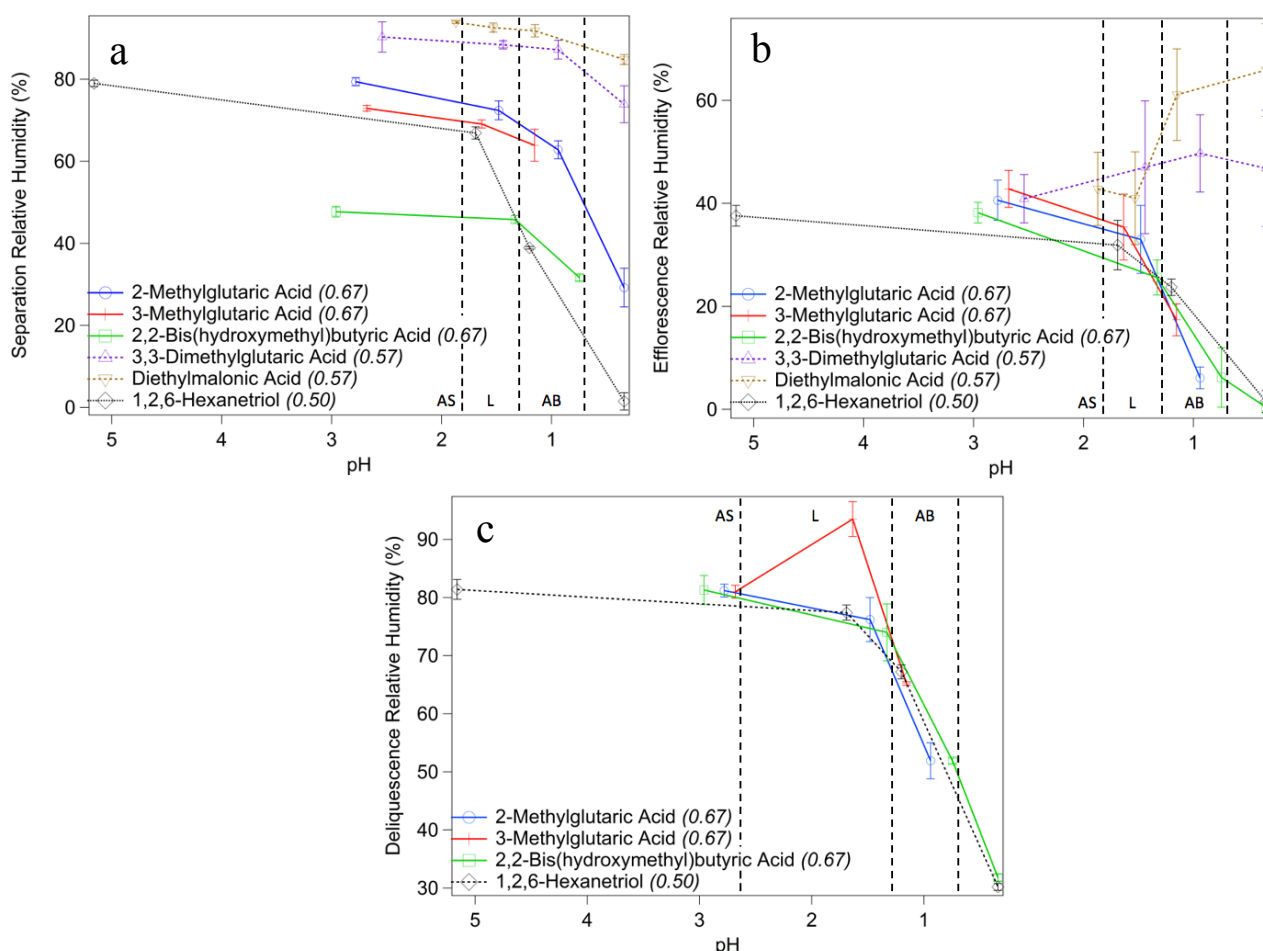


Figure 3-5: The separation relative humidities (a), efflorescence relative humidities (b), and deliquescence relative humidities (c) for each system studied plotted against bulk pH. The regions where the ammonium sulfate (AS), letovicite (L), and ammonium bisulfate (AB) are shown. Note: Ammonium bisulfate is expected to be the identity of the inorganic at low pH as well.

3.6 References

1. Ciobanu, V. G.; Marcolli, C.; Krieger, U. K.; Weers, U.; Peter, T. Liquid-Liquid Phase Separation in Mixed Organic/Inorganic Aerosol Particles. *J. Phys. Chem. A* **2009**, *113*, 41, 10966-10978.
2. Guo, H.; Xu, L.; Bougiatioti, A.; Cerully, K. M.; Capps, S. L.; Hite Jr, J. R.; Carlton, A. G.; Lee, S. H.; Bergin, M. H.; Ng, N. L.; Nenes, A.; Weber, R. J. Fine-particle water and pH in the southeastern United States. *Atmos. Chem. Phys.* **2015**, *15*, 9, 5211-5228.
3. Guo, H.; Sullivan, A. P.; Campuzano-Jost, P.; Schroder, J. C.; Lopez-Hilfiker, F. D.; Dibb, J. E.; Jimenez, J. L.; Thornton, J. A.; Brown, S. S.; Nenes, A.; Weber,

- R. J. Fine particle pH and the partitioning of nitric acid during winter in the northeastern United States. *J. Geophys. Res.-Atmos.* **2016**, *121*, 1-22.
4. Bougiatioti, A.; Nikolaou, P.; Stavroulas, I.; Kouvarakis, G.; Weber, R.; Nenes, A.; Kanakidou, M.; Mihalopoulos, N. Particle water and pH in the eastern Mediterranean: source variability and implications for nutrient availability. *Atmos. Chem. Phys.* **2016**, *16*, 7, 4579-4591.
5. Guo, H.; Liu, J.; Froyd, K. D.; Roberts, J. M.; Veres, P. R.; Hayes, P. L.; Jimenez, J. L.; Nenes, A.; Weber, R. J. Fine particle pH and gas-particle phase partitioning of inorganic species in Pasadena, California, during the 2010 CalNex campaign. *Atmos. Chem. Phys.* **2017**, *17*, 9, 5703-5719.
6. Losey, D. J.; Parker, R. G.; Freedman, M. A. pH Dependence of Liquid-Liquid Phase Separation in Organic Aerosol. *J. Phys. Chem. Lett.* **2016**, *7*, 19, 3861-3865.
7. You, Y.; Renbaum-Wolff, L.; Bertram, A. K. Liquid-liquid phase separation in particles containing organics mixed with ammonium sulfate, ammonium bisulfate, ammonium nitrate or sodium chloride. *Atmos. Chem. Phys.* **2013**, *13*, 23, 11723-11734.
8. Cacace, M. G.; Landau, E. M.; Ramsden, J. J. The Hofmeister series: salt and solvent effects on interfacial phenomena. *Q. Rev. Biophys.* **1997**, *30*, 3, 241-277.
9. Dentener, F. J.; Crutzen, P. J. A three-dimensional model of the global ammonia cycle. *J. Atmos. Chem.* **1994**, *19*, 4, 331-369.
10. Weber, R. J.; Guo, H.; Russell, A. G.; Nenes, A. High aerosol acidity despite declining atmospheric sulfate concentrations over the past 15 years. *Nature Geosci* **2016**, *9*, 4, 282-285.
11. Silvern, R. F.; Jacob, D. J.; Kim, P. S.; Marais, E. A.; Turner, J. R.; Campuzano-Jost, P.; Jimenez, J. L. Inconsistency of ammonium-sulfate aerosol ratios with thermodynamic models in the eastern US: a possible role of organic aerosol. *Atmos. Chem. Phys.* **2017**, *17*, 8, 5107-5118.
12. Colberg, C. A.; Krieger, U. K.; Peter, T. Morphological Investigations of Single Levitated H₂SO₄/NH₃/H₂O Aerosol Particles during Deliquescence/Efflorescence Experiments. *J. Phys. Chem. A* **2004**, *108*, 14, 2700-2709.
13. Colberg, C. A.; Luo, B. P.; Wernli, H.; Koop, T.; Peter, T. A novel model to predict the physical state of atmospheric H₂SO₄/NH₃/H₂O aerosol particles. *Atmos. Chem. Phys.* **2003**, *3*, 4, 909-924.
14. Martin, S. T.; Hung, H. M.; Park, R. J.; Jacob, D. J.; Spurr, R. J. D.; Chance, K. V.; Chin, M. Effects of the physical state of tropospheric ammonium-sulfate-nitrate particles on global aerosol direct radiative forcing. *Atmos. Chem. Phys.* **2004**, *4*, 1, 183-214.
15. Wang, J.; Hoffmann, A. A.; Park, R. J.; Jacob, D. J.; Martin, S. T. Global distribution of solid and aqueous sulfate aerosols: Effect of the hysteresis of particle phase transitions. *J. Geophys. Res.-Atmos.* **2008**, *113*, D11, 1-11.
16. Yao, X.; Ling, T. Y.; Fang, M.; Chan, C. K. Size dependence of in situ pH in submicron atmospheric particles in Hong Kong. *Atmos. Environ.* **2007**, *41*, 2, 382-393.
17. Koop, T.; Bertram, A. K.; Molina, L. T.; Molina, M. J. Phase Transitions in Aqueous NH₄HSO₄ Solutions. *J. Phys. Chem. A* **1999**, *103*, 45, 9042-9048.

18. Martin, S. T. Phase Transitions of Aqueous Atmospheric Particles. *Chem. Rev.* **2000**, *100*, 9, 3403-3454.
19. Clegg, S. L.; Seinfeld, J. H.; Brimblecombe, P. Thermodynamic modelling of aqueous aerosols containing electrolytes and dissolved organic compounds. *J. Aerosol Sci.* **2001**, *32*, 6, 713-738.
20. Lin, J.-S.; Tabazadeh, A. The effect of nitric acid uptake on the deliquescence and efflorescence of binary ammoniated salts in the upper troposphere. *Geophys. Res. Lett.* **2002**, *29*, 10, 1-4.
21. Martin, S. T.; Schlenker, J. C.; Malinowski, A.; Hung, H.-M.; Rudich, Y. Crystallization of atmospheric sulfate-nitrate-ammonium particles. *Geophys. Res. Lett.* **2003**, *30*, 21, 1-4.
22. Schlenker, J. C.; Martin, S. T. Crystallization Pathways of Sulfate–Nitrate–Ammonium Aerosol Particles. *J. Phys. Chem. A* **2005**, *109*, 44, 9980-9985.
23. Parsons, M. T.; Riffell, J. L.; Bertram, A. K. Crystallization of Aqueous Inorganic–Malonic Acid Particles: Nucleation Rates, Dependence on Size, and Dependence on the Ammonium-to-Sulfate Ratio. *J. Phys. Chem. A* **2006**, *110*, 26, 8108-8115.
24. Rosenoern, T.; Schlenker, J. C.; Martin, S. T. Hygroscopic Growth of Multicomponent Aerosol Particles Influenced by Several Cycles of Relative Humidity. *J. Phys. Chem. A* **2008**, *112*, 11, 2378-2385.
25. Li, Y. J.; Liu, P. F.; Bergoend, C.; Bateman, A. P.; Martin, S. T. Rebounding hygroscopic inorganic aerosol particles: Liquids, gels, and hydrates. *Aerosol. Sci. Tech.* **2017**, *51*, 3, 388-396.
26. Tabazadeh, A.; Toon, O. B. The role of ammoniated aerosols in cirrus cloud nucleation. *Geophys. Res. Lett.* **1998**, *25*, 9, 1379-1382.
27. Chen, Y.; DeMott, P. J.; Kreidenweis, S. M.; Rogers, D. C.; Sherman, D. E. Ice Formation by Sulfate and Sulfuric Acid Aerosol Particles under Upper-Tropospheric Conditions. *J. Atmos. Sci.* **2000**, *57*, 22, 3752-3766.
28. Zuberi, B.; Bertram, A. K.; Koop, T.; Molina, L. T.; Molina, M. J. Heterogeneous Freezing of Aqueous Particles Induced by Crystallized (NH₄)₂SO₄, Ice, and Letovicite. *J. Phys. Chem. A* **2001**, *105*, 26, 6458-6464.
29. Beyer, K. D.; Bothe, J. Ammonium Bisulfate/Water: A Pseudobinary System. *J. Phys. Chem. A* **2006**, *110*, 22, 7105-7112.
30. Murray, B. J.; Bertram, A. K. Inhibition of solute crystallisation in aqueous H⁺–NH₄⁺–SO₄²⁻–H₂O droplets. *Phys. Chem. Chem. Phys.* **2008**, *10*, 22, 3287-3301.
31. Froyd, K. D.; Murphy, D. M.; Lawson, P.; Baumgardner, D.; Herman, R. L. Aerosols that form subvisible cirrus at the tropical tropopause. *Atmos. Chem. Phys.* **2010**, *10*, 1, 209-218.
32. Bogdan, A.; Molina, M. J. Physical Chemistry of the Freezing Process of Atmospheric Aqueous Drops. *J. Phys. Chem. A* **2017**, *121*, 16, 3109-3116.
33. Seinfeld, J. H.; Pandis, S. N., *Atmospheric Chemistry and Physics: From Air Pollution to Climate Change*. John Wiley & Sons, Inc.: New York, 1998.
34. Rindelaub, J. D.; Craig, R. L.; Nandy, L.; Bondy, A. L.; Dutcher, C. S.; Shepson, P. B.; Ault, A. P. Direct Measurement of pH in Individual Particles via Raman

- Microspectroscopy and Variation in Acidity with Relative Humidity. *J. Phys. Chem. A* **2016**, *120*, 6, 911-917.
35. Dallemagne, M. A.; Huang, X. Y.; Eddingsaas, N. C. Variation in pH of Model Secondary Organic Aerosol during Liquid-Liquid Phase Separation. *J. Phys. Chem. A* **2016**, *120*, 18, 2868-2876.
 36. Craig, R. L.; Nandy, L.; Axson, J. L.; Dutcher, C. S.; Ault, A. P. Spectroscopic Determination of Aerosol pH from Acid-Base Equilibria in Inorganic, Organic, and Mixed Systems. *J. Phys. Chem. A* **2017**, *121*, 30, 5690-5699.
 37. Jang, M.; Czoschke, N. M.; Lee, S.; Kamens, R. M. Heterogeneous Atmospheric Aerosol Production by Acid-Catalyzed Particle-Phase Reactions. *Science* **2002**, *298*, 5594, 814-817.
 38. Limbeck, A.; Kulmala, M.; Puxbaum, H. Secondary organic aerosol formation in the atmosphere via heterogeneous reaction of gaseous isoprene on acidic particles. *Geophys. Res. Lett.* **2003**, *30*, 19, 1-4.
 39. Iinuma, Y.; Böge, O.; Gnauk, T.; Herrmann, H. Aerosol-chamber study of the α -pinene/O₃ reaction: influence of particle acidity on aerosol yields and products. *Atmos. Environ.* **2004**, *38*, 5, 761-773.
 40. Surratt, J. D.; Lewandowski, M.; Offenberg, J. H.; Jaoui, M.; Kleindienst, T. E.; Edney, E. O.; Seinfeld, J. H. Effect of Acidity on Secondary Organic Aerosol Formation from Isoprene. *Environ. Sci. Technol.* **2007**, *41*, 15, 5363-5369.
 41. Zhou, S.; Wang, Z.; Gao, R.; Xue, L.; Yuan, C.; Wang, T.; Gao, X.; Wang, X.; Nie, W.; Xu, Z.; Zhang, Q.; Wang, W. Formation of secondary organic carbon and long-range transport of carbonaceous aerosols at Mount Heng in South China. *Atmos. Environ.* **2012**, *63*, 203-212.
 42. Hinrichs, R. Z.; Buczek, P.; Trivedi, J. J. Solar Absorption by Aerosol-Bound Nitrophenols Compared to Aqueous and Gaseous Nitrophenols. *Environ. Sci. Technol.* **2016**, *50*, 11, 5661-5667.
 43. Gao, S.; Ng, N. L.; Keywood, M.; Varutbangkul, V.; Bahreini, R.; Nenes, A.; He, J.; Yoo, K. Y.; Beauchamp, J. L.; Hodyss, R. P.; Flagan, R. C.; Seinfeld, J. H. Particle Phase Acidity and Oligomer Formation in Secondary Organic Aerosol. *Environ. Sci. Technol.* **2004**, *38*, 24, 6582-6589.
 44. Zhang, Q.; Jimenez, J. L.; Worsnop, D. R.; Canagaratna, M. A Case Study of Urban Particle Acidity and Its Influence on Secondary Organic Aerosol. *Environ. Sci. Technol.* **2007**, *41*, 9, 3213-3219.
 45. Williams, L. R.; Long, F. S. Viscosity of supercooled sulfuric acid solutions. *J. Phys. Chem-US* **1995**, *99*, 11, 3748-3751.
 46. Williams, L. R.; Golden, D. M. Solubility of HCl in sulfuric acid at stratospheric temperatures. *Geophys. Res. Lett.* **1993**, *20*, 20, 2227-2230.
 47. Zobrist, B.; Marcolli, C.; Pedernera, D. A.; Koop, T. Do atmospheric aerosols form glasses? *Atmos. Chem. Phys.* **2008**, *8*, 17, 5221-5244.
 48. Koop, T.; Bookhold, J.; Shiraiwa, M.; Pöschl, U. Glass transition and phase state of organic compounds: dependency on molecular properties and implications for secondary organic aerosols in the atmosphere. *Phys. Chem. Chem. Phys.* **2011**, *13*, 43, 19238-19255.

49. Bodsworth, A.; Zobrist, B.; Bertram, A. K. Inhibition of efflorescence in mixed organic-inorganic particles at temperatures less than 250 K. *Phys. Chem. Chem. Phys.* **2010**, *12*, 38, 12259-66.
50. You, Y.; Bertram, A. K. Effects of molecular weight and temperature on liquid-liquid phase separation in particles containing organic species and inorganic salts. *Atmos. Chem. Phys.* **2015**, *15*, 3, 1351-1365.
51. Chebbi, A.; Carlier, P. Carboxylic acids in the troposphere, occurrence, sources, and sinks: A review. *Atmos. Environ.* **1996**, *30*, 24, 4233-4249.
52. Khare, P.; Kumar, N.; Kumari, K. M.; Srivastava, S. S. Atmospheric formic and acetic acids: An overview. *Rev. Geophys.* **1999**, *37*, 2, 227-248.
53. Grosjean, D. Atmospheric chemistry of alcohols. *J. Brazil. Chem. Soc.* **1997**, *8*, 433-442.
54. Kesselmeier, J.; Staudt, M. Biogenic Volatile Organic Compounds (VOC): An Overview on Emission, Physiology and Ecology. *J. Atmos. Chem.* **1999**, *33*, 1, 23-88.
55. Nguyen, H. T.-H.; Takenaka, N.; Bandow, H.; Maeda, Y.; de Oliva, S. T.; Botelho, M. M. f.; Tavares, T. M. Atmospheric alcohols and aldehydes concentrations measured in Osaka, Japan and in Sao Paulo, Brazil. *Atmos. Environ.* **2001**, *35*, 18, 3075-3083.
56. Bertram, A. K.; Martin, S. T.; Hanna, S. J.; Smith, M. L.; Bodsworth, A.; Chen, Q.; Kuwata, M.; Liu, A.; You, Y.; Zorn, S. R. Predicting the relative humidities of liquid-liquid phase separation, efflorescence, and deliquescence of mixed particles of ammonium sulfate, organic material, and water using the organic-to-sulfate mass ratio of the particle and the oxygen-to-carbon elemental ratio of the organic component. *Atmos. Chem. Phys.* **2011**, *11*, 21, 10995-11006.
57. Renbaum-Wolff, L.; Song, M.; Marcolli, C.; Zhang, Y.; Liu, P. F.; Grayson, J. W.; Geiger, F. M.; Martin, S. T.; Bertram, A. K. Observations and implications of liquid-liquid phase separation at high relative humidities in secondary organic material produced by α -pinene ozonolysis without inorganic salts. *Atmos. Chem. Phys.* **2016**, *16*, 12, 7969-7979.
58. Song, M.; Liu, P.; Martin, S. T.; Bertram, A. K. Liquid-liquid phase separation in particles containing secondary organic material free of inorganic salts. *Atmos. Chem. Phys. Discuss.* **2017**, *2017*, 1-29.
59. Choi, M. Y.; Chan, C. K. The Effects of Organic Species on the Hygroscopic Behaviors of Inorganic Aerosols. *Environ. Sci. Technol.* **2002**, *36*, 11, 2422-2428.

Chapter 4

Effect of Acidic Processing on Ice Nucleation on Fly Ash

Author Contributions: Sarah Sihvonen in the Freedman Lab began this project and did the XRD, ATR-IR, and ICP-AES analysis while overseeing the TEM, EDS, SAED, and sample preparation done by Daniel Veghte (Ph.D. 2014) and Andrea Sitton (rotating graduate student 2014). Losey contributed BET and immersion freezing data.

4.1 Introduction

Aerosol particles can serve as seeds for cloud condensation and ice formation. Cirrus clouds are of particular interest due to their ability to impact climate.¹⁻⁶ As cirrus clouds are made of ice crystals, factors promoting these clouds are of great interest to the scientific community.⁷⁻²⁴ Ice formation can take place using a foreign substance as a seed particle, called heterogeneous freezing, or freezing water droplets free of solid impurities, called homogeneous freezing. Homogeneous ice nucleation occurs at very low temperatures of <-40 °C,²⁵ while heterogeneous freezing can occur at higher

temperatures. Because of this, the properties of the substances that can serve as ice nuclei have been and continue to be extensively studied. While homogeneous ice nucleation has long been thought to be the primary pathway for ice nucleation, recent studies have cast doubt on that mechanism.^{11, 20, 26-27}

Combustion processes contribute significantly to aerosol content across the globe.²⁸⁻³⁰ These combustion processes can be natural in origin, such as in biomass burning, or anthropogenic, such as in industrial emissions related to coal combustion. The anthropogenic combustion of coal produces many materials that are emitted into the atmosphere, one of which is fly ash, a major byproduct of the coal burning process. Fly ash is a silicate glassy material that primarily contains oxides of silica, aluminum, calcium and iron.³¹ An estimated 8000 million tons of coal are burned daily worldwide, resulting in sizable amounts of produced fly ash.³² The produced fly ash is collected and is often reused in concrete and grouting production.³¹ However, some fly ash is stored in landfills, and emission into the atmosphere can occur from wind action.³¹ Additionally, a portion of fly ash produced is also emitted into the atmosphere as field studies close to coal burning stacks have found.³³ Once in the atmosphere, fly ash can contribute to cloud formation by serving as cloud condensation nuclei to form a liquid drop or ice nucleating material to form an ice particle.^{26, 34} Because most fly ash is sub-micron sized and able to undergo long range atmospheric transport,³³ it can be involved in heterogeneous chemistry, such as acidic processing. This can alter the fly ash properties and atmospheric impact. Fly ash particles are alkaline because they contain CaO and MgO, which could increase the complexity of reactions that fly ash undergoes.³⁵ Exposure to acidic materials is likely since SO₂ and NO₂, which can be oxidized to

sulfuric and nitric acid, are co-emitted with fly ash. The effect of this exposure to sulfuric acid on the ice nucleation of fly ash has not been explored despite the co-location of the two substances, but sulfuric acid coatings and acid treatment has been extensively investigated on mineral dust.^{9, 12, 14-16, 19, 21} Sulfuric acid treatment decreased the ice nucleation efficiency of the studied mineral dust. Sullivan et al. found that exposure to sulfuric acid led to irreversible effects on the ice nucleation efficiency, even with heating and exposure to ammonia, suggesting that the effect is a chemical and/or physical change in the particles.¹²

Acidic processing of fly ash has been extensively studied to understand leaching of aluminum, iron, and magnesium.³⁶⁻³⁷ In large regions of the oceans, phytoplankton are iron-limited, and the availability of iron dictates the productivity of these organisms.³⁸⁻⁴⁰ If the phytoplankton were not iron limited they could significantly reduce atmospheric levels of CO₂.³⁸⁻³⁹ A large portion of the iron for these organisms comes from iron dissolved from atmospheric deposits into the ocean. This fact highlights the importance of understanding the amount of bioavailable iron in aerosol deposits into these nutrient poor regions of the ocean. While aluminosilicate-containing mineral dust is considered a significant source of iron to these regions, the iron in mineral dust is difficult to leach from the well-ordered aluminosilicate framework.³⁵ Similar to mineral dust, fly ash also only has a small amount of soluble material,³³ and the amount of soluble material changes during sulfuric acid processing. Changes to the iron content of fly ash and mineral dust due to acidic processing have been shown to significantly increase the content of bioavailable iron.^{35, 37, 41-42} The leaching of the iron from the fly ash particles can create pores.⁴³ More iron is made bioavailable from acid-processed fly ash than acid-

processed mineral dust.³⁵ As a result, fly ash is expected to be an important source of iron to the oceans. The acidic processing of the fly ash is self-inhibited, however, through the production of calcium sulfate which can coat the particles, blocking pores, and reactive material within the particle.^{41, 43-44}

The composition and morphology of fly ash differs based on the type of coal.³¹ Fly ash can be described as Class C, resulting from the burning of lignite or sub-bituminous coal, or Class F, resulting from the burning of anthracite or bituminous coal. The primary difference between the two classes is that Class C has a high amount of calcium, while Class F has a high amount of iron. When pulverized coal is burned in the furnace, the impurities in the coal melt and convert to a new form. Clays convert to amorphous, aluminosilicate glass spheres, and other metal-containing phases generally convert to the oxide of the metal. The molten materials form into spheres, which then rapidly cool, locking the shape into place. These changes occur during the average 3-4 seconds coal spends in the furnace.³¹ The resulting fly ash is mostly amorphous spheres of Si and some Al with a smaller fraction of crystalline metal oxide, which is mainly calcium or iron oxide.^{31, 33-35}

A more complete understanding of the impact of fly ash in the atmosphere is limited because fly ash is challenging to distinguish from mineral dust in field studies using commonly employed instrumentation such as mass spectrometry, due to their similar elemental compositions. However, their morphologies vary, empowering microscopy techniques to differentiate the two species. Mineral dust is usually irregularly shaped as a layered, crystalline structure, and fly ash tends to be spherical with small irregularly shaped crystalline particles, that are hard to distinguish from mineral dust,

interspersed throughout. Once the samples are mixed, however, only the spherical particles in fly ash can be readily distinguished from mineral dust. In addition, laboratory studies, as opposed to field studies, can take advantage of more composition-probing techniques that would be difficult to translate to field work. It is worthwhile to distinguish between mineral dust and fly ash because while their atmospheric impact may be similar, their emission sources are different. The emission of fly ash is influenced by the worldwide use of coal and is impacted by legislation, while mineral dust is emitted by wind action over arid areas of the Earth. If fly ash is always counted as mineral dust and the emissions of fly ash change significantly or the proportions of the types of coal burnt changed then the predicted climatic impact of these materials will be incorrect.

Fly ash can alter cloud properties in the lower troposphere by serving as a cloud condensation nucleus.³³ To serve as a cloud condensation nucleus, the particle needs to uptake water and form a droplet. Thin, hygroscopic coatings containing Ca, Na, and S exist on the surface of fly ash.^{33, 35} This water-soluble coating forms as the particles cool after the coal is combusted. As Si and Al are less volatile than the coating elements, Ca, Na, and S deposit onto the surface of the Si- and Al-containing spheres.³³ Parungo et al. found that 60% of fly ash can uptake water even at water-subsaturated regions.³³ This small amount of material is sufficient to allow fly ash to serve as a cloud condensation nucleus.³³

The efficiency of fly ash to serve as an ice nucleating particle is not well understood. Due to the water-soluble coating found on fly ash, immersion (when the particle is in a water droplet) and/or condensation freezing (when water condenses before freezing) is likely. Since fly ash is commonly identified as mineral dust in field studies,

not as much work has been done exploring the ice nucleating properties of fly ash. Only a couple studies have explored the ice nucleation ability of fly ash. Umo et al. concluded that the ice nucleation activity of fly ash had similar ice nucleating activity to clay minerals, but is less active than quartz, feldspars, and desert dusts in the immersion mode.³⁴ Another study that compared different types of ash, including wood ash from different sources, coal bottom ash, and fly ash, concluded that of the systems studied, fly ash had the highest ice nucleation efficiency.⁴⁵ Based on laboratory measurements, quartz has been suggested to be the second most efficient immersion mode nucleus after feldspars.⁴⁶ Since fly ash does contain quartz, that component may play a favorable role in the immersion mode freezing results. The presence of quartz in volcanic ash samples has been suggested to play a role in the immersion freezing behavior.²⁴ Parungo et al. also found fly ash to be capable of serving as an ice nucleating particle.³³ The freshly emitted fly ash was less efficient than fly ash that was stored in a vacuum chamber, indicating that the volatile material that is co-emitted with fly ash can reduce the ice nucleating efficiency of fly ash. One field study that distinguished between mineral dust and fly ash particles in ice residues in cirrus clouds using microscopy and found that ~7% of the ice formed from nucleating on fly ash.²⁶ These results demonstrate that fly ash can play an important role for ice nucleation. The properties of fly ash are likely to change with atmospheric processing as well.³⁴ No studies have investigated the ice nucleation activity of aged fly ash, but aging possible ice nuclei through acidic processing has been shown previously to have an effect on the ice nucleation behavior of mineral dust.²¹

In this study, the physical and chemical properties of four fly ash samples representative of emission from around the United States are explored before and after

acid treatment. X-ray diffraction (XRD), attenuated total reflectance infrared spectroscopy (ATR-IR), transmission electron microscopy (TEM) with selected area electron diffraction (SAED) and energy dispersive spectroscopy (EDS), inductively coupled plasma-atomic emission spectroscopy (ICP-AES), Brunauer-Emmett-Teller (BET) surface area analysis, and immersion freezing are used to explore the properties of fly ash and its freezing activity. The effects of sulfuric acid-treatment and water-treatment are investigated to mimic atmospheric processing.

4.2 Experimental Methods

Four fly ash samples of three different Class types were chosen. Two Class C fly ash, Joppa (Joppa Generating Station, Joppa IL) and Welsh (Welsh Generation Station, Pittsburg, TX), a hybrid Class C/F fly ash, Clifty (Clifty Creek Power Plant, Madison, IN), and a Class F fly ash, Miami (Miami Fort Generation Station, North Ben, OH) were used for these studies. All fly ash samples were obtained through Fly Ash Direct, a service of Waste Management, Inc. The fly ash was treated with sulfuric acid or water following the same procedure. 0.4 grams of fly ash was combined with 15 mL 0.10 M sulfuric acid (EMD, ACS Reagent grade) or ultrapure water (HPLC grade, Fisher). After agitation for 1.5 hours at an atmospherically relevant pH range for the upper troposphere,⁴⁷ the samples were centrifuged and the supernatant was collected for analysis. The fly ash was allowed to dry by evaporation for several days and/or put into an oven for 3 hours at 110 °C to aid in this process. The supernatant collected was used in ICP-AES analysis. The samples were lightly ground with a mortar and pestle before analysis. The samples were each submitted for Brunauer-Emmett-Teller analysis to determine surface area with N₂ as the flow gas.

For the XRD experiments, an X-ray diffractometer with Cu K α radiation with a current of 40 mA and a voltage of 45 kV was used. Bulk powder samples were front loaded in a zero-background silicon holder. Goniometer angles were set from 5 to 70° 2 θ with a 0.0263° 2 θ step size and a scan step time of 96.4 s. A beam knife was used to reduce low angle scattering. The XRD diffractograms were analyzed using Jade XRD libraries. The ATR-IR spectra were obtained using an average of 100 scans at resolution of 4 cm⁻¹. Samples for TEM were prepared using aerosol that was dry-generated from the untreated and acid-treated minerals, which were impacted on continuous carbon coated copper grids (SPI Supplies). During the TEM analysis, SAED and EDS were performed to investigate the degree of crystallinity and elemental composition, respectively.

The immersion ice nucleation experiments were performed using the lab-built immersion chamber (Figure 4-1). 2 μ L droplets of a 0.3 wt% fly ash in ultrapure water solution were pipetted onto a hydrophobically coated slide (Hampton research) which is then placed inside the chamber. While taking pictures every 0.5 C, the chamber is cooled by flowing nitrogen through a copper coil submerged in liquid nitrogen. The flow was adjusted to allow for a -3 deg C/minute cooling rate.

The cumulative number of particles frozen at a given temperature ($n(T)$) were recorded to calculate the cumulative fraction of particles frozen (f_{ice}) using the following equation:

$$f_{ice} = \frac{n(T)}{N} \quad (4-1)$$

where N is the total number of particles. In order to rule out background freezing from the Millipore water, freezing experiments were done with pure Millipore water (206

particles in total). Using the procedure outlined in O'Sullivan et al., the fraction of particles frozen at a specific temperature, $F(T)$, from each trial was used to calculate $K(T)$, the number of nucleation sites per milliliter water at that temperature for each Millipore and fly ash trial as follows:

$$K(T) = \frac{-\ln(1-F(T))}{V} \times d \quad (4-2)$$

where V is the droplet volume in milliliters and d is the dilution factor.⁴⁸ The average $K(T)$ at each temperature for the Millipore water is then subtracted from the average $K(T)$ calculated for each fly ash experiment. The cumulative number of surface sites per unit area as a function of temperature (n_s) is calculated from the $K(T)$ using the following equation:

$$n_s = K(T) \times C^{-1} \quad (4-3)$$

where C is the total surface area of fly ash in a given volume, which is calculated using the BET surface area and mass percent fly ash in each experiment. The n_s is calculated at each temperature and its standard deviation is calculated using the standard deviation of $K(T)$ over each trial.

4.3 Results and Discussion

The fly ash used in this study is classified into 3 categories: Class C, Class F, and a hybrid Class C/F. The elemental compositions for each fly ash sample were determined using wet chemical techniques as specified by regulatory guidelines and were certified by Resource Materials Testing Inc.⁴⁹ As seen in Table 4-1, Si is the primary component of all fly ash with Al also being a major component. Class C fly ash, Joppa and Welsh, have

a high amount of Ca. Class F has the smallest amount of Ca, but the highest amount of Fe. Class C/F has almost equal amounts of Ca and Fe. To a lesser extent, Mg, Na, K, and S are also present in every fly ash type. It is important to note that the metal element in the sample may not be in the form of the chemical formula listed in Table 4-1.

Table 4-1: The composition of the fly ash samples

Chemical	Class C		Class C/F	Class F
	Joppa (%)	Welsh (%)	Clifty (%)	Miami (%)
SiO ₂	38.84	34.03	43.13	46.47
Al ₂ O ₃	19.53	18.23	21.31	21.50
Fe ₂ O ₃	5.44	5.68	12.39	22.17
CaO	24.27	26.89	11.78	3.41
MgO	4.88	6.32	2.51	1.02
Na ₂ O	1.62	2.52	2.22	0.64
K ₂ O	0.69	0.42	1.34	2.32
SO ₃	1.42	1.98	2.82	1.13

The XRD results show only the crystalline phases present in each fly ash sample. Table 4-2 and Figure 4-1 show the results of this analysis. The results indicate many crystalline components, but a fair amount of amorphous material is present, which is most notable in the Clifty and Miami samples, indicated by the large hump in the background of each sample. The primary crystalline component of each sample is quartz and is identified as Q in the diffraction patterns. Smaller amounts of mullite, hematite, magnetite, anhydrite, lime, calcite, and periclase are also present in most samples (Table 4-2). Each fly ash type is composed of a complex mixture of these components. XRD shows that fly ash is largely composed of amorphous material such as an aluminosilicate glass with some crystalline components, a description that is largely supported by literature.^{31, 34} The water wash did not change the overall diffraction pattern compared to

the untreated fly ash for every samples indicating that the amount of crystalline water-soluble material is low and that the crystalline components are unaffected by water. This is expected from previous studies.^{31, 34} After acid-treatment however, gypsum ($\text{Ca}(\text{SO}_4) \cdot 2\text{H}_2\text{O}$) is present as the major product (Table 4-2 and Figure 4-1). This product is only detected on the fly ash from Class C and Class C/F. This is expected because the high amount of Ca in these fly ash types. The amount of gypsum formed by the Class C samples, Joppa and Welsh, appears to be higher than the amount formed by Clifty, which is Class C/F. This directly corresponds to the overall amount of Ca in these samples as indicated by Table 4-1. Even after acid treatment, calcium oxide peaks are still present in the diffraction pattern for these samples indicating that not all of the Ca is available for the reaction and/or unreactive. The Clifty sample also has hematite and magnetite present, but these components are present to a much smaller extent than gypsum and quartz.

The Class F Miami sample does not have the same reactivity as the Class C and C/F samples. First, as seen in Table 4-2 and Figure 4-1, the Class F sample has Fe present as hematite and magnetite like the Clifty sample but to a greater extent. These components, along with quartz compose most of the crystalline material of each Miami sample. There is a high amount of amorphous material present in the Miami sample as indicated by the broad hump in the data. The high noise in the data is a result of the Fe in the sample fluorescing in the copper X-ray beam. It is present in the Clifty sample as well, although to a lesser extent. Overall, there are no major changes in the Miami sample with water or acid treatment. This indicates that no crystalline phases are created or

altered through these treatments. A small amount of salt is possible, but it is below the detection limit.

Table 4-2: Crystalline fly ash components identified using XRD.

Mineral	Chemical Formula	Class C		Class C/F	Class F
		Joppa	Welsh	Clifty	Miami
Quartz	SiO_2	X	X	X	X
Mullite	$\text{Al}_{2.35}\text{Si}_{0.64}\text{O}_{4.82}$	X	X		X
Hematite	Fe_2O_3		X	X	X
Magnetite	Fe_3O_4	X		X	X
Anhydrite	CaSO_4	X	X	X	
Lime	CaO	X	X	X	X
Calcite	CaCO_3	X	X	X	
Periclase	MgO	X	X	X	X
Products after acid-treatment					
Gypsum	$\text{Ca}(\text{SO}_4) \cdot 2\text{H}_2\text{O}$	X	X	X	

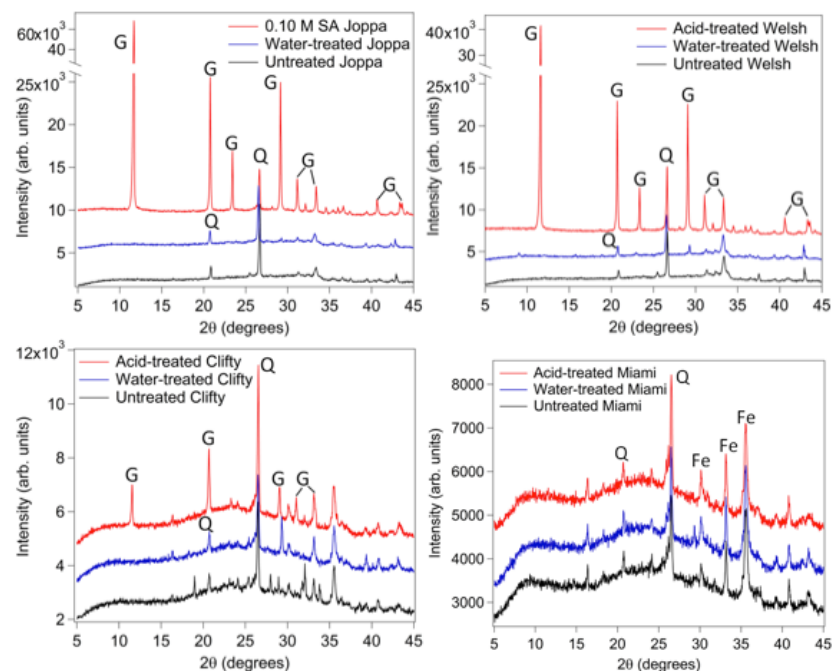


Figure 4-1: The XRD data for untreated, acid-treated, and water-treated Class C Joppa and Welsh, Class C/F Clifty, and Class F Miami fly ash. Major components, quartz (Q), gypsum (G), and iron oxide (Fe) are marked on each diffraction pattern.

ATR-IR was used to further characterize the fly ash samples to examine the samples for changes in the functional groups present. A small amount of water is still present in several of the water-treated samples as seen with a broad stretch at 1200 and 3200 cm^{-1} (Figure 4-2). The broad stretches at $<1300 \text{ cm}^{-1}$ indicate metal bonding such as Al-O, Si-O, Ca-O, and Fe-O and are present in all the fly ash samples.⁵⁰ As the XRD results indicated, there are no major changes between the water-treated and untreated fly ash samples. In the Class C and Class C/F fly ash, gypsum can be seen as indicated by the broad stretch at 1100 cm^{-1} and sharper stretches at 1624, 1681, 3396, and 3521 cm^{-1} .⁵¹ The results for the Miami fly ash also support the results from the XRD analysis where there is no change with acid-treatment (Figure 4-1 and Figure 4-2).

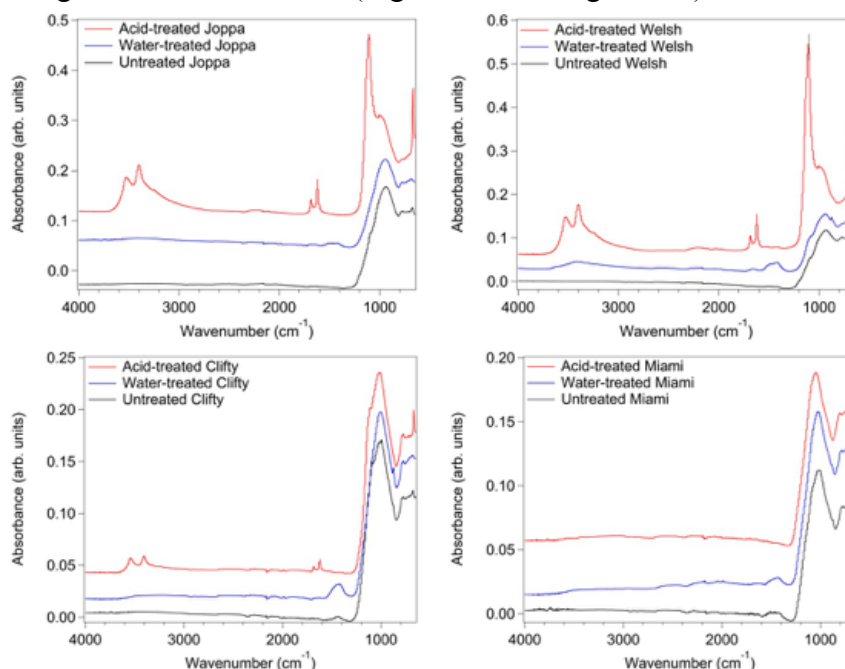


Figure 4-2: The ATR-IR data for untreated, acid-treated, and water-treated Class C Joppa and Welsh, Class C/F Clifty, and Class F Miami fly ash.

The TEM analysis provides information about the morphology of the fly ash samples. Selected area diffraction (SAD) was also used to determine the crystallinity of

the particles present. Additionally, EDS was used to determine the elemental composition of selected particles. Representative TEM images of the particle types observed in the untreated Class C samples and Class C/F Clifty are shown in Figure 4-3 a and b, and representative TEM images for the same samples after acid treatment are shown in Figure 4-3 b and c. The elemental compositions of the particles shown in Figure 4-3 are shown in Figure 4-4 as EDS spectra. As indicated by the diffuse halo in the SAD in the inset of Figure 4-3a the samples have many amorphous spherical particles, consistent with the silicate glass being a component of fly ash. Attached to the larger spherical particles are smaller, irregularly shaped crystalline materials as indicated by the bright spots in the SAD inset in Figure 4-3b. The large particle and attached smaller particles contain primarily Ca with smaller signals from Mg, Al, Si, P, Ti, and Fe (Figure 4-4a). The presence of Ti was unexpected based on the elemental analysis in Table 4-1 and XRD analysis in Table 4-2. However, small concentrations of Ti are found in the ICP-AES results of the Class C/F Clifty sample. In Figure 4-4b corresponding to the small crystalline particles seen in Figure 4-3b calcium is again the primary signal with smaller signals from Si, P, and S. This analysis is consistent with a quartz particle with a soluble coating containing P and S. The mixture of many elements in the EDS results highlights how the formation of fly ash results from the cooling of many intermixed impurities in coal. Overall, these results are in agreement with Table 4-1 and other studies that performed elemental analysis on fly ash.³³⁻³⁴

After acid exposure, large crystals appeared throughout the Class C and Class C/F samples as shown in Figure 4-3c. The well-ordered bright spots in the SAD inset indicates the material is highly crystalline and the EDS spectra of the particle in Figure 4-

4c shows the presence of Ca and S indicating that this particle is likely the gypsum also observed in the XRD and ATR-IR. The morphology around the large spherical particles changed slightly, such that the smaller particles appear to be more of a coating than before acid treatment, as shown in Figure 4-3d. The larger particle with coating in Figure 4-3d is composed of primarily Al and Si with smaller signals from K, Ca, and Fe as shown in the EDS spectrum in Figure 4-4d. The lack of S signal indicates that the gypsum crystals are localized. The Clifty sample behaves like the Class C samples, but with less calcium sulfate observed.

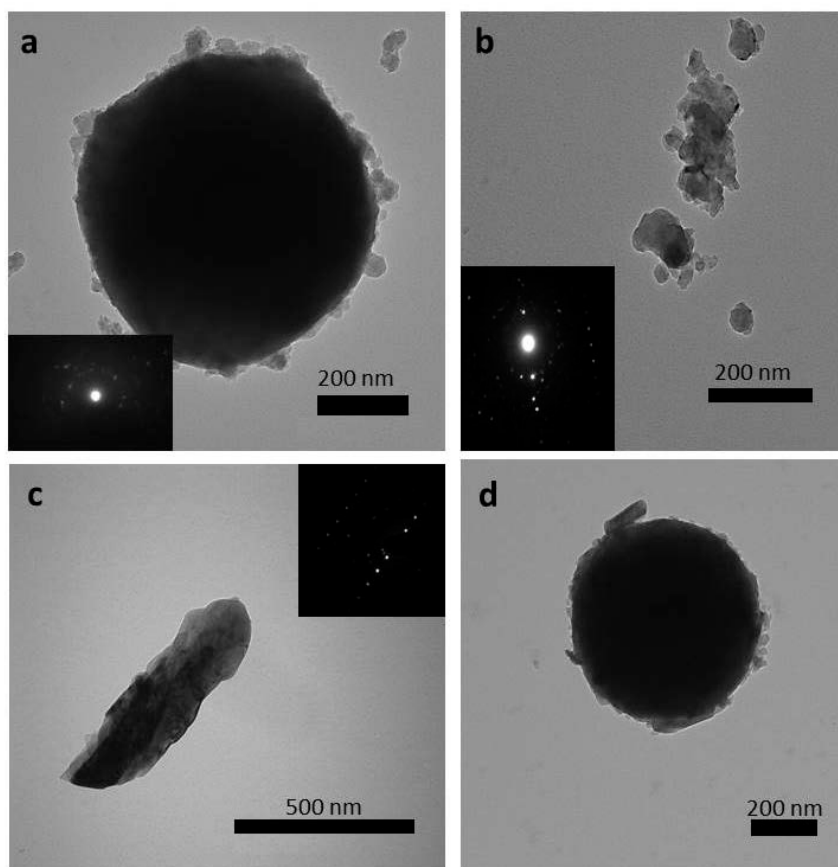


Figure 4-3: Representative TEM images for Class C and C/F fly ash particles (a and b) and acid-treated Class C and C/F fly ash particles (c and d). Insets in a, b, and c are SAD patterns showing crystallinity.

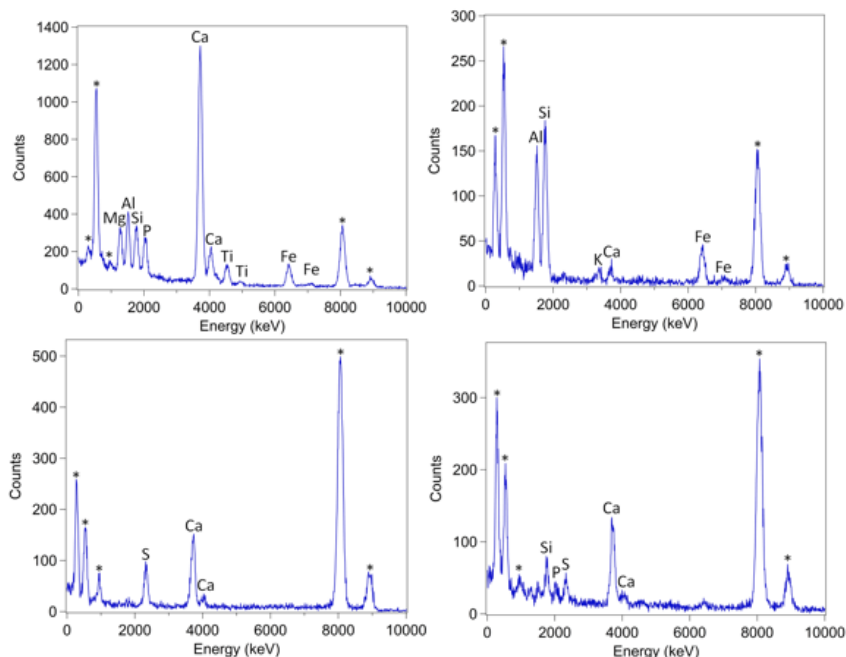


Figure 4-4: EDS spectra of the particles shown in Figure 4-4. The untreated samples are shown in a and b and the acid-treated samples are shown in c and d. The labels from Figure 4-4 correspond to the same letter in this figure. The elements are labeled by symbol in each spectrum. EDS peaks from background signals of C, O, and Cu are denoted by *.

The morphology of the Miami sample as seen in the TEM images in Figure 4-5 a and b is different from the other fly ash samples. While the spheres with small amounts of crystalline materials around them are observed, some soot-like structures and more irregular particles with a similar appearance to mineral dust are observed as well as seen in Figure 4-5 a and b. The soot-like structure is not composed of C, but is composed of relatively equal amounts of Si, Al, S, Ca, and Fe as seen in the EDS spectrum in Figure 4-6a. The mineral-like structure in Figure 4-5 b is primarily composed of Si with smaller signals from Al, Mg, K, and Fe as seen in Figure 4-6b. After acid treatment, the particle shapes were less distinct, and fewer small particles were observed, perhaps a result of dissolution (Figure 4-5 c and d). The mineral structure after acid treatment

appears eroded and is primarily composed of Si with smaller amounts of Al, S, and Fe (Figure 4-6c). The spherical particle in Figure 4-5d is primarily composed of Si and Al with smaller amounts of S, K, and Fe as seen in Figure 4-6d. The XRD and ATR-IR results indicate that the Miami sample is less reactive than the Class C Joppa and Welsh and Class C/F Clifty samples. However, the TEM shows that there are morphological changes as a result of acid treatment.

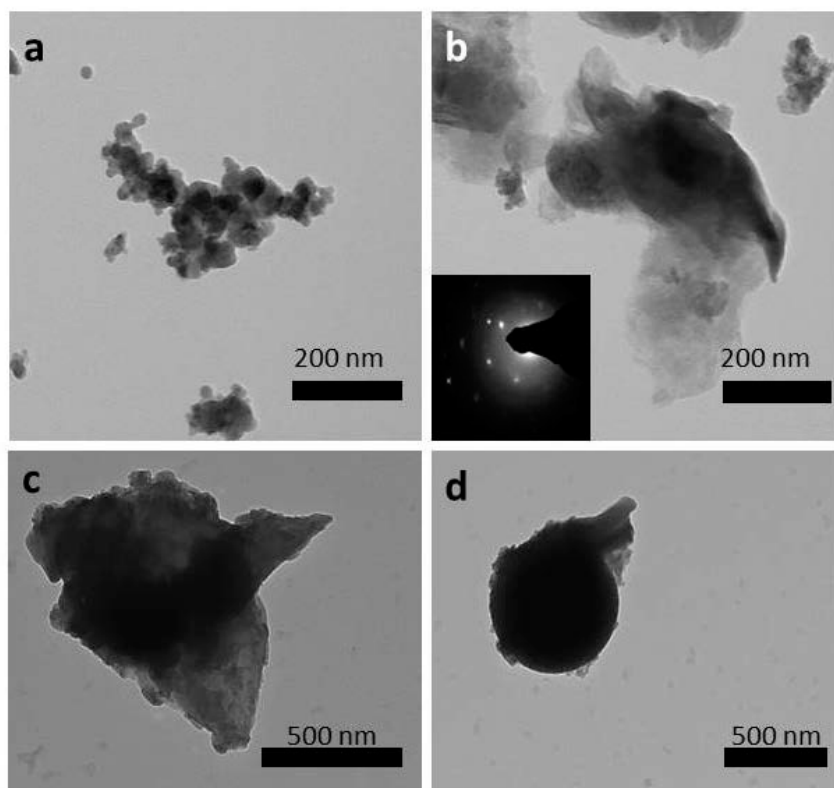


Figure 4-5: Representative TEM images for Class F Miami fly ash particles (a and b) and acid-treated Class F Miami fly ash particles (c and d). Insets in a, b, and c are SAD patterns showing crystallinity.

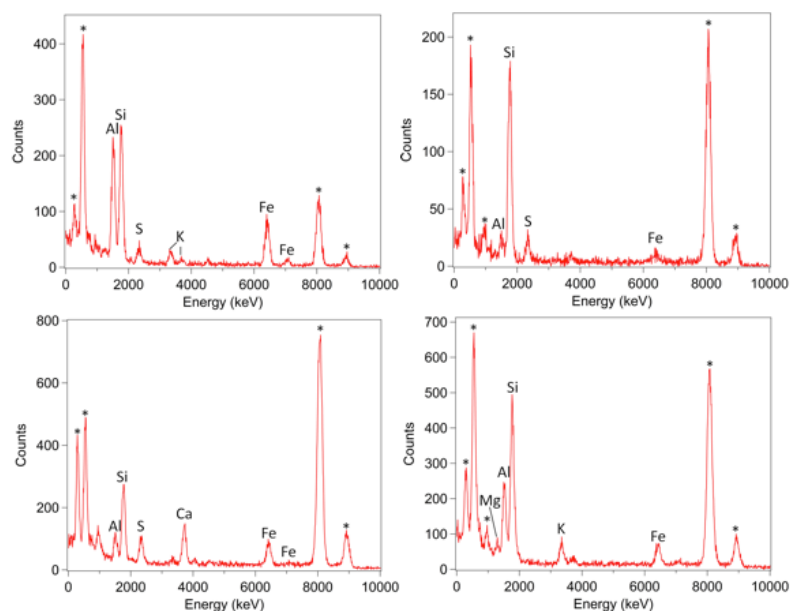


Figure 4-6: EDS spectra of the particles shown in Figure 4-5. The untreated samples are shown in a and b and the acid-treated samples are shown in c and d. The labels from Figure 4-5 correspond to the same letter in this figure. The elements are labeled by symbol in each spectrum. EDS peaks from background signals of C, O, and Cu are denoted by *.

ICP-AES analysis was performed on the supernatants in order to quantitatively examine the cations after water and acid treatment. The Class C fly ash samples released small amounts of Ca, Na and S into the supernatant during the water wash, as seen in Figure 4-7. The Clifty sample released mainly Na and S into the supernatant during water treatment. The high amount of Na in the water-treated Class C/F Clifty sample relative to the other samples indicates that the sodium content of Clifty is primarily in a water-soluble form. These results indicate (aside from Na in Clifty) that there is a small amount of water soluble material containing S, Na and Ca on these samples. Parungo et al. also found only small amounts of soluble material containing S.³³ The sulfuric acid leached a greater quantity and variety of cations from the fly ash than the water did. Data for S in the acid-treated samples is shown as 0 because the S from the fly ash is masked

by the S in the sulfuric acid. The release of Ca, Mg, Si and Al were the most enhanced in the Joppa and Welsh samples. The Clifty sample released mainly Ca, Na, Al, and Si, along with some Fe. The release of multiple cations suggests the possibility that a larger variety of sulfate salts are made in addition to gypsum, but that they are in too small of an amount to distinguish in the diffractograms and ATR-IR spectra. The ICP-AES results for Miami show that some soluble Ca and S dissolved upon water treatment (Figure 4-7). Smaller amounts of Al and Si were removed during acid treatment than in the Class C and Class C/F fly ash samples. However, the Class F Miami and Class C/F Clifty sample released more Fe during the acid-treatment. The Miami sample released approximately the same amount of Ca as the other fly ash samples during acid-treatment. However, no evidence of the formation of gypsum was found in the XRD, ATR-IR, or EDS analysis. These finding indicate that samples with high amounts of Ca are more reactive to acid treatment, but the samples with high Fe content release more Fe during acid treatment.

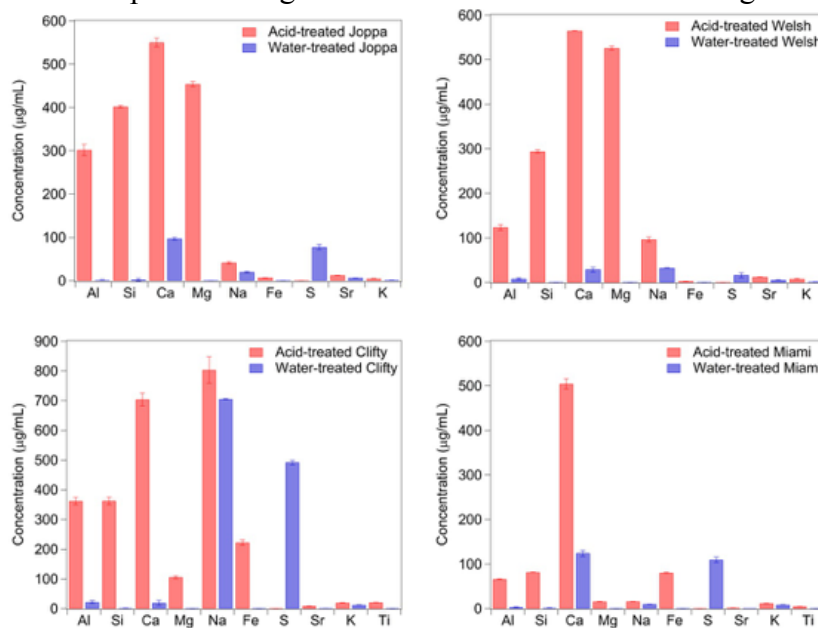


Figure 4-7: The ICP-AES results for the supernatant collected from the water-treated and acid-treated Class C Joppa and Welsh, Class C/F Clifty, and Class F Miami fly ash samples.

Immersion freezing analysis was done to determine the effect of the elemental and morphological changes on ice nucleation. Low weight percent suspensions of the fly ash were made to ensure that the fly ash was well mixed during the experiments (Table 4-3). In order to parameterize the freezing events against the surface area available for nucleation, BET analysis was performed (Table 4-3). Class C fly ash, Joppa and Welsh, and Class F ash both showed an increase in the surface area of the acid-treated samples compared to the water-treated samples. This could be attributed to acid exposure etching away the edges of particles leading to a higher overall surface area. The Class C/F Clifty fly ash showed a slight decrease in surface area with the acid-treated samples. Recent literature has suggested the importance of pore size on ice nucleation behavior,⁵² so the pore width of each sample was also recorded. In every case, the pore width was smaller for the acid-treated sample. This is somewhat unexpected due to previous studies observing an increase in pore size when kaolinite and montmorillonite, different aluminosilicate clays, were treated with sulfuric acid,⁵³⁻⁵⁴ but the complexity of the fly ash in comparison could explain the difference.

Table 4-3: The BET, pore width, and onset, end, and 50% frozen part for each fly ash experiment.

			BET (m ² /g)	Pore width (nm)	IN Onset (°C)	IN End (°C)	50% Frozen (°C)
Class C	Joppa	Water-treated	8.72	9.38	-8	-30	-24
		Acid-treated	21.69	5.06	-17.5	-28	-25
	Welsh	Water-treated	7.76	9.84	-16	-29.5	-23
		Acid-treated	19.58	6.68	-16.5	-26	-23.5
Class C/F	Clifty	Water-treated	8.88	7.02	-18.5	-29	-25
		Acid-treated	6.24	5.07	-15.5	-28	-24.5
Class F	Miami	Water-treated	3.92	5.40	-12.5	-28.5	-23.5
		Acid-treated	6.17	3.41	-13.5	-24	-20.5

Table 4-3 and Figure 4-8a also show the freezing behavior of each fly ash sample. The onset of freezing ranges from -8 to -18.5 °C, and the end of freezing is from -24 to -30 °C. The temperature at which 50% of the particles are frozen is listed. Using this information, it is clear that each fly ash Class behaved differently. The Class C fly ash samples, Joppa and Welsh, had the water-treated samples freeze at slightly higher temperatures compared to the acid-treated samples. The opposite is seen for the Class C/F sample, Clifty. The biggest difference is seen in the Class F, Miami, sample which has the acid-treated sample freeze several degrees warmer than the water-treated sample. The background freezing of Millipore water is also plotted in the fraction frozen plot showing that every fly ash sample led to heterogeneous freezing of the water droplets.

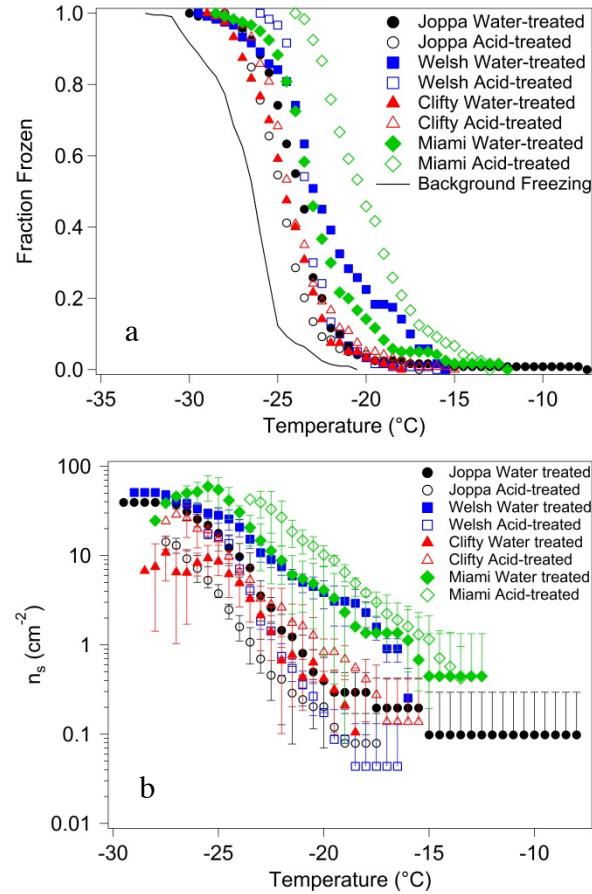


Figure 4-8: The fraction frozen for the water-treated and acid-treated (marked with SA) fly ash samples with the background freezing due to Millipore water (a) and the n_s plot for each sample with the standard deviation.

To control for the effect of particle size on the freezing behavior of the fly ash samples, the BET results were used to parameterize the results according to surface area. These results are plotted as the number of active sites in a given surface area vs temperature (Figure 4-8b). These results confirm that the Class F Miami acid-treated sample is a better immersion freezing ice nucleus than both its water-treated counterpart and every other sample. Similarly, the Class C/F, Clifty, sample also showed better freezing efficiency with the acid-treated sample compared to the water-treated sample.

The Class C samples, Joppa and Welsh, however, both showed better freezing efficiency with the water-treated samples.

The freezing efficiency showed no correlation to the overall pore width across all samples so the change in pore size is not the reason for the changes in ice nucleation. Instead, it could be related to the reaction products from acid-treatment. When Class C fly ash is treated with sulfuric acid, gypsum is produced and this could block sites for ice nucleation during these experiments. Class C/F and F fly ash both produced little to no gypsum so this was not a factor. Unlike previous studies however, the sulfuric acid-treatment led to better ice nucleation ability. No products were produced and the only major difference was the specific leaching of Fe, which is not expected to have a major difference than leaching of Al, Si, Ca, Mg, or Na which were major leachants for the other samples. Further characterization should be done to better understand why ice nucleation efficiency is affected in this way.

4.4 Conclusions and Atmospheric Implications

This study indicates that fly ash is capable of participating in heterogeneous reactions in the atmosphere. Since fly ash has a soluble coating, it is likely to undergo aqueous chemistry. The fate of Fe in the fly ash before and after acidic-processing is of particular interest due to its importance in the biogeochemical cycle. The solubility of Fe from fly ash was found to be greater than in mineral dust. Chen et al. found that after 1.5 hours of acidic processing at pH 1, about 3 mg Fe/g fly ash was released from a class F fly ash.³⁵ This study used sulfuric acid at a pH of 1 to process the fly ash, but no control was taken to monitor the pH after addition. The class C/F Clifty fly ash sample in this study released 8.3 mg Fe/g fly ash, and the Class F Miami sample released 3.0 mg Fe/g

fly ash after 1.5 hours of acidic processing. The Class C fly ash samples Joppa and Welsh released 0.25 and 0.084 g Fe/g fly ash, respectively. This result is consistent with previous literature which found that the total iron released does not always correspond to the surface area or the iron content of the sample, indicating that the speciation and chemical environment is necessary to know how much leaching will occur.⁴² These results highlight the importance of the type of fly ash on the heterogeneous chemistry and overall environmental impact. Ultimately, acidic processing in the aqueous phase in contact with the solid fly ash surfaces does alter the environmental impact of fly ash.

Fly ash treated with sulfuric acid reacted, in most cases, to form gypsum ($\text{CaSO}_4 \cdot 2\text{H}_2\text{O}$). Only the Class F Miami sample, with its low calcium content, failed to produce this product. In general, the Class F sample does not appear to react to the same extent as the other fly ash samples. Acidic processing was found to increase the amount of soluble iron present especially in the Class C/F and F samples. Increased soluble iron has important implications for the biogeochemical cycle. The ICP-AES measurements indicate that fly ash has soluble material on the surface and is therefore likely to serve as a cloud condensation nucleus. Serving as a cloud condensation nucleus would limit the availability of fly ash in the upper troposphere to serve as an ice nucleus. Fly ash with higher Fe content may be more prevalent in the upper troposphere due to it being less reactive and less likely to serve as a cloud condensation nucleus.

The immersion freezing experiments done on the water- and acid-treated samples revealed that for the Class C samples, Joppa and Welsh, the water-treated samples had the highest ice nucleation activity, and for the Class C/F, Clifty, and Class F, Miami, the acid-treated samples demonstrated the best ice nucleation activity. These results can

partially be explained by the production of gypsum, which is greater for Class C samples and could be covering active sites for ice nucleation. While the Class C/F sample produced some gypsum, it is not to the same degree due to its smaller Ca amount. The results for Class C/F and Class F are not correlated with any major changes to pore width or reaction products. Further work needs to be done in order to discover the cause. Also, deposition freezing should be done to further characterize the freezing activity of the fly ash. Immersion and deposition freezing rely on different properties to induce freezing. Immersion freezing requires that the particle is already in a liquid droplet, whereas deposition freezing occurs through the direct formation of ice onto the particle. Because of this, deposition freezing can be more sensitive to the surface of the particle. Differences in these modes for the same particles have been explored in literature.^{24, 55} These studies have found that the ice nucleation efficiency of the particles is dependent on the mode used. Gypsum has been previously studied before using deposition freezing, which revealed that it can serve as an ice nucleus, but it is unknown whether its presence in the acid-treated Class C and Class C/F fly ash would improve its ice nucleation efficiency.⁵⁶ Exploring this new mode would provide a more rounded discussion of the affect acid processing has on fly ash.

In summary, sulfuric-acid treatment has major physical and chemical effects on fly ash. These effects are dependent on the class and therefore composition of the fly ash. Acid-treatment results in gypsum being created and a variety of metals to be leached. These changes affected the immersion ice nucleation activity of the samples. In future studies, care should be taken to thoroughly characterize samples because small changes in composition across classes of fly ash can lead to very different results in ice nucleation

activity. Furthermore, each fly ash class, whether acid-treated or not, has the potential to be serve as a cloud condensation nucleus or ice nucleus and can play a role in affecting climate.

4.5 References

1. Chen, T.; Rossow, W. B.; Zhang, Y. Radiative Effects of Cloud-Type Variations. *J. Climate*. **2000**, *13*, 1, 264-286.
2. Luo, B. P.; Peter, T.; Fueglistaler, S.; Wernli, H.; Wirth, M.; Kiemle, C.; Flentje, H.; Yushkov, V. A.; Khattatov, V.; Rudakov, V.; Thomas, A.; Borrmann, S.; Toci, G.; Mazzinghi, P.; Beuermann, J.; Schiller, C.; Cairo, F.; Di Donfrancesco, G.; Adriani, A.; Volk, C. M.; Strom, J.; Noone, K.; Mitev, V.; MacKenzie, R. A.; Carslaw, K. S.; Trautmann, T.; Santacesaria, V.; Stefanutti, L. Dehydration potential of ultrathin clouds at the tropical tropopause. *Geophys. Res. Lett.* **2003**, *30*, 11, 1-4.
3. Jensen, E.; Pfister, L. Transport and freeze-drying in the tropical tropopause layer. *J. Geophys. Res.-Atmos.* **2004**, *109*, D2, 1-16.
4. Mitchell, D. L.; Rasch, P.; Ivanova, D.; McFarquhar, G.; Nousiainen, T. Impact of small ice crystal assumptions on ice sedimentation rates in cirrus clouds and GCM simulations. *Geophys. Res. Lett.* **2008**, *35*, 9, 1-5.
5. Fueglistaler, S.; Dessler, A. E.; Dunkerton, T. J.; Folkins, I.; Fu, Q.; Mote, P. W. Tropical tropopause layer. *Rev. Geophys.* **2009**, *47*, 1, 1-31.
6. IPCC, 2013: Summary for Policymakers. In: Climate Change 2013: The Physical Science Basis. Contribution of Working Group I to the Fifth Assessment Report of the Intergovernmental Panel on Climate Change [Stocker, T.F., D. Qin, G.-K. Plattner, M. Tignor, S.K. Allen, J. Boschung, A. Nauels, Y. Xia, V. Bex and P.M. Midgley (eds.)]. Cambridge University Press, Cambridge, United Kingdom and New York, NY, USA.
7. Knopf, D. A.; Koop, T. Heterogeneous nucleation of ice on surrogates of mineral dust. *J. Geophys. Res.-Atmos.* **2006**, *111*, D12, 1-10.
8. Zobrist, B.; Marcolli, C.; Pedernera, D. A.; Koop, T. Do atmospheric aerosols form glasses? *Atmos. Chem. Phys.* **2008**, *8*, 17, 5221-5244.
9. Eastwood, M. L.; Cremel, S.; Wheeler, M.; Murray, B. J.; Girard, E.; Bertram, A. K. Effects of sulfuric acid and ammonium sulfate coatings on the ice nucleation properties of kaolinite particles. *Geophys. Res. Lett.* **2009**, *36*, 2, 1-5.
10. Cziczo, D. J.; Froyd, K. D.; Gallavardin, S. J.; Moehler, O.; Benz, S.; Saathoff, H.; Murphy, D. M. Deactivation of ice nuclei due to atmospherically relevant surface coatings. *Environ. Res. Lett.* **2009**, *4*, 4, 044013.
11. Froyd, K. D.; Murphy, D. M.; Lawson, P.; Baumgardner, D.; Herman, R. L. Aerosols that form subvisible cirrus at the tropical tropopause. *Atmos. Chem. Phys.* **2010**, *10*, 1, 209-218.
12. Sullivan, R.; Petters, M.; DeMott, P.; Kreidenweis, S.; Wex, H.; Niedermeier, D.; Hartmann, S.; Clauss, T.; Stratmann, F.; Reitz, P. Irreversible loss of ice

- nucleation active sites in mineral dust particles caused by sulphuric acid condensation. *Atmos. Chem. Phys.* **2010**, *10*, 23, 11471-11487.
13. Sullivan, R. C.; Miñambres, L.; DeMott, P. J.; Prenni, A. J.; Carrico, C. M.; Levin, E. J. T.; Kreidenweis, S. M. Chemical processing does not always impair heterogeneous ice nucleation of mineral dust particles. *Geophys. Res. Lett.* **2010**, *37*, 24, 1-5.
 14. Chernoff, D. I.; Bertram, A. K. Effects of sulfate coatings on the ice nucleation properties of a biological ice nucleus and several types of minerals. *J. Geophys. Res-Atmos.* **2010**, *115*, D20, 1-12.
 15. Niedermeier, D.; Hartmann, S.; Shaw, R.; Covert, D.; Mentel, T.; Schneider, J.; Poulain, L.; Reitz, P.; Spindler, C.; Clauss, T. Heterogeneous freezing of droplets with immersed mineral dust particles—measurements and parameterization. *Atmos. Chem. Phys.* **2010**, *10*, 8, 3601-3614.
 16. Yang, Z.; Bertram, A. K.; Chou, K. C. Why Do Sulfuric Acid Coatings Influence the Ice Nucleation Properties of Mineral Dust Particles in the Atmosphere? *J. Phys. Chem. Lett.* **2011**, *2*, 11, 1232-1236.
 17. Schill, G. P.; Tolbert, M. A. Depositional Ice Nucleation on Monocarboxylic Acids: Effect of the O:C Ratio. *J. Phys. Chem. A* **2012**, *116*, 25, 6817-6822.
 18. Murray, B.; O'sullivan, D.; Atkinson, J.; Webb, M. Ice nucleation by particles immersed in supercooled cloud droplets. *Chem. Soc. Rev.* **2012**, *41*, 19, 6519-6554.
 19. Tobo, Y.; DeMott, P. J.; Raddatz, M.; Niedermeier, D.; Hartmann, S.; Kreidenweis, S. M.; Stratmann, F.; Wex, H. Impacts of chemical reactivity on ice nucleation of kaolinite particles: A case study of levoglucosan and sulfuric acid. *Geophys. Res. Lett.* **2012**, *39*, 19, 1-5.
 20. Cziczo, D. J.; Froyd, K. D.; Hoose, C.; Jensen, E. J.; Diao, M.; Zondlo, M. A.; Smith, J. B.; Twohy, C. H.; Murphy, D. M. Clarifying the Dominant Sources and Mechanisms of Cirrus Cloud Formation. *Science* **2013**, *340*, 6138, 1320-1324.
 21. Sihvonen, S. K.; Schill, G. P.; Lykтей, N. A.; Veghte, D. P.; Tolbert, M. A.; Freedman, M. A. Chemical and Physical Transformations of Aluminosilicate Clay Minerals Due to Acid Treatment and Consequences for Heterogeneous Ice Nucleation. *J. Phys. Chem. A* **2014**, *118*, 38, 8787-8796.
 22. Schill, G. P.; De Haan, D. O.; Tolbert, M. A. Heterogeneous Ice Nucleation on Simulated Secondary Organic Aerosol. *Environ. Sci. Technol.* **2014**, *48*, 3, 1675-1682.
 23. Schill, G. P.; Tolbert, M. A. Heterogeneous Ice Nucleation on Simulated Sea-Spray Aerosol Using Raman Microscopy. *J. Phys. Chem. C* **2014**, *118*, 50, 29234-29241.
 24. Schill, G. P.; Genareau, K.; Tolbert, M. A. Deposition and immersion-mode nucleation of ice by three distinct samples of volcanic ash. *Atmos. Chem. Phys.* **2015**, *15*, 13, 7523-7536.
 25. Vali, G. Ice nucleation—A review. *Nucleation and atmospheric aerosols* **1996**, 271-279.
 26. DeMott, P. J.; Cziczo, D. J.; Prenni, A. J.; Murphy, D. M.; Kreidenweis, S. M.; Thomson, D. S.; Borys, R.; Rogers, D. C. Measurements of the concentration and

- composition of nuclei for cirrus formation. *Proc. Natl. Acad. Sci. U.S.A.* **2003**, *100*, 25, 14655-14660.
27. Haag, W.; Kärcher, B. The impact of aerosols and gravity waves on cirrus clouds at midlatitudes. *J. Geophys. Res.-Atmos.* **2004**, *109*, D12, 1-18.
 28. Li, J.; Pósfai, M.; Hobbs, P. V.; Buseck, P. R. Individual aerosol particles from biomass burning in southern Africa: 2, Compositions and aging of inorganic particles. *J. Geophys. Res.-Atmos.* **2003**, *108*, D13, 1-12.
 29. Pósfai, M.; Simonics, R.; Li, J.; Hobbs, P. V.; Buseck, P. R. Individual aerosol particles from biomass burning in southern Africa: 1. Compositions and size distributions of carbonaceous particles. *J. Geophys. Res.-Atmos.* **2003**, *108*, D13, 1-13.
 30. Bond, T. C.; Doherty, S. J.; Fahey, D. W.; Forster, P. M.; Bernsten, T.; DeAngelo, B. J.; Flanner, M. G.; Ghan, S.; Kärcher, B.; Koch, D.; Kinne, S.; Kondo, Y.; Quinn, P. K.; Sarofim, M. C.; Schultz, M. G.; Schulz, M.; Venkataraman, C.; Zhang, H.; Zhang, S.; Bellouin, N.; Guttikunda, S. K.; Hopke, P. K.; Jacobson, M. Z.; Kaiser, J. W.; Klimont, Z.; Lohmann, U.; Schwarz, J. P.; Shindell, D.; Storelvmo, T.; Warren, S. G.; Zender, C. S. Bounding the role of black carbon in the climate system: A scientific assessment. *J. Geophys. Res.-Atmos.* **2013**, *118*, 11, 5380-5552.
 31. Sear, L. K. A., *Properties and use of coal fly ash*. Thomas Telford: London, 2001.
 32. WCA: Coal Combustion Products Report. World Coal Association: London, 2013.
 33. Parungo, F.; Ackerman, E.; Proulx, H.; Pueschel, R. Nucleation properties of fly ash in a coal-fired power-plant plume. *Atmos. Environ.* **1978**, *12*, 4, 929-935.
 34. Umo, N. S.; Murray, B. J.; Baeza-Romero, M. T.; Jones, J. M.; Lea-Langton, A. R.; Malkin, T. L.; O'Sullivan, D.; Neve, L.; Plane, J. M. C.; Williams, A. Ice nucleation by combustion ash particles at conditions relevant to mixed-phase clouds. *Atmos. Chem. Phys.* **2015**, *15*, 9, 5195-5210.
 35. Chen, H.; Laskin, A.; Baltrusaitis, J.; Gorski, C. A.; Scherer, M. M.; Grassian, V. H. Coal Fly Ash as a Source of Iron in Atmospheric Dust. *Environ. Sci. Technol.* **2012**, *46*, 4, 2112-2120.
 36. Nagib, S.; Inoue, K. Recovery of lead and zinc from fly ash generated from municipal incineration plants by means of acid and/or alkaline leaching. *Hydrometallurgy* **2000**, *56*, 3, 269-292.
 37. Izquierdo, M.; Querol, X. Leaching behaviour of elements from coal combustion fly ash: An overview. *Int. J. Coal Geol.* **2012**, *94*, Supplement C, 54-66.
 38. Martin, J. H. Glacial-interglacial CO₂ change: The Iron Hypothesis. *Paleoceanography* **1990**, *5*, 1, 1-13.
 39. Martin, J. H.; Coale, K. H.; Johnson, K. S.; Fitzwater, S. E.; Gordon, R. M.; Tanner, S. J.; Hunter, C. N.; Elrod, V. A.; Nowicki, J. L.; Coley, T. L.; Barber, R. T.; Lindley, S.; Watson, A. J.; Van Scoy, K.; Law, C. S.; Liddicoat, M. I.; Ling, R.; Stanton, T.; Stockel, J.; Collins, C.; Anderson, A.; Bidigare, R.; Ondrusek, M.; Latasa, M.; Millero, F. J.; Lee, K.; Yao, W.; Zhang, J. Z.; Friederich, G.; Sakamoto, C.; Chavez, F.; Buck, K.; Kolber, Z.; Greene, R.; Falkowski, P.; Chisholm, S. W.; Hoge, F.; Swift, R.; Yungel, J.; Turner, S.; Nightingale, P.;

- Hatton, A.; Liss, P.; Tindale, N. W. Testing the iron hypothesis in ecosystems of the equatorial Pacific Ocean. *Nature* **1994**, *371*, 6493, 123-129.
40. Moore, J. K.; Doney, S. C.; Glover, D. M.; Fung, I. Y. Iron cycling and nutrient-limitation patterns in surface waters of the World Ocean. *Deep-Sea Res. Part II*. **2001**, *49*, 1, 463-507.
 41. Iyer, R. The surface chemistry of leaching coal fly ash. *J. Hazard. Mater.* **2002**, *93*, 3, 321-329.
 42. Cwiertny, D. M.; Baltrusaitis, J.; Hunter, G. J.; Laskin, A.; Scherer, M. M.; Grassian, V. H. Characterization and acid-mobilization study of iron-containing mineral dust source materials. *J. Geophys. Res-Atmos.* **2008**, *113*, D5, 1-18.
 43. Seidel, A.; Zimmels, Y. Mechanism and kinetics of aluminum and iron leaching from coal fly ash by sulfuric acid. *Chem. Eng. Sci.* **1998**, *53*, 22, 3835-3852.
 44. Seidel, A.; Sluszný, A.; Shelef, G.; Zimmels, Y. Self inhibition of aluminum leaching from coal fly ash by sulfuric acid. *Chem. Eng. J.* **1999**, *72*, 3, 195-207.
 45. Grawe, S.; Augustin-Bauditz, S.; Hartmann, S.; Hellner, L.; Pettersson, J. B. C.; Prager, A.; Stratmann, F.; Wex, H. The immersion freezing behavior of ash particles from wood and brown coal burning. *Atmos. Chem. Phys.* **2016**, *16*, 21, 13911-13928.
 46. Atkinson, J. D.; Murray, B. J.; Woodhouse, M. T.; Whale, T. F.; Baustian, K. J.; Carslaw, K. S.; Dobbie, S.; O'Sullivan, D.; Malkin, T. L. The importance of feldspar for ice nucleation by mineral dust in mixed-phase clouds. *Nature* **2013**, *498*, 7454, 355-358.
 47. Meskhidze, N.; Chameides, W. L.; Nenes, A.; Chen, G. Iron mobilization in mineral dust: Can anthropogenic SO₂ emissions affect ocean productivity? *Geophys. Res. Lett.* **2003**, *30*, 21, 1-5.
 48. O'Sullivan, D.; Murray, B. J.; Ross, J. F.; Whale, T. F.; Price, H. C.; Atkinson, J. D.; Umo, N. S.; Webb, M. E. The relevance of nanoscale biological fragments for ice nucleation in clouds. *Sci. Rep.-UK* **2015**, *5*, 8082.
 49. International, A., Standard Test Methods for Sampling and Testing Fly Ash of Natural Pozzolans for Use in Portland-Cement Concrete. International, A., Ed. 2013.
 50. Povnennykh, A.; SSR, K. U. The use of infrared spectra for the determination of minerals. *Am. Mineral.* **1978**, *63*, 956-959.
 51. Prasad, P. S. R.; Chaitanya, V. K.; Prasad, K. S.; Rao, D. N. Direct formation of the γ -CaSO₄ phase in dehydration process of gypsum: In situ FTIR study. *Am. Mineral.* **2005**, *90*, 4, 672-678.
 52. Marcolli, C. Deposition nucleation viewed as homogeneous or immersion freezing in pores and cavities. *Atmos. Chem. Phys.* **2014**, *14*, 4, 2071-2104.
 53. Kumar, P.; Jasra, R. V.; Bhat, T. S. Evolution of porosity and surface acidity in montmorillonite clay on acid activation. *Ind. Eng. Chem. Res.* **1995**, *34*, 4, 1440-1448.
 54. Panda, A. K.; Mishra, B. G.; Mishra, D. K.; Singh, R. K. Effect of sulphuric acid treatment on the physico-chemical characteristics of kaolin clay. *Colloid Surface A* **2010**, *363*, 1, 98-104.
 55. Steinke, I.; Möhler, O.; Kiselev, A.; Niemand, M.; Saathoff, H.; Schnaiter, M.; Skrotzki, J.; Hoose, C.; Leisner, T. Ice nucleation properties of fine ash particles

- from the Eyjafjallajökull eruption in April 2010. *Atmos. Chem. Phys.* **2011**, *11*, 24, 12945-12958.
56. Zimmermann, F.; Weinbruch, S.; Schütz, L.; Hofmann, H.; Ebert, M.; Kandler, K.; Wörzinger, A. Ice nucleation properties of the most abundant mineral dust phases. *J. Geophys. Res.-Atmos.* **2008**, *113*, D23, 1-11.

Chapter 5

Conclusions and Future Directions

5.1 Conclusions

This dissertation explored how different properties of aerosol particles can affect their phase transitions and their ability to nucleate ice to form ice clouds. Both of these effects can influence how these particles interact in the atmosphere with radiation and other species. Chapters 2 and 3 used optical microscopy to determine the effect of differences in bulk pH on phase transitions in organic-inorganic aerosol model systems. Chapter 4 explored the effect of acid-treatment on different types of fly ash. Physical and chemical characterization of the fly ash using XRD, ATR-IR, TEM, EDS, SAED, and ICP-AES was performed and immersion freezing was used to determine the effects on ice nucleation activity after processing.

The results on phase transitions revealed that aerosol particle pH significantly affect the separation, mixing, efflorescence, and deliquescence relative humidities of

organic-inorganic systems. As 3-methylglutaric acid becomes more deprotonated at higher pH, the separation relative humidity decreases making phase separation more difficult. This is attributed to the increased solubility of the organic component. The efflorescence relative humidity increases and becomes controlled by the organic component at higher pH as well. The deliquescence and mixing relative humidities change little over the range of pH values, indicating that transitions requiring the formation of a nucleus were more susceptible to the pH changes. A previously-unobserved hysteresis between the separation and mixing transitions was seen at high pH as well, which could mean that particles can be phase separated for longer periods of time in the atmosphere when deprotonated. The importance of pH in phase transitions of organic-inorganic aerosol particles was also demonstrated with the low pH studies done on systems containing 3-methylglutaric acid, 2-methylglutaric acid, 3,3-dimethylglutaric acid, diethylmalonic acid, 2,2-Bis(hydroxymethyl)butyric acid, and 1,2,6-hexanetriol. Sulfuric acid was used because it is quickly produced in the atmosphere when SO_2 and water combine. It also serves as an important catalyst for reactions leading to secondary organic matter. This study found that with increased amounts of sulfuric acid, the separation relative humidity decreased for every system. This was attributed to the change in the identity of the inorganic component, because ammonium bisulfate and letovicite are expected to have less salting-out ability than ammonium sulfate according to the Hofmeister series. At the lowest pH studied the separation relative humidities were low enough to not phase separate at all in atmospherically relevant conditions. The efflorescence and deliquescence relative humidities were also affected by the addition of sulfuric acid underlining the importance of composition on phase transitions.

Interestingly, this study also observed phase separation in several systems with no inorganic salt present, just sulfuric acid and the organic component. These results could affect mass transfer and water uptake for systems at low pH.

The effects of sulfuric acid-treatment on different types of fly ash was also investigated. The effects of acid-treatment were dependent on the type (i.e. composition) of the fly ash studied. The fly ash that contained calcium, Class C and C/F fly ash, produced a coating of gypsum ($\text{CaSO}_4 \cdot 2\text{H}_2\text{O}$) during acid-treatment. Class C/F and Class F fly ash, leached soluble iron during acid-treatment as well. The characterization results reveal that fly ash contains water-soluble material before acid-treatment making it a probable cloud condensation nucleus, and that after acid-treatment, more soluble material is produced or leached. The Class F sample did not react to the same extent as the other samples but did have better immersion freezing activity following acid-treatment. This freezing behavior was also observed for Class C/F, but Class C had better freezing activity after only water-treatment indicating that the production of gypsum may have blocked sites active to freezing. The freezing behavior of the Class F and Class C/F samples could not be explained using the characterization techniques employed.

5.2 Future Directions

The phase transition studies have many different avenues for future exploration. First, the effect of the addition of sulfuric acid with no inorganic salt can be further explored. Of the six organic compounds studied here, three phase separated with just acid. Due to sulfuric acid's ability to cause phase separation without the aid of a salt, an organic coating could form and creating a barrier for uptake of ammonia, preventing its

neutralization in the atmosphere.¹ Further characterization of what organic compounds can induce phase separation in particles and when this phenomenon occurs would be beneficial to aerosol scientists. Also, another step that future pH studies could take is to investigate the effect of sulfuric acid in the submicron regime. The dependence on size of phase separation has been explored previously, but pH has not been investigated and could lead to interesting implications on the morphology of submicron aerosol particles.² One further study that could help to explain the data collected in the low pH research would be to directly characterize the particle viscosity as a function of sulfuric acid content and relative humidity. Because the phase separation and efflorescence behavior could be possibly due to a viscosity inhibited phase transition, fully characterizing the viscosity across the particle could confirm this.

In order to expand the current study of acid-treatment on fly ash, deposition freezing experiments should be done to further characterize the freezing activity of the fly ash. Immersion and deposition freezing rely on different properties to induce freezing. Because immersion freezing is studied with the particle already in a liquid droplet, it does not require uptake onto the particle to nucleate ice. Because of this, deposition freezing can be more sensitive to the surface of the particle. Differences in immersion and deposition freezing behavior of the same particles has been explored in literature.³⁻⁴ These studies have found that the ice nucleation efficiency of the particles is dependent on the mode being used. Gypsum has been studied before using deposition freezing, which revealed that it can serve as an ice nucleus using this freezing mode, but it is unknown whether its presence in the acid-treated Class C and Class C/F fly ash would

improve its ice nucleation efficiency.⁵ Exploring this new mode would provide a more rounded discussion of the affect acid processing has on fly ash.

5.3 Outlook

This work's objective was to better understand what influences aerosol particles can have in the environment. This was done in several ways. The phase transitions of organic-inorganic aerosol particles were explored as a function of pH and relative humidity. Also, the chemical, morphological, and ice nucleation effects of water- and acid-treatment of different fly ash compositions was investigated. The results from both of these research areas can be expanded to include further characterization of the role of sulfuric acid in phase transitions of aerosol particles including submicron particles and particle viscosity and of the ice nucleation activity of treated fly ash samples.

5.4 References

1. Silvern, R. F.; Jacob, D. J.; Kim, P. S.; Marais, E. A.; Turner, J. R.; Campuzano-Jost, P.; Jimenez, J. L. Inconsistency of ammonium–sulfate aerosol ratios with thermodynamic models in the eastern US: a possible role of organic aerosol. *Atmos. Chem. Phys.* **2017**, *17*, 8, 5107-5118.
2. Veghte, D. P.; Altaf, M. B.; Freedman, M. A. Size Dependence of the Structure of Organic Aerosol. *J. Am. Chem. Soc.* **2013**, *135*, 43, 16046-16049.
3. Schill, G. P.; Genareau, K.; Tolbert, M. A. Deposition and immersion-mode nucleation of ice by three distinct samples of volcanic ash. *Atmos. Chem. Phys.* **2015**, *15*, 13, 7523-7536.
4. Steinke, I.; Möhler, O.; Kiselev, A.; Niemand, M.; Saathoff, H.; Schnaiter, M.; Skrotzki, J.; Hoose, C.; Leisner, T. Ice nucleation properties of fine ash particles from the Eyjafjallajökull eruption in April 2010. *Atmos. Chem. Phys.* **2011**, *11*, 24, 12945-12958.
5. Zimmermann, F.; Weinbruch, S.; Schütz, L.; Hofmann, H.; Ebert, M.; Kandler, K.; Wörzinger, A. Ice nucleation properties of the most abundant mineral dust phases. *J. Geophys. Res.-Atmos.* **2008**, *113*, D23, 1-11.

VITA

Delanie Jean Losey

EDUCATION

The Pennsylvania State University, University Park, PA 2012-2017
Ph.D. in Chemistry
Advisor: Dr. Miriam Freedman

Manchester University, North Manchester, IN 2008-2012
B.A. Chemistry and Environmental Studies, *Magna Cum Laude*

PUBLICATIONS

- Alstadt, V.; Dawson, J. N.; Losey, D. J.; Sihvonen, S. K.; Freedman, M. A. Heterogeneous Freezing of Carbon Nanotubes: A Model System for Pore Condensation and Freezing in the Atmosphere. *J. Phys. Chem. A* **2017**, *121*, 8166-8175.
- Losey, D. J.; Parker, R. G.; Freedman, M. A. pH Dependence of Liquid-Liquid Phase Separation in Organic Aerosol. *J. Phys. Chem. Lett.* **2016**, *7*, 3861-3865.
- Losey, D. J.; Frenzel, B. A.; Smith, W. M.; Hightower, S. E.; Hamaker, C. G. Tricarbonyl rhenium complex of 2,6-bis(8'-quinoliny)pyridine: Synthesis, spectroscopic characterization, X-ray structure and DFT calculations. *Inorg. Chem. Commun.* **2013**, *30*, 46-48.

FELLOWSHIPS, HONORS, AND AWARDS

2015-2016 Penn State Chemistry Graduate Student Travel Award
2013-2014 Dan H. Waugh Memorial Teaching Award
Graduate Fellowship Award (Penn State University, Fall 2012)

LEADERSHIP EXPERIENCE

Organic Lab Section Supervisor	January 2016-April 2017
VOICES Conference Co-Chair/Organizer/Volunteer	June 2014-February 2017
Public Relations Officer/Executive Board Member	June 2014-May 2015